

Nano Particle and Fiber Reinforced Injection Molded Polymeric Materials

by

Reyhan Keskin

A dissertation submitted to the Graduate Faculty of
Auburn University
in partial fulfillment of the
requirements for the Degree of
Philosophy

Auburn, Alabama
August 09, 2010

Keywords: Polypropylene, glass fibers, carbon fibers, nanoclay, modeling, tensile strength

Copyright 2010 by Reyhan Keskin

Approved by

Sabit Adanur, Chair, Professor of Polymer and Fiber Engineering
Peter Schwartz, Professor of Polymer and Fiber Engineering
Carol Larson Warfield, Professor of Consumer Affairs

Abstract

Fiber reinforced polymers have been widely used for many years. Despite of their higher cost of production compared to metals, their improved properties make them widely used.

Modeling of fiber reinforced polymers is necessary to predict the final product properties, and to decide on production conditions and material properties to be used in manufacturing.

In 1987, Fukushima and Inagaki who were researchers in Toyota investigated the effects of nano sized clay on the strength properties of timer belts. Their trial started the nanocomposite era. The discovery of carbon nanotubes and fullerenes gave more options for nanocomposites production. Due to the difference between nano scale and micron scale, nanocomposites have different properties compared to conventional composites.

In this study, polypropylene (PP) is reinforced with elastomers, fibers and nanoclay. To improve the toughness of PP, two thermoplastic elastomers were added separately. Tensile tests were conducted according to the ASTM D638-3 standard test method on Instron universal testing machine. Rubber particle distributions were observed on SEM. Tensile test results give an increase in energy at break which is the toughness of the material. Increase in toughness proves that adding thermoplastic elastomers toughens the PP.

For fiber and nanoclay reinforcement, polypropylene based composites having glass fiber, carbon fiber, and nanoclay reinforcements at 1 wt%, 4 wt% and 7 wt% are produced. The

fibers are in the micron scale while the clay is in nano scale. Pure polypropylene samples are used as control samples. The effect of compatibilizer on nanoclay/polypropylene is also investigated using a montmorillonite nanoclay. The mechanical properties (tensile strength, flexural strength and impact strength) of the samples are tested. The cross-sections of the samples are studied using scanning electron microscopy. Fiber length distributions are studied using scanning electron microscopy and light microscopy.

The processing characteristics of PP/F1 and PP/F2 blends have been studied. Addition of thermoplastic elastomers F1 and F2 to PP decreased the yield stress of the blend and decreased its modulus. Toughening of polypropylene was achieved by blending of PP with the thermoplastic elastomers. Tensile tests show that brittle characteristics of PP turns to be ductile both in PP/F1 and PP/F2 blends.

Addition of carbon fibers and glass fibers to PP matrix, enhances tensile, flexural and impact properties of the composite; while the addition of nanoclay decreases the composite properties. This may be due to poor dispersion of nanoclay, for this reason compatibilizer is added to the nanoclay/polypropylene composites and improvement in properties is achieved.

Models are developed for predictions of tensile strength, impact energy and flexural strength depending on the fiber volume content, interfacial shear strength, void volume, matrix volume, fiber volume, fiber orientation degrees and total fiber area of glass and carbon fiber reinforced samples. The difference between measured and calculated values does not exceed 10%; model predictions for tensile strength, impact energy and flexural strength give good correlation between measured and calculated values.

Acknowledgments

This study would not have been possible without the help of several people that I would like to thank: Dr. Ramsis Farag for teaching how to conduct tensile and impact tests, and how to operate the machines, Dr. Miller for helping in SEM analysis, and Dr. Edward Davis for giving information and helping while operating the injection molding machine. I also appreciate the help of Mr. Jeff Thomson, and Mr. Steve Howard in several steps of this study; and the guidance of Dr. Christopher Roberts, Dr. Ram Gupta, Dr. Bart Prorok and Mr. Roy Howard in sample preparation and evaluation for SEM.

I would also like to thank Dr. Maria Auad and Dr. Esaam for their contributions in sample preparation and testing; and Mr. David Clark for operating the injection molding machine during sample production.

This research is supported by the *U.S. Department of Commerce* (DOC-ITA-O8-TBD-E), which is appreciated.

Table of Contents

Abstract	ii
Acknowledgments	iv
List of Tables	ix
List of Figures	xi
Chapter 1. Introduction	1
1.1. References	3
Chapter 2. Literature review	5
2.1. Fiber reinforced polymeric materials (FRMPs)	5
2.2. Reinforcers	11
2.2.1. Fiber reinforcers	11
2.2.2. Nanoparticle reinforcers	11
2.2.3. Rubber reinforcers	13
2.3. Importance of predicting mechanical properties of IMPM	15
2.3.1. Macromechanics approach	16
2.3.2. Micromechanics approach	17
2.3.2.1. Rule of mixtures (ROM)	17
2.3.2.2. Halpin-Tsai equation	20
2.4. References	21

Chapter 3. Improving Toughness of Polypropylene (PP) with Thermoplastic Elastomers in	
Injection Molding	26
3.1. Introduction	26
3.2. Experimental	30
3.2.1. Materials	30
3.2.2. Sample preparation	30
3.3. Results and discussion	31
3.3.1. Mechanical properties	31
3.3.1.1. Impact and tensile tests	31
3.3.1.2. Three-point bending tests.....	35
3.3.2. DSC analysis.....	37
3.3.3. SEM analysis	40
3.4. Conclusions.....	44
3.5. References.....	45
Chapter 4. Fiber and nanoclay reinforced PP composites	51
4.1. Materials used	51
4.1.1. Polypropylene (PP)	51
4.1.2. Glass fibers	52
4.1.3. Carbon fibers	53
4.1.4. Nanoclay	54
4.1.5. Compatibilizer	55
4.2. Machines used	55
4.2.1. Injection molding machine EM 50/300 Battenfeld	56

4.2.1.1. Operation of the EM 50/300 Battenfeld IMM	60
4.2.2. Instron 5565 Universal Tester	69
4.2.3. Instron DynaTup 8250	69
4.3. Sample preparation	70
4.4. Tests	72
4.4.1. Tensile strength	72
4.4.1.1. SEM analysis of the samples	76
4.4.2. Impact strength	83
4.4.3. Flexural strength	92
4. 5. References	96
Chapter 5. Model development	98
5.1. Objective	98
5.2. Approach	99
5.3. Factors affecting the mechanical properties of IMPM	100
5.3.1. Fiber length and diameter	100
5.3.1.1. Critical length	104
5.3.2. Void volume	109
5.3.3. Fiber orientation degree (FOD)	110
5.3.4. Interfacial shear strength (IFSS)	117
5.4. Suggested models	119
5.4.1. Rule of mixtures for tensile strength	119
5.4.1.1. Fiber reinforcement parallel to the flow direction	119
5.4.1.2. Fiber reinforcement transverse to the flow direction	121

5.4.2. Model for tensile testing	122
5.4.2.1. Effect of fiber orientation degree	122
5.4.2.2. Effect of void	123
5.4.2.3. Effect of total fiber surface area and IFSS	124
5.4.3. Model for flexural testing	126
5.4.3.1. Determination of force applied	127
5.4.3.2. Effect of void volume	127
5.4.3.3. Effect of fiber orientation degree	128
5.4.4. Model for impact testing.....	130
5.4. References.....	133
Chapter 6. Conclusions and recommendations	135
6.1. Conclusions	135
6.2. Recommendations	136

List of Tables

Table 3.1. Sample codes and blend compositions	31
Table 3.2. Results of tensile and impact tests for PP, F1, F2, PP/F1 and PP/F2 samples	32
Table 3.3. 3-point bending test results of PP, F1, F2, PP/F1 and PP/F2 samples	35
Table 3.4. Thermal properties of PP, F1, F2, PP/F1 and PP/F2 samples obtained from DSC analysis	39
Table 4.1. Properties of glass and carbon fibers used	52
Table 4.2. Machines used for the manufacturing and testing of samples	55
Table 4.3. Parts of the control panel	62
Table 4.4. Symbols of the most widely used keys on the Unilog.....	64
Table 4.5. Sample codes and blend compositions	71
Table 4.6. Results of the tensile tests.....	72
Table 4.7. Results of the impact tests for pure polypropylene and glass fiber, carbon fiber and nanoclay reinforced polypropylene samples.....	83
Table 4.8. Three point bending test results for pure polypropylene and glass fiber, carbon fiber and nanoclay reinforced polypropylene (mean \pm standard deviation).....	92
Table 5.1. Parameters to be included in modeling.....	100
Table 5.2. Fiber length distribution mean values ' l_m ' (mean \pm standard deviation).....	104
Table 5.3. Calculated critical length ' l_c ' values for the fibers used	105

Table 5.4. The fiber volume, matrix volume and void volume of pure polypropylene and glass fiber, carbon fiber and nanoclay reinforced polypropylene (mean \pm standard deviation) 110

Table 5.5. FOD angle percentages for the samples 115

Table 5.6. IFSS of glass fibers and carbon fibers used 119

List of Figures

Figure 2.1. Structure of MMT.....	12
Figure 2.2. Intercalated and delaminated structures of polymer- nanoclay nanocomposites	12
Figure 2.3. Dispersion mechanism of nanoclays during mixing	13
Figure 2.4. Classification of modeling techniques for materials	16
Figure 2.5. Force and fiber alignment in the longitudinal loading condition	18
Figure 2.6. Force and fiber alignment in perpendicular loading condition	20
Figure 3.1. Dimensions of big dog-bone shaped samples	32
Figure 3.2. Stress- strain curves of PP, F1, F2, PP/F1 and PP/F2 samples	33
Figure 3.3. Stress- strain curve of PP	35
Figure 3.4. 3-point bending test stress-strain curves of PP, F1, F2, PP/F1 and PP/F2	36
Figure 3.5. DSC thermograms of PP, F1 and PP/F1 samples.....	38
Figure 3.6. DSC thermograms of PP, F2 and PP/F2 samples.....	38
Figure 3.7. SEM micrograph of etched PP/F1 blend	40
Figure 3.8. SEM micrograph of etched PP/F2 blend.....	41
Figure 3.9. SEM micrograph of F1 particle sizes in etched PP/F1 blend.....	42
Figure 3.10. SEM micrograph of F2 particle sizes in etched PP/F2 blend.....	42
Figure 3.11. Histogram of particle diameter of F1 in etched PP/F1 blend	43
Figure 3.12. Histogram of particle diameter of F2 in etched PP/F2 blend	44
Figure 4.1. Repeating unit of polypropylene	51

Figure 4.2. Carbonization step for producing carbon fibers	53
Figure 4.3. Graphitization step for producing carbon fibers.....	54
Figure 4.4. Chemical structure of Nanofil 919®	54
Figure 4.5. Injection molding machine	57
Figure 4.6. Shear rate and velocity profiles for nonisothermal flow during injection molding process.....	59
Figure 4.7. Fountain flow in injection molding	59
Figure 4.8. Injection molding machine used to produce samples.....	60
Figure 4.9. Control panel of the machine	61
Figure 4.10. Appearance of the interrupt list of the Battenfeld EM 50/300 IMM.....	63
Figure 4.11. Logon panel of the IMM	65
Figure 4.12. Main menu showing real data for the machine during production.....	67
Figure 4.13. Carbon fibers in bundle form(a) and opened fibers using pressurized air (b).....	70
Figure 4.14. Tensile graph of glass fiber reinforced samples	73
Figure 4.15. Tensile graph of carbon fiber reinforced samples	74
Figure 4.16. Tensile graph of NN1	74
Figure 4.17. Tensile graph of NN4 and NN7.....	75
Figure 4.18. Tensile graph of nanoclay and compatibilizer reinforced samples	75
Figure 4.19. SEM micrograph of C1	76
Figure 4.20. SEM micrograph of C4	77
Figure 4.21. SEM micrograph of C7	77
Figure 4.22. SEM micrograph of GF1	78
Figure 4.23. SEM micrograph of GF4.....	78

Figure 4.24. SEM micrograph of GF7	79
Figure 4.25. SEM micrograph of NN1	80
Figure 4.26. SEM micrograph of NN4	80
Figure 4.27. SEM micrograph of NN7	81
Figure 4.28. SEM micrograph of CMP-NN1.....	81
Figure 4.29. SEM micrograph of CMP-NN4.....	82
Figure 4.30. SEM micrograph of CMP-NN7.....	82
Figure 4.31. Load-deformation graph of PP	85
Figure 4.32. Velocity-time graph of PP	85
Figure 4.33. Load-deformation graph of GF1	86
Figure 4.34. Velocity-time graph of GF1	86
Figure 4.35. Load-deformation graph of GF4	87
Figure 4.36. Velocity-time graph of GF4	87
Figure 4.37. Load-deformation graph of GF7	88
Figure 4.38. Velocity-time graph of GF7	88
Figure 4.39. Load-deformation graph of C1	89
Figure 4.40. Velocity-time graph of C1	89
Figure 4.41. Load-deformation graph of C4.....	90
Figure 4.42. Velocity-time graph of C4.....	90
Figure 4.43. Load-deformation graph of C7.....	91
Figure 4.44. Velocity-time graph of C7.....	91
Figure 4.45. Three point bending graph for pure polypropylene.....	94
Figure 4.46. Three point bending results for glass fiber reinforced PP	94

Figure 4.47. Three point bending results for carbon fiber reinforced PP	95
Figure 4.48. Three point bending results for nanoclay reinforced PP	95
Figure 5.1. Fiber length distribution of GF1	101
Figure 5.2. Fiber length distribution of GF4.....	101
Figure 5.3. Fiber length distribution of GF7.....	102
Figure 5.4. Fiber length distribution of C1	102
Figure 5.5. Fiber length distribution of C4	103
Figure 5.6. Fiber length distribution of C7	103
Figure 5.7. SEM micrograph of GF1	106
Figure 5.8. SEM micrograph of GF4.....	106
Figure 5.9. SEM micrograph of GF7	107
Figure 5.10. SEM micrograph of C1	107
Figure 5.11. SEM micrograph of C4	108
Figure 5.12. SEM micrograph of C7	108
Figure 5.13. SEM micrograph of a fiber orientation angle of GF1	111
Figure 5.14. SEM micrograph of a fiber orientation angle of GF4	111
Figure 5.15. SEM micrograph of a fiber orientation angle of GF7	112
Figure 5.16. FOD for dogbone shaped GF1	112
Figure 5.17. FOD for dogbone shaped GF4	113
Figure 5.18. FOD for dogbone shaped GF7	113
Figure 5.19. FOD for dogbone shaped C1	114
Figure 5.20. FOD for dogbone shaped C4.....	114
Figure 5.21. FOD for dogbone shaped C7.....	115

Figure 5.22. Schematic of fiber orientation development in injection molding	116
Figure 5.23. Example of fiber orientations	117
Figure 5.24. Simulation for fiber reinforcement parallel to the flow direction	120
Figure 5.25. Simulation for fiber reinforcement transverse to the flow direction	121
Figure 5.26. Measured and calculated tensile strength values of GF1, GF4 and GF7	125
Figure 5.27. Measured and calculated tensile strength values of C1, C4 and C7.....	126
Figure 5.28. Measured and calculated values for flexural strength of glass fiber and carbon fiber reinforced samples	129
Figure 5.29. Measured and calculated values for impact energy of glass fiber and carbon fiber reinforced samples	132

CHAPTER 1

INTRODUCTION

Fiber reinforced polymers have been widely used for many years. Despite of their higher cost of production compared to metals, their improved properties make them widely used.

As production costs of fiber reinforced polymers are high, final product property prediction is very important in fiber reinforced composites. Modeling of fiber reinforced polymers is necessary to predict the final product properties, and to decide on production conditions and material properties to be used in production such as fiber type, fiber length, fiber content, matrix type, etc.

Some polymers are widely used in sectors such as automotive and aerospace due to their high impact properties. Toughness is a desired property for polymers. Toughness is defined as ‘the material’s ability to withstand an applied sudden load without failure’. There are several methods of impact testing such as impact resistance, tensile elongation tests, tensile impact tests, falling weight tests and pendulum tests. There are three main methods to increase the impact property of a polymer:

- 1- By changing its crystallinity ratio.
- 2- By adding a rubbery phase into the polymer.
- 3- By adding a fibrous or non-fibrous reinforcement into the polymer structure [1].

In fiber reinforced composites, it is possible to enable the desired fiber location and

fiber orientation in the polymer matrix. Polymer molecules transfer load between fibers. High performance fibers such as glass fibers, carbon fibers or Kevlar ®49 aramid fibers reinforce the matrix. Weight reduction is essential in aircraft, military and space applications, so fiber reinforced composites have advantages over metals for weight reduction applications in sectors such as military, aerospace, marine engineering and sporting goods [2].

The need of energy consumption reduction in vehicles requires improving vehicle efficiency by reducing weight. Light weight improves fuel efficiency and driving performance, and gives lower vehicle emission rates [3].

In 1987, Fukushima and Inagaki, who were researchers in Toyota, investigated the effects of nano sized clay on the strength properties of timer belts. Their trial started the nanocomposite era. The discovery of carbon nanotubes and fullerenes gave more options to nanocomposites production. Due to the difference between nano scale and micro scale, nanocomposites have different properties compared to conventional composites [4].

It is possible to have big increases such as 10 % in mechanical properties even with very small amounts of nano particles such as 1 wt% [5]. Increase of mechanical properties of nano particle reinforced composites is possible if a good load transfer between matrix and reinforcement is present [6, 7, 8, 9].

The objective of this study is to improve properties of polypropylene (PP) by adding fiber reinforcements and nanoclay, as well as forming models to predict the overall properties of the composites reinforced with glass fibers and carbon fibers.

In this study, polypropylene based composites having glass fiber, carbon fiber, and nanoclay reinforcements at 1 wt%, 4 wt% and 7 wt% are produced. The fibers are in the micron scale while the clay is in nano scale. Pure polypropylene samples were used as control

samples. The effect of compatibilizer on nanoclay/polypropylene is also investigated using montmorillonite nanoclay. The mechanical properties (tensile strength, flexural strength and impact strength) of the samples are tested. The fiber length distributions of the samples are studied using scanning electron microscopy and light microscopy. Models to predict tensile strength, flexural strength and impact strength of the fiber reinforced composites are developed.

1.1. References

- [1] Perkins, W. G., Polymer Toughness and Impact Resistance, *Polymer Engineering and Science*, **39**, 2445-2460 (1999).
- [2] Mallick, P. K., “Fiber Reinforced Composites Materials, Manufacturing and Design”, CRC Press, 2-23 (1993).
- [3] Fuchs, E. R. H., Field, F. R., Roth, R., and Kirchain, E., Strategic Materials Selection In The Automobile Body: Economic Opportunities For Polymer Composite Design, *Composites Science and Technology*, **68**, 1989-2002 (2008).
- [4] Xiao, Y., Zhang, X. Q., Cao, W., Wang, K., Tan, H., Zhang, Q., Du, R. N., and Fu, Q., Dispersion and Mechanical Properties of Polypropylene/Multiwall Carbon Nanotubes Composites Obtained via Dynamic Packing Injection Molding, *Journal of Applied Polymer Science*, **104**(3), 1880-1886 (2007).
- [5] Qian, D., Dickey, E. C., Andrews, R., and Rantell, T., Load Transfer and Deformation Mechanisms in Carbon Nanotube–Polystyrene Composites , *Applied Physics Letters*, **76**, 2868-2870 (2000).

- [6] Frankland, S. J. V., Caglar, A., Brenner, D. W., and Greibel, M., Molecular Simulation of the Influence of Chemical Cross-Links on the Shear Strength of Carbon Nanotube-Polymer Interfaces, *J. Phys. Chem. B* **106**, 3046-3050 (2002).
- [7] Hu, Y., and Sinnott, S. B., Modification of Carbon Nanotube Polymer-Matrix Composites through Polyatomic-Ion Beam Deposition: Predictions from Molecular Dynamics Simulations, *Composite Science and Technology*, **63**, 1663-1669 (2003).
- [8] Hu, Y., Jang, I., and Sinnott, S. B., Molecular Dynamics Simulations of Polyatomic-Ion Beam Deposition Induced Chemical Modification of Carbon Nanotube/Polymer Composites, *Journal of Materials Chemistry*, **14**, 719-729 (2004).
- [9] Valavala, P. K., and Odegard, G. M., Modeling Techniques for Determination of Mechanical Properties of Polymer Nanocomposites, *Rev. Adv. Mater. Sci.*, **9**, 34-44 (2005).

CHAPTER 2

LITERATURE REVIEW

2.1. Fiber Reinforced Polymeric Materials (FRPMs)

Even though fiber reinforced materials were used in history before (such as straw reinforced bricks), fiber reinforced polymeric materials history starts with the Second World War. The purpose of trying to produce stronger materials for the military/ aerospace market is the initiator of fiber reinforced polymeric materials production. Fiber reinforced polymeric materials are widely used in several sectors such as communication satellites, aircrafts, sporting goods, transportation, energy sector, wind turbines, automotive and sporting goods. Fiber reinforced composites have two components: reinforcing fibers and matrix. Fibers are providing high strength and modulus to the structure and are embedded in the matrix; and matrix protects fibers [1]. FRPMs can be in laminate form, or they may be extruded or injection molded.

Widely used, cheap polymers such as polypropylene, polyethylene, polystyrene and PVC as well as engineering thermoplastics such as PMMA, polycarbonate, polysulfone may be used as matrices [2]. When processing polymers, if the neat polymer does not provide the desired final product properties, reinforcers (fibers, fillers or additives) may be embedded in the polymer. Fibers may be natural (which degrade) or man-made according to end use aims.

Fillers may be silica products (quartz, silica), silicates (mica, talc, Wollastonite, calcium silicate, aluminum silicate), glass (glass flakes, hollow glass spheres, cellular glass nodules),

calcium carbonate (chalk, limestone), metallic oxides (zinc oxide, alumina, magnesia, titania), other inorganic components (barium sulfate, silicon carbide, molybdenum disulfide, barium ferrite), metal powders (aluminum, bronze, lead, stainless steel, zinc), carbon (carbon black, ground petroleum coke, intercalated graphite, exfoliated graphite), and cellulosic fillers (wood flour, shell flour). Additives may be antioxidants, antistatic agents, colorants and pigments, coupling agents, compatibilizers, flame retardants, fillers, foaming agents, heat stabilizers, mold release agents, odor suppressors, plasticizers, processing aids (emulsifiers, lubricants), ultraviolet stabilizers or viscosity depressants [3].

When metallic materials and FRPMs are compared, FRPMs have higher strength advantage and lower weight advantage. FRPMs have lower specific gravities, higher strength/weight ratios, higher modulus/weight ratios compared to traditional metallic materials. The possibility of improving properties of FRPMs in the desired direction is another advantage. Metallic materials are isotropic and they exhibit similar properties in all directions [1].

Fu and Lauke, (1996) developed an analytical model considering the effects of fiber length and fiber orientation distributions on the tensile strength of short fiber reinforced composites. They studied the effects of mean fiber length, critical fiber length, and fiber orientation coefficient. They concluded that the strength of composites increases with an increase of mean fiber length, and a decrease of critical fiber length. They showed that the tensile strength of composites increases with an increase of fiber orientation coefficient [4].

Thomason et al., (1996) studied the effect of fiber length (0.1-50 mm) and concentration (3-60 wt %) on tensile and flexural strengths of polypropylene laminates. They concluded that laminate tensile strength increased linearly with fiber concentration and fiber length. Sizing the glass fibers increased the tensile strength. The fiber orientation of the samples was found to be

close to parallel with the loading direction. They compared experimental data with a modified version of the Kelly-Tyson model and found a strong correlation between them [5].

Cauvin et al. (2010) studied the tensile behavior of injection molded polypropylene reinforced with montmorillonite clay platelets. They concluded that Young's modulus and yield stress increased with nanoclay reinforcement even at low volume fractions. They modeled the elastic region of the tensile behavior with the Ponte Castaneda and Willis lower bound method and found a good correlation between the predicted and calculated results [6].

Kalaitzidou et al., (2007) produced injection molded polypropylene parts reinforced with exfoliated graphite nanoplatelets, carbon fibers, nanosize carbon black, and montmorillonite clay. They compared the experimental results with the Halpin-Tsai and Tandon-Weng models and concluded that for low reinforcements there is a good relation between experimental and calculated results. As nanoclay platelets were forming large aggregates, the models overestimated the modulus of nanoclay reinforced composites. Even for low contents, the nanoclay reinforced composites experimental results were far under the predicted results. For all samples, the predicted results differed from the measured results; this difference was concluded to be caused by the large interface between reinforcement and matrix at high reinforcement levels [7].

Fu et al. (2001) investigated the tensile properties of injection molded polypropylene (PP) composites reinforced with short glass fibers and short carbon fibers. They used the fiber reinforcements at 8 vol %, 16 vol %, and 25 vol %. They studied the influence of mean fiber length (fiber aspect ratio) and fiber volume fraction on tensile properties. They observed that an increase in fiber volume fraction results in a decrease in mean fiber length. They described the relationship between mean fiber length and fiber volume fraction as [8]:

$$l_m = -0.000234 \times e^{(20.482 \times v_f)} + 0.2882 \dots\dots\dots (2.1)$$

where: l_m : Mean fiber length (mm)

v_f : Fiber volume fraction

The SEM micrographs of the fracture surfaces show the brittle nature of their tensile failure. Their study shows that the composite strength depends on mean fiber length more than fiber volume fraction, and the composite modulus is more dependent on fiber volume fraction [8].

De Morais, (2006) improved his own analytical model to predict the longitudinal tensile strength of carbon fiber reinforced polymeric composites in laminate form (Equation 2.2). He defined fiber strength by Weibull distribution and his model predictions showed a good correlation with the experimental results [9].

$$\sigma_{utl} = V_f \left[\frac{16 \times \tau_{pm}^2 \times L_o \times \sigma_{f0}^\rho}{(\rho + 2) \times d_f^2} \right] \times e^{-\frac{1}{\rho+2}} \dots\dots\dots (2.2)$$

where: σ_{utl} : Ultimate tensile strength

τ_{pm} : Shear stress in the matrix yielding zone

L_o : Gauge length

σ_{f0} : Characteristic strength of fiber

ρ : Weibull modulus

d_f : Fiber diameter

V_f : Fiber volume fraction

Mohsen et al., (2008) reinforced polyamide 66 with CaCO_3 both at micron and nano size, and investigated its tensile properties. They compared their experimental results with the Guth, Nicolais-Nargis, Rule of Mixtures, Hashin-Shtrikman, and Halpin-Tsai equations. The microcomposites and nanocomposites had higher modulus and lower tensile strength than neat polyamide samples. When nanocomposites and microcomposites are compared, nanocomposites had higher modulus and strength values. They found out that none of those equations could predict the tensile properties of their samples. As the experimental results showed higher values than the predicted values, those models could be used to predict the elastic modulus [10].

Lee and Jang (1998), investigated the tensile, flexural, and impact properties of glass fiber mat reinforced polypropylene at various glass fiber contents between 10-30 vol %. The tensile and flexural modulus increased with an increase in glass fiber content until maximum glass fiber content, which is between 15-20 vol %. The impact absorption energy also showed an increase until 20 vol %, and then decreased. They observed that the void content was increasing as glass fiber content increased. They concluded that polypropylene was not able to wet the glass fibers [11].

Hagstrand et al., (2005) evaluated the effect of void content on the mechanical properties of glass fiber reinforced polypropylene composites. By changing the molding pressure application time, they produced different samples having 1 to 14% void contents. They concluded that voids had a negative effect on the flexural modulus and strength. On the other hand, void content had a positive effect on stiffness; an increase of 1% void volume was causing a 2% increase in stiffness. The flexural failure load did not show a significant increase with increasing void content [12].

As fiber reinforced polymer composite production increased, the need to identify the micromechanical properties that control the structure-property relations aroused. The properties of composites result from a combined effect of fiber and matrix properties and the stress transfer ability in the fiber-matrix interface [13].

As mentioned in Chapter 1, in 1987, Fukushima and Inagaki investigated the effects of nanoclay on timer belts and observed an increase in strength. The nanocomposite history starts with this research conducted in Toyota. The discovery of carbon nanotubes in 1991 accelerated the studies on nanocomposites. Nanocomposites have much higher mechanical properties than conventional composites [14]. However, the mechanical properties of nano particle reinforced composites may be increased only in the presence of a good load transfer between matrix and reinforcement [15, 16, 17]. The increase of elastic modulus obtained with 1 wt% carbon nanotube is nearly equal to the increase caused with a 10 wt% reinforcement of carbon fibers [18].

Boutaleb et al., (2009) proposed a micromechanical model for the yield stress and modulus of nanoparticle reinforced polymers [19]. The Young modulus at any layer is defined as:

$$(E_l)_i = \frac{r_\Sigma}{r_i} \times E_M + \left(\frac{r_\Sigma - r_i}{e}\right)^\beta \times \left(E_P - \frac{r_\Sigma}{r_P} \times E_M\right) \dots\dots\dots (2.3)$$

where: r_p : The particle radius

r_Σ : The entire inclusion radius

r_i : The interface radius

e : The distance to particle center

E_p : Elastic modulus of the particle

E_M : Elastic modulus of the matrix

β : Exponent that introduces the interfacial characteristics

2.2. Reinforcers

2.2.1. Fiber reinforcers

Fibers are load carrying members of the composite which may be either in continuous or discontinuous lengths; they give reinforcement to the matrix [1].

Fibers used for reinforcing thermoplastics are cellulose fibers (α -cellulose, pulp preforms, cotton flock, jute, sisal, rayon), synthetic organic fibers (polyamides, polyester (PET), polyacrylonitrile (PAN), polyvinyl alcohol (PVOH)), carbon fibers, asbestos fibers, fibrous glass (filaments, chopped strand, reinforcing mat, glass yarn, glass ribbon), whiskers (aluminum oxide, titanium dioxide, boron, boron nitride, boron carbide), and metallic fibers (aluminum, stainless steel, copper, tungsten) [3].

2.2.2. Nanoparticle reinforcers

Nanoclays are composed of organic modified laminar silicate structures, and they have a hybrid organic-inorganic structure. Montmorillonite (MMT) is a nanoclay that is composed of aluminum replacing different amounts of silicate and cations as shown in Figure 2.1.

MMT has weak bonding between the cations, water molecules and silicate layers; also MMT has a relatively open structure that is called 'smectite structure' [20].

Nanoclays can swell and shrink depending on the amount of water. The spacing between layers can vary between 1.0 nm- 2.1 nm. Since MMT may be swelled by organic molecules, it is

suitable to produce nanocomposites having polymers and nanoclay. Small amounts of MMT based nanoclays improve the overall properties of polymer matrix [21].

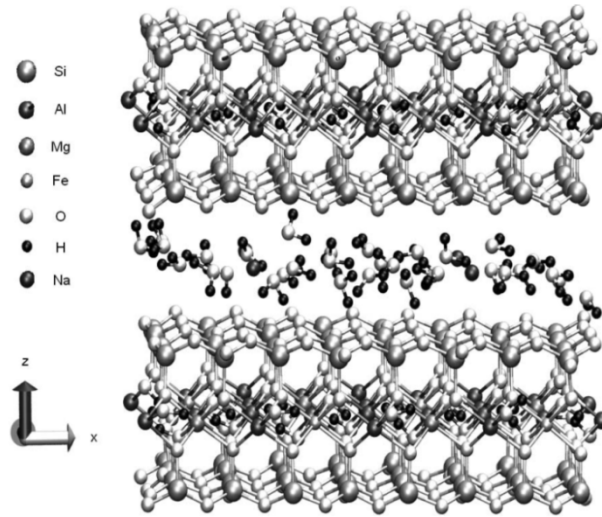


Figure 2.1. Structure of MMT [20].

Polymer-clay nanocomposites are classified into three groups according to their dispersion: intercalated, delaminated (exfoliated) and conventionally mixed nanocomposites. Intercalated and delaminated dispersions are shown in Figure 2.2.

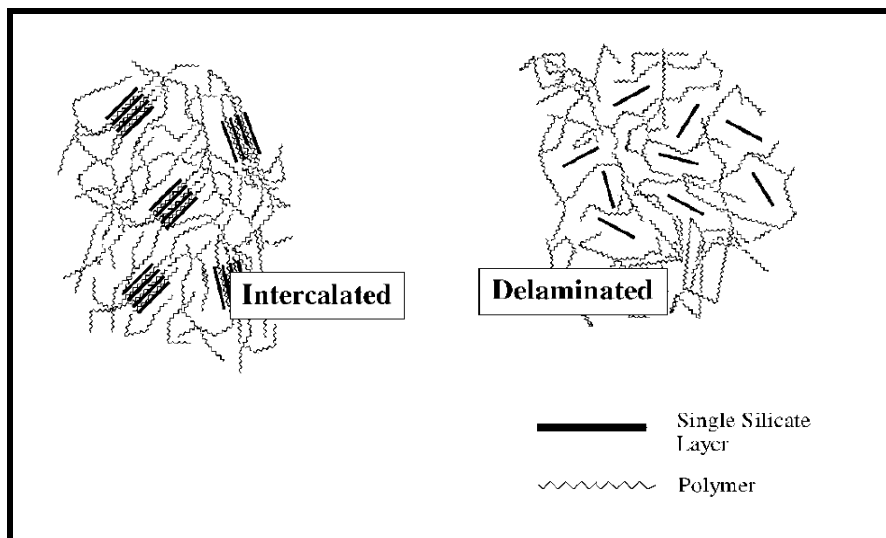


Figure 2.2. Intercalated and delaminated structures of polymer-nanoclay nanocomposites [21].

In intercalated nanocomposites a small amount of polymer moves into the spacing between clay platelets; in delaminated (exfoliated) nanocomposites clay platelets are fully dispersed in polymer matrix; and in conventionally mixed nanocomposites the nanoclay acts as filler [22]. The dispersion mechanism of nanoclays during mixing is illustrated in Figure 2.3.

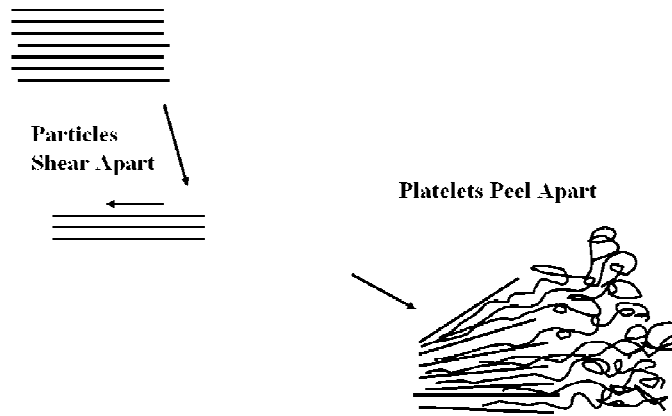


Figure 2.3. Dispersion mechanism of nanoclays during mixing [23].

2.2.3. Rubber reinforcers

Blending polymers with rubbers is a method for toughening. In the last several decades, many studies were conducted to increase toughness of materials by increasing their impact strength [24].

Materials may have two different failure types: brittle (weak) fracture and ductile (tough) fracture. In brittle fracture, the load/deflection curve has a linear characteristic. Materials showing brittle fracture usually have small volumes of crazes in their structure. The breakage of glass is a typical 'brittle fracture'. In ductile fracture, the load/deflection curve has an incline in the plastic region. [25].

In the failure of a material there are two steps. The first step is called 'crack initiation'. In crack initiation microcracks form which are very small cracks invisible to the human eye. When

a material is subjected to a stress, molecular bonds of the material's molecules are affected by the stress applied. Molecular bonds break as stress increases. The second step is 'crack propagation' in which cracks develop and cause failure of the material. Due to broken molecular bonds, microcracks increase in the material's structure. [25].

There are several theories explaining toughening mechanism of plastics with rubbers such as: the multiple crazing theory, the cavitation theory and the critical matrix ligament thickness theory.

According to the multiple crazing theory, the stretched rubber molecules during fracture absorb most of the energy released [25].

According to the cavitation theory, a big fracture energy is released due to dispersed rubber particles. Due to cavitation, the surface area of the blend increases. When compared to pure polymer, the plastic deformation increases and fracture energy increases [26].

The critical matrix ligament thickness theory explains the impact toughness with the 'ligament thickness' which is the distance between dispersed particles. When the ligament thickness is smaller than the critical thickness, ductile transition occurs [27]

In immiscible blends of polymers and rubbers, while an increase in impact strength is observed, elastic modulus and yield stress are decreased. To obtain balanced properties, uniform elastomer distribution in the end-product, and some degree of interfacial adhesion between matrix and elastomer are essential. For toughening and therefore for improving impact strength, elastomer modulus has to be smaller than the modulus of PP and the elastomer must have low crystallinity. The impact strength of a polymer is the result of all contributing processes to dissipate the energy of the impact blow. Impact strength is the most important property of plastics as it is related to the service life of the material and its safety [28].

It is important to know the failure mode of a material according to its end use aim. Impact testing is a method to determine the failure mode. Testing speed and environmental temperature may change the mode of failure. The glass transition temperature of a material and if it is higher or lower than the environment temperature during test changes the failure mode of the material. When disk samples are impact tested, glassy polymers exhibit a cracking behavior and they break into pieces; while more crystalline polymer samples are less damaged [29].

2.3. Importance of predicting mechanical properties of IMPM

Predicting the properties of reinforced polymeric materials is important as they have important applications especially in automotive and aerospace sectors.

Valavala and Odegard (2005), reviewed various modeling techniques for nanocomposites. Figure 2.4 shows the diagram of modeling techniques for nanocomposites. Computational chemistry methods which deal with bonds in the molecular or atomic level are based on the assumption of a unique molecular structure of the material, while computational mechanics methods assume there is a continuous structure in the material and they neglect the chemical bonds between phases. Computational mechanics methods do not include the chemical interactions between the matrix and reinforcement phases in the composite assuming perfect bonding between the two phases. Eshelby, Mori Tanaka, Halpin-Tsai, Rule of Mixtures, finite element method and boundary element method are among the computational mechanics methods [30].

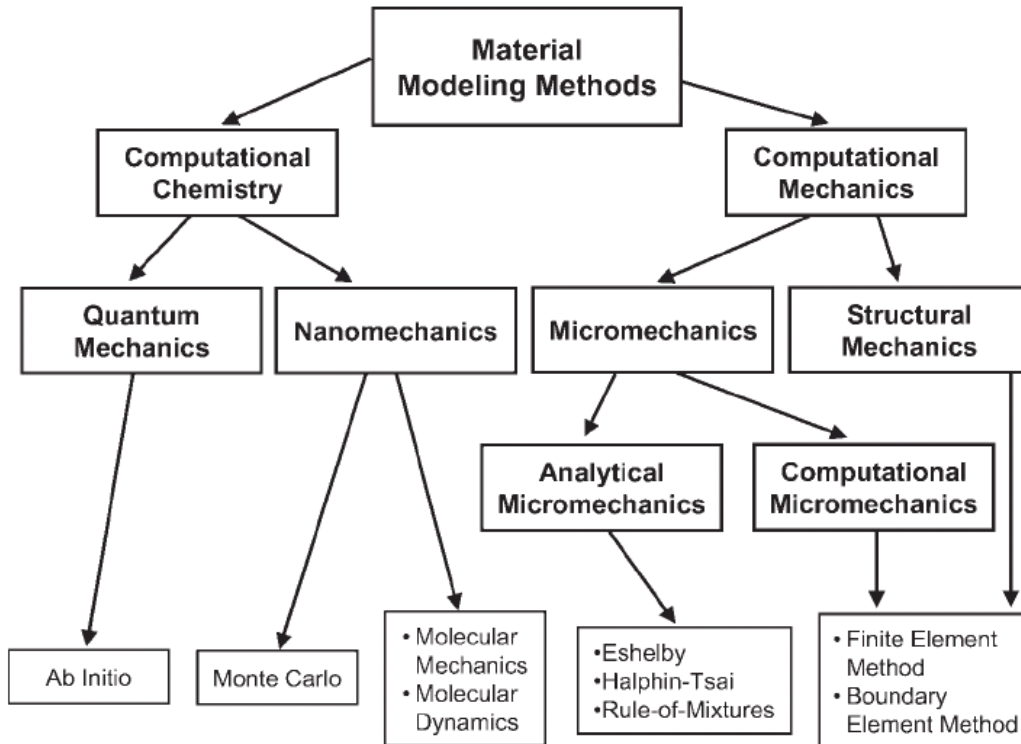


Figure 2.4. Classification of modeling techniques for materials [30].

As predicting the overall properties of composites is very essential, models predicting final properties of composites are being developed. Knowledge of the final mechanical properties of fiber reinforced polymeric materials (FRPMs) matrices is useful to prevent performance loss, failure and extra production costs.

Composite material modeling can be studied in two main methods: macromechanics and micromechanics.

2.3.1. Macromechanics approach

In macromechanics studies, it is assumed that the composite material is homogeneous and the effects of the constituent materials are detected only as averaged properties of the composite [31].

2.3.2. Micromechanics approach

In micromechanics approach, composite behavior is studied by the interaction between phases in the material. The interaction between phases is based on a microscopic scale. The aim of micromechanics methods is to predict the composite material overall properties using the elastic properties such as strain of the constituent materials [1]. The mechanics of the materials approach models assume that there is perfect adhesion between the phases, the particles are spherical and evenly dispersed, and that the properties of composite materials are independent of the size of particles. Even though this may be correct for systems with micron sized reinforcements, it may not be correct for nanocomposite systems. In mechanics of materials approach, some simplifying assumptions are made. The most important assumption is that the strain in the matrix is equal to the strain in the reinforcer [31]. There are two main methods for modeling of composites: mechanics of materials approach and elasticity approach [32].

2.3.2.1. Rule of Mixtures (ROM)

‘The Rule of Mixtures’ is one of the most widely used methods of predicting the modulus of a composite. The Rule of Mixtures can be obtained using the assumption of equal strain in the fiber and matrix. In the Rule of mixtures, the failure of the composite is explained by broken fibers . In ductile fiber reinforced brittle matrix composites, matrix fracture is observed since the maximum fiber strain is higher than the maximum matrix strain. In the elasticity approach, there are subclasses such as self-consistent models, various techniques that use energy bounding principles, exact solutions, statistical approaches, finite element methods, semi empirical approaches and microstructure theories [33].

For homogeneous materials, properties do not change with direction; for fiber reinforced materials location and orientation changes the properties of the material [1]. Fibers have high modulus along their axis and a lower modulus perpendicular to their axis. Fiber reinforced materials' modulus is affected by the fiber orientation and the direction of applied force to the material [34]. When calculating modulus of fiber reinforced composites in the longitudinal direction, in which force is applied along the fiber, “the rule of mixtures” assumes perfect bonding between matrix and fibers [1]. Figure 2.5 gives a representative illustration for the longitudinal loading condition.

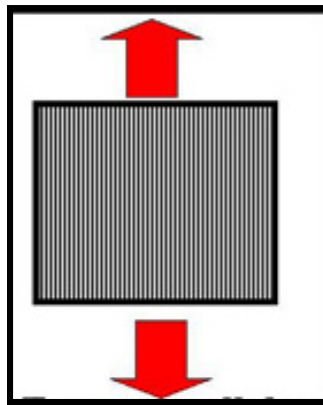


Figure 2.5. Force and fiber alignment in the longitudinal loading condition [34].

It is assumed that ‘ ϵ_m ’ deformation (strain) of matrix and ‘ ϵ_f ’ deformation of fibers are the same for the longitudinal loading condition ($\epsilon_m = \epsilon_f$) which is the “isostrain condition”. Isostrain condition means that deformation of matrix and deformation of fibers are the same [34]. Equation 2.4 and Equation 2.5 give the formulas for composite strength and modulus, respectively.

$$\sigma_c = \sigma_m \times v_m + \sigma_f \times v_f \dots\dots\dots (2.4)$$

$$E_c = E_m \times v_m + E_f \times v_f \dots\dots\dots (2.5)$$

Volume and volume fraction equations are as follows:

$$v_m = \frac{V_m}{V_c} \dots\dots\dots (2.6)$$

$$v_f = \frac{V_f}{V_c} \dots\dots\dots (2.7)$$

$$V_c = V_m + V_f \dots\dots\dots (2.8)$$

$$v_c = v_m + v_f = 1 \dots\dots\dots (2.9)$$

where: σ_m : Tensile strength of matrix

σ_f : Tensile strength of fiber

σ_c : Tensile strength of composite

V_m : Volume of matrix (mm³)

V_f : Volume of fiber (mm³)

V_c : Volume of composite (mm³)

v_m : Volume fraction of matrix

v_f : Volume fraction of fiber

v_c : Volume fraction of composite

E_m : Elasticity modulus of matrix

E_f : Elasticity modulus of fiber

E_c : Elasticity modulus of composite

In transverse loading, fibers are vertical to the force direction. Using Rule of Mixtures, modulus of fiber reinforced composites in the transverse loading condition is determined by Equation 2.10, assuming “isostress condition”, which means that matrix and fibers are under the same stress and acting as a series of springs. Figure 2.6 gives a representative illustration for the perpendicular loading condition [34].

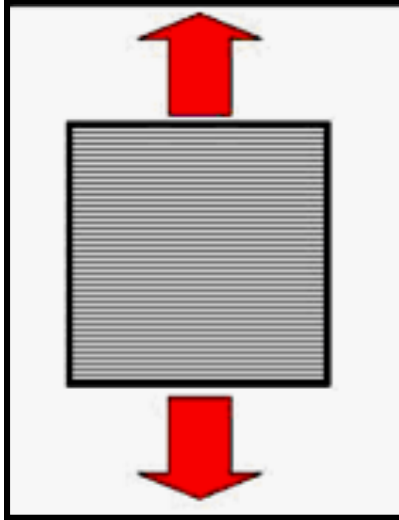


Figure 2.6. Force and fiber alignment in perpendicular loading condition [34].

The elastic modulus of the composite is given by:

$$E_C = \frac{1}{\left(\frac{v_m}{E_m}\right) + \left(\frac{v_f}{E_f}\right)} \dots\dots\dots (2.10)$$

2.3.2.2. Halpin-Tsai Equation

Halpin-Tsai equation is one of the most widely used elasticity approach equations, which is given in Equation 2.11. It is a modification of the Rule of Mixtures by using ‘ξ’ fiber reinforcement measure and ‘η’ correction factor for the reinforcer (Equation 2.12).

‘ξ’ is a measure of fiber reinforcement of the composite material and is dependent on fiber geometry, packing geometry, and loading conditions. One of the most important issues in Halpin-Tsai equation is the determination of ξ [35].

$$\frac{E_c}{E_m} = \frac{1 + \xi \eta v_f}{1 - \eta v_f} \dots\dots\dots (2.11)$$

where:

$$\eta = \frac{(E_f/E_m)^{-1}}{(E_f/E_m)^{+\xi}} \dots\dots\dots (2.12)$$

The lower and upper limits for Halpin-Tsai equation are given in Equation 2.13 and Equation 2.14, respectively.

For the lower limiting cases of Halpin-Tsai equation, Equation 2.13 is obtained by assuming that $\xi = 0$. Equation 2.13 represents the transverse loading of reinforcers perpendicular to the flow direction in the composite [35].

$$E_c = \frac{1}{v_m/E_m + v_f/E_f} \dots\dots\dots (2.13)$$

For the upper limiting cases, Equation 2.14 is obtained by assuming that $\xi = \infty$.

$$E_c = E_m \times v_m + E_f \times v_f \dots\dots\dots (2.14)$$

The upper limiting condition represents the longitudinal loading condition of the Rule of Mixtures (ROM). In this condition, the maximum reinforcement is achieved as the fibers are loaded parallel to the flow direction in the composite.

2.4. References

[1] Mallick, P. K., “Fiber Reinforced Composites Materials, Manufacturing and Design”, CRC Press, 119-128, 240-361,587-588 (1993).

[2] McCrum, N. G. , Buckley, C. P., and Bucknall, C. B., “Principles of Polymer Engineering”, Oxford Science Publications, second edition (1997).

[3] Peters, S. T., “Handbook of Composites”, Chapman &Hall, 131-155 (1998).

- [4] Fu, S. Y., and Lauke, B., Effects of Fiber Length and Fiber Orientation Distributions on the Tensile Strength of Short-Fiber-Reinforced Polymers, *Composites Science and Technology*, **56**, 1179-1190 (1996).
- [5] Thomason, J. L., Vlug, M. A., Schipper, G., and Krikort, H. G. L. T., Influence of Fiber Length and Concentration on the Properties of Glass Fiber-Reinforced Polypropylene: Part 3. Strength and Strain at Failure, *Composites Part A*, **27A**, 1075-1084 (1996).
- [6] Cauvin, L., Kondo, D., Brieu, M., and Bhatnagar, N., Mechanical Behavior of a PP Platelet-Reinforced Nanocomposite: Experimental Characterization and Two Scale Modeling of Linear and Non-Linear Response, *Materials Science and Engineering A*, 527(4-5), 1102-1108 (2010).
- [7] Kalaitzidou, K., Fukushima, H., Miyagawa, H., and Drzal, L. T., Flexural and Tensile Moduli of Polypropylene Nanocomposites and Comparison of Experimental Data to Halpin-Tsai and Tandon-Wang Models, *Polymer Engineering and Science*, **47**(11), 1796-1803 (2007).
- [8] Fu, S. Y., Lauke, B., Mader, E., Yue, C. Y., Hu, X., and Mai, Y. W., Hybrid Effects on Tensile Properties of Hybrid Short-Glass-Fiber- and Short-Carbon-Fiber-Reinforced Polypropylene Composites, *Journal of Materials Science*, **36**(5), 1243-1251 (2001).
- [9] De Morais, A. B., Prediction of the Longitudinal Tensile Strength of Polymer Matrix Composites, *Composites Science and Technology*, **66**, 2990-2996 (2006).
- [10] Mohsen, R. S., Saied, N. K., Ali Z., Hosein E. M., and Hasan P., Theoretical and Experimental Determination of Tensile Properties of Nanosized and Micron-Sized CaCO₃/PA66 Composites, *Polymer Composites*, **30**(3), 274-280 (2008).

- [11] Lee, N. J., Jang, J., The Use of Mixed Coupling Agents to Improve the Performance of Polypropylene Based Composites Reinforced with Short Glass Fiber, *Composites Science and Technology*, **57**(12), 1559-1569 (1998).
- [12] Hagstrand, P. O., Bonjour, F., and Manson, J. A. E., The Influence of Void Content on the Structural Flexural Performance of Unidirectional Glass Fiber Reinforced Polypropylene Composites, *Composites Part A: Applied Science and Manufacturing*, **36**, 705-714 (2005).
- [13] Thomason, J. L., Micromechanical Parameters From Macromechanical Measurements on Glass Reinforced Polyamide 66, *Composites Science and Technology*, **61**, 2007-2016 (2001).
- [14] Xiao, Y., Zhang, X. Q., Cao, W., Wang, K., Tan, H., Zhang, Q., Du, R. N., and Fu, Q., Dispersion and Mechanical Properties of Polypropylene/Multiwall Carbon Nanotubes Composites Obtained via Dynamic Packing Injection Molding, *Journal of Applied Polymer Science*, **104**(3), 1880-1886 (2007).
- [15] Frankland, S. J. V., Caglar, A., Brenner, D. W., and Greibel, M., Molecular Simulation of the Influence of Chemical Cross-Links on the Shear Strength of Carbon Nanotube-Polymer Interfaces, *J. Phys. Chem.*, B106, 3046-3050 (2002).
- [16] Hu, Y., and Sinnott, S. B., Modification of Carbon Nanotube Polymer-Matrix Composites through Polyatomic-Ion Beam Deposition: Predictions from Molecular Dynamics Simulations, *Composite Science and Technology*, **63**, 1663-1669 (2003).
- [17] Hu, Y., Jang, I., and Sinnott, S. B., Molecular Dynamics Simulations of Polyatomic-Ion Beam Deposition Induced Chemical Modification of Carbon Nanotube/Polymer Composites, *Journal of Materials Chemistry*, **14**, 719-729 (2004).

- [18] Qian, D., Dickey, E. C., Andrews, R., and Rantell, T., Load transfer and Deformation Mechanisms in Carbon Nanotube–Polystyrene Composites , *Applied Physics Letters*, **76**, 2868-2870 (2000).
- [19] Boutaleb, S., Zairi, F., Mesbah, A., Nait-Abdelaziz, M., Gloaguen, J. M., Boukharouba, T., and Lefebvre, J. M., Micromechanical Modelling of the Yield of Polymer-Particulate Nanocomposites with an Inhomogeneous Interphase, *Procedia Engineering*, **1**, 217-220 (2009).
- [20] Katti, D. R., Schmitdt, S. R., Ghosh, P., and Katti, K. S., Molecular Modeling of the Mechanical Behavior and Interactions in Dry and Slightly Hydrated Sodium Montmorillonite Interlayer, *Ca. Geotech. J.*, **44**, 425-435 (2007).
- [21] Porter, D., Metcalfe, E., and Thomas, M. J. K., Nanocomposite Fire Retardants-A Review, *Fire and Materials*, **24**, 45-52 (2000).
- [22] Lopez-Quintanilla, M. L., Sanchez-Valdes, S., Ramos de Valle, L. F., and Medellin-Rodriguez, F. J., Effect of Some Compatibilizing Agents on Clay Dispersion of Polypropylene-Clay Nanocomposites, *Journal of Applied Polymer Science*, **100**, 4748-4756 (2006).
- [23]<http://www.nanoclay.com/pdfs/ANTEC%20Presentation%20wNotes%20052200.ppt#295,19>, Dispersion Mechanism, access date 05.23.2009.
- [24] Karger-Kocsis, J., “*Structure and Morphology, Polypropylene Structure, Blends and Composites*”, 50-51, Chapman & Hall, Cambridge (1995).
- [25] Zabaleta, A., Gonzalez, L., Eguiazabal, J. I., and Nazabal, J., Rubber Toughening of Poly(ether imide) by Modification with Poly(butylenes terephthalate), *European Pol. Journal*, **45**(2), 466-473 (2009).

- [26] Tortorella, N., and Beatty, C. L., Morphology and Mechanical Properties of Impact Modified Polypropylene Blends, *Polymer Engineering and Science*, **48**(11), 2098-2110 (2008).
- [27] Perkins, W. G., Polymer Toughness and Impact Resistance, *Polymer Engineering and Science*, **39**(12), 2445-2460 (1999).
- [28] Fu, Q., Wang, Y., Li, Q., and Zhang, G., Adding EPDM Rubber Makes Poly(propylene) Brittle, *Macromol. Mater. Eng.*, **287**(6), 391-394 (2002).
- [29] Duan Y., Saigal A., Greif R., and Zimmerman M. A., Impact Behavior and Modeling of Engineering Polymers, *Polymer Engineering and Science*, 43(1), 112-124 (2003).
- [30] Valavala, P. K., and Odegard, G. M., Modeling Techniques for Determination of Mechanical Properties of Polymer Nanocomposites, *Rev. Adv. Mater. Sci.*, **9**, 34-44 (2005).
- [31] Haghghat, M., Zadhoush, A., and Horasani, S. N., Physicomechanical Properties of α -cellulose Filled Styrene-Butadiene Rubber Composites, *Journal of Applied Polymer Science*, **96**, 2203-2211 (2005).
- [32] Jones, R. M., "Mechanics of Composite Materials", Taylor & Francis, 137-143 (1999).
- [33] Chou, T. W., "Microstructural Design of Fiber Composites", Cambridge University Press, 81-87 (1992).
- [34] <http://info.lu.farmingdale.edu/depts/met/met205/composites.html>, access date 04.10.2009.
- [35] Halpin J. C., The Halpin-Tsai Equations: A Review, *Polymer and Engineering Science*, 16(5), 344-352 (1976).

CHAPTER 3

IMPROVING TOUGHNESS OF POLYPROPYLENE (PP) WITH THERMOPLASTIC ELASTOMERS IN INJECTION MOLDING

ABSTRACT: Polypropylene (PP) is one of the most widely used polymers commercially; however it exhibits brittle fracture. To improve the toughness of PP, two thermoplastic elastomers were added separately. Tensile tests were conducted according to the ASTM D638-3 standard test method on Instron universal testing machine. Rubber particle distributions were observed on SEM. Tensile test results show an increase in energy at break which is the toughness of the material. Increase in toughness proves that adding thermoplastic elastomers toughens the PP.

KEYWORDS: toughness, properties, processing, testing, measurement

3.1. Introduction

Polypropylene (PP) was invented in the 1950s and became one of the most widely used polymers among thermoplastics due to its availability and low cost. PP has many industrial applications including interior and exterior automobile parts such as injection molded bumpers and dashboards for cars [1]. PP is a low cost, multi-functional thermoplastic; however, it shows brittle failure under certain loading conditions at or below room temperature or in notched state. Brittle failure can be prevented by adding energy-absorption mechanisms [2]. Mixing brittle thermoplastic matrices such as PP, PE as well as polyamides, polycarbonate and poly(ethylene

terephthalate) (PET) with rubber makes them tougher [3]. Rubber toughening should result in greater ductility, greater crack resistance and higher impact strength of the material [4].

Studies on toughening of PP with several rubbers such as octene ethylene copolymer (EOC) [5-7], styrene butadiene rubber (SBR) [8-10], ethylene propylene rubber (EPR) [11-13], styrene ethylene butadiene styrene rubber (SEBS) [14-16] and ethylene propylene diene monomer (EPDM) [17-21] have been conducted. Ternary blends of PP/polyethylene/EPDM are also studied for toughening of polypropylene [22, 23]. Oksuz and Eroglu [19] studied the effect of elastomer type and elastomer content on the mechanical properties of polypropylene. They used three types of elastomers EPDM, SBSR and ethylene vinyl acetate (EVA). EVA had three vinyl acetate concentrations named EVA 9, EVA 18 and EVA 28. All blends were produced at five different elastomer contents (3, 6, 9, 12, and 15 wt %). As a result, they found out that EPDM at 15 wt % and EVA 28 at 15 wt % are the most effective blends in impact strength.

Mighri et al., [12] observed that the addition of ethylene based elastomers to polypropylene increases the ductility and impact resistance. Wang et al., [24] investigated the toughness of blended Nylon 1212 and EPDM-graft-maleated acid (MA). Due to the reaction between the anhydride of EPDM-graft-MA and the amine of Nylon 1212, Nylon 1212/EPDM-graft-MA copolymer forms and the copolymer reduces the tension between Nylon 1212 and EPDM-graft-MA, resulting in a tougher Nylon 1212.

Polypropylene blends with polyethylene (PE), ethylene-propylene copolymer (EPR), ethylene propylene diene monomer (EPDM) and polyamides (PA) are produced in big quantities and therefore those blends are very important commercially. EPR and EPDM elastomers are the largest portion among the blends of PP [1]. PP toughened with styrene-ethylene-butadiene-

styrene (SEBS) is being used in automotive parts due to its higher impact strength properties [14].

Mechanical properties of polymer-rubber blends are mainly controlled by their morphology. For rubber toughened polymers the shape, content, size, and size distribution of the dispersed phase particles have major effects on mechanical properties of polymer elastomer blends [14]. Multiple crazing, damage competition, shear yielding, microvoids and cavitation theories are major theories on toughening mechanisms of blends but those mechanisms cannot yet completely explain toughening of polymers. To get better toughening, it is essential to have uniform size and distribution of toughening material in the matrix [25].

In rubber toughened thermoplastic blends, the dispersed rubber particles in the thermoplastic matrix cause a large increase in the new surface area, and as a result, they increase the fracture energy of the blend [14]. Fu et al., [17] conducted tensile strength and impact strength tests as well as SEM and finite element method (FEM) analysis on polypropylene/EPDM blends. According to the FEM analysis, they concluded that during impact fracture, dispersed particles act as stress concentrators.

A traditional approach for toughening PP is blending PP with rubber particles. In rubber blended PP, the toughness increases, but elastic modulus of PP decreases [26].

Impact behavior can be improved by decreasing crystalline morphology of semicrystalline polymers with controlled heating, by blending a rubbery phase, or by adding reinforcers such as fibers or fillers to the matrix [4]. The properties of a polymer are determined by the crystallization and its structure. As a result, crystallization of PP and its blends is essential in both polymer science and engineering [27].

George et al., [28] studied the crystallinity of PP/nitrile rubber (NBR) blends at increasing NBR content. They observed that the crystallinity of the blends decreased with the increase of NBR content.

The effect of crystallization of isotactic PP on stress-strain behavior was investigated by Barish [29] who observed that completely crystalline films of isotactic poly(propylene) were cracking during elongational force application.

Da Costa et al., [18] conducted research on the impact strength of polypropylene/scrap rubber tires (PP/SRT) and polypropylene/ethylene-propylene-diene/scrap rubber tires (PP/EPDM/SRT) extruded blends and observed no change in the impact of PP/SRT blends and an increase in the impact strength of PP/EPDM/SRT blends compared to PP. The degree of crystallinity decreased with the increase of EPDM loading into PP matrix.

The toughening of isotactic polypropylene (iPP) with ethylene-co-propylene (EPR) having 80/20 weight ratio was investigated in several studies [30-33].

D’Orazio et al., [34] studied 60/40 weight ratio blends of iPP with two different EPR copolymer synthesized with different catalysts. The EPR_{Ti} is synthesized with a Titanium based catalyst and EPR_{Va} is synthesized with a Vanadium based catalyst. At low temperatures, impact strength of EPR_{Ti} showed better properties. DSC results showed that EPR_{Ti} has lower crystallinity rate than EPR_{Va} . Better impact strength of EPR_{Ti} is related to its lower crystallinity.

In the present study, PP blends with two different thermoplastic elastomers at 50/50 weight ratio are evaluated for mechanical, morphological and thermal properties. Mechanical properties are investigated by conducting impact, tensile, and 3-point bending tests; morphology is investigated by scanning electron microscopy (SEM) analysis; and thermal properties are

investigated by differential scanning calorimetry (DSC) analysis. The results of this research would be useful to produce tougher PP fibers using the extrusion process.

3.2. Experimental

3.2.1. Materials

Polypropylene copolymer (PP) from Premier Plastic Resins (30 Melt Copolymer Natural Polypropylene) having a melt flow rate (MFR) of 34g/10 min at 230°C and a density of 0.910 g/cm³ was used in this study. Two different thermoplastic elastomers used with the codes of F1 and F2 are Versaflex®OM 3060-1 and Versaflex®OM 9-802 CL from GLS Corporation, respectively. F1, which is a poly(ethylene:propylene:diene) copolymer, has an apparent viscosity of 15.0 Pa·s at 200°C and a specific gravity of 0.900 g/cm³; F2, which is a styrene butadiene block polymer, has an apparent viscosity of 16.0 Pa·s at 200°C and a specific gravity of 0.930 g/cm³.

3.2.2. Sample Preparation

The pellets used in blends were dried in a vacuum oven at 100°C overnight before using. The blends were prepared by in-situ mixing using an EM 50/300 Battenfeld injection molding machine, with a 180-185-185-180°C temperature profile from nozzle to barrel and at 50°C mold temperature. The pressure values were set to 383 bars for injection pressure, and 364 bar for melt pressure. The nozzle's radius is 13 mm and the screw size is 30 mm. The blends and their compositions are given in Table 3.1.

Table 3.1. Sample codes and blend compositions.

Sample Code	PP (wt %)	F1 (wt %)	F2 (wt %)
PP	100	–	–
F1	–	100	–
F2	–	–	100
PP/F1	50	50	–
PP/F2	50	–	50

The samples were injected into a mold to produce impact (ASTM D3763-06), tensile (ASTM D638-03), and 3-point bending (ASTM D790) testing bars. An average value of at least five measurements was reported. Differential scanning calorimetry (DSC) analysis and scanning electron microscopy (SEM) analysis were done on the samples to investigate the thermal and morphological properties.

3.3. Results and Discussion

3.3.1. Mechanical Properties

3.3.1.1. Impact and Tensile Tests

Polymer toughness is a measure of a material's ability to withstand an applied sudden load without failure. The impact tests were conducted according to the ASTM D3763-06 standard test method using falling weight. Rectangular samples at 12.7 mm x 3.18 mm x 76.2 mm dimensions were tested on Instron Dynatup 8250 universal impact tester; an average of at least five specimens was taken for impact strength results. The impact strength results of the samples are given in Table 3.2.

Table 3.2. Results of tensile and impact tests for PP, F1, F2, PP/F1 and PP/F2 samples (mean \pm standard deviation).

Sample Code	Tensile stress at Maximum Load (MPa)	Tensile strain at Maximum Load (%)	Energy at Maximum Load (J)	Elastic Modulus (MPa)	Impact Strength (J/m)
PP	18.64 \pm 8.79	2.2 \pm 0.45	0.36 \pm 0.06	1226.32 \pm 4.13	49.13 \pm 5.02
F1	5.64 \pm 0.05	634.8 \pm 4.87	50.22 \pm 1.19	2.00 \pm 0.01	5.36 \pm 0.68
F2	5.35 \pm 0.17	1054.5 \pm 9.56	73.23 \pm 4.90	1.54 \pm 0.04	6.74 \pm 0.33
PP/F1	7.30 \pm 0.30	62 \pm 15.85	8.20 \pm 2.18	66.00 \pm 18.04	124.39 \pm 3.37
PP/F2	10.90 \pm 0.62	728 \pm 79.92	141.28 \pm 21.34	122.38 \pm 26.65	105.63 \pm 9.37

All tensile properties were measured with an Instron 5565 universal testing machine. Standard tensile tests were carried out according to the ASTM D 638-03 standard test method on injection-molded dog-bone specimens. The test specimens had 102 mm length, 13 mm width and 3.16 mm thickness. Figure 3.1 shows the dimensions of dogbone-shaped tensile samples in mm.

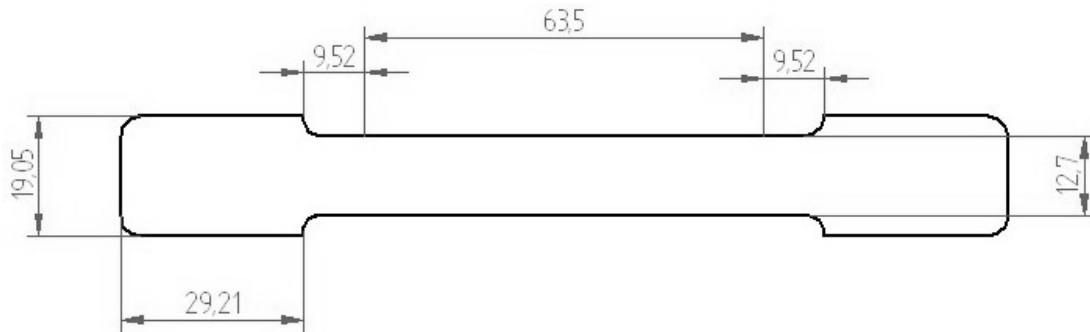


Figure 3.1. Dimensions of big dog-bone shaped samples.

The gauge length was 51 mm. An average of at least five specimens was taken for tensile testing results. The speed of testing was chosen according to the Table 1 of the ASTM Standard D 638-03. The recommended speeds of testing for the sample, which is Type IV, are 5 mm/min

$\pm 25 \%$, $50 \text{ mm/min} \pm 10 \%$ or $500 \text{ mm/min} \pm 10 \%$ and the speed of testing shall be chosen to produce rupture in 0.5 to 5 min for the specimen geometry being used. As F1 and F2 samples have high elongations, their rupture was taking longer than 5 min at 50.8 mm/min so the speed of testing was chosen to be 508 mm/min . The crosshead speed was set at 508 mm/min for F1, F2, PP/F1 and PP/F2 samples. But as polypropylene is brittle, cross-head speed of 50.8 mm/min was used for the PP.

The tensile stress at maximum load, tensile strain at maximum load, energy at maximum load, and elastic modulus were measured. The tensile test values obtained from the samples are listed in Table 3.2 and the stress-strain curves are given in Figure 3.2.

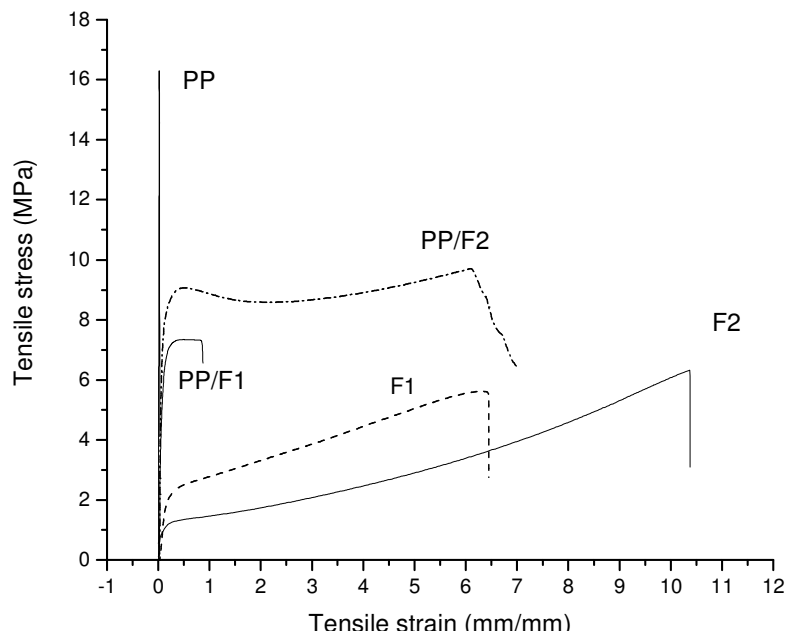


Figure 3.2. Stress- strain curves of PP, F1, F2, PP/F1 and PP/F2 samples.

When polymers are blended with rubbers, an increase in impact strength is observed while, on the other hand, elastic modulus and yield stress decrease. For improving impact

strength by toughening with elastomer, the elastomer modulus has to be smaller than the modulus of PP, and the elastomer must have low crystallinity [35].

Impact strength of PP/F1 and PP/F2 blends, which are 124.39 J/m and 105.63 J/m respectively, are higher than the impact strength of PP sample which is 49.13 J/m. The increase in impact strength values of elastomer blended samples PP/F1 and PP/F2 indicates that toughening of PP is achieved by both F1 and F2 blends of PP.

When tensile testing values are compared, it is seen that tensile stresses at maximum load of PP/F1 and PP/F2 samples (7.30 MPa and 10.90 MPa, respectively) are lower than the tensile stress at maximum load of PP which is 18.64 MPa. Similarly, elastic modulus of PP is higher than the moduli of both PP/F1 and PP/F2 blends. Fine and uniform distribution of elastomer as well as smaller elastomer modulus than elastic modulus of PP are given as the necessary conditions to have optimum impact strength improvement in PP/elastomer blends by Inoue [35].

The moduli of both elastomers F1 and F2 are smaller than the elastic modulus of PP. This is a requirement for improving impact strength. In this study this requirement and an improvement in impact strength are both achieved.

Toughness may be measured by the energy transferred to a polymer at break or the area under a conventional stress-strain curve [4]. In Figure 3.2, the bigger areas under the stress-strain curves of PP/F1 and PP/F2 indicate that PP/F1 and PP/F2 samples are tougher than PP samples. In Figure 3.2, it is seen that PP has a brittle failure while PP/F1 and PP/F2 samples have ductile characteristics. Ductility is one of the expected results of rubber toughening. Since PP had a brittle behaviour compared to the other samples, its stress-strain curve in Figure 3.2 seems like a straight vertical line due to the scale of the X axis. For this reason, the stress-strain curve of the PP is redrawn in Figure 3.3 to show the details.

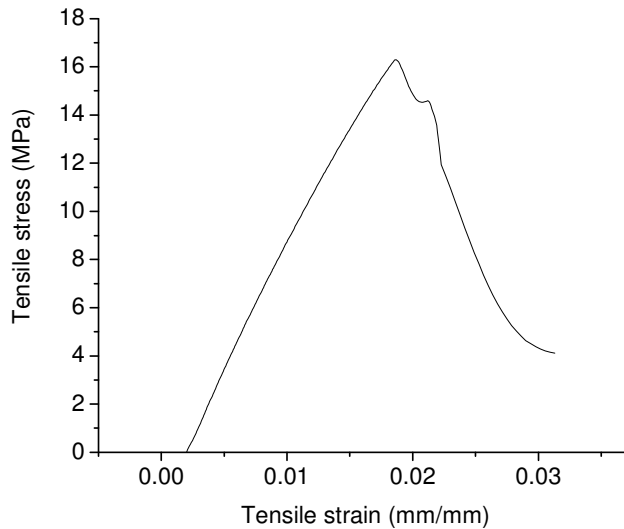


Figure 3.3. Stress-strain curve of PP.

3.3.1.2. Three-Point Bending Tests

3-point bending tests are carried out according to the ASTM D790 standard test method at a 0.47 mm/min crosshead speed using Instron 5565 universal testing machine. An average of at least five specimens was taken for 3-point bending test results. The results are shown in Table 3.3 and Figure 3.4.

Table 3.3. 3-point bending test results of PP, F1, F2, PP/F1 and PP/F2 samples (mean \pm standard deviation).

Sample	Maximum Load (N)	Maximum Flexural Stress (MPa)	Flexural Modulus (MPa)	Flexural Strain at Maximum Stress (%)
PP	82.44 \pm 2.37	49.59 \pm 0.61	1713.93 \pm 48.10	9.56 \pm 0.22
F1	2.93 \pm 0.05	1.87 \pm 0.04	39.05 \pm 0.63	8.57 \pm 0.45
F2	1.51 \pm 0.17	0.92 \pm 0.06	16.48 \pm 1.53	11.22 \pm 1.46
PP/F1	13.70 \pm 0.46	8.23 \pm 0.28	218.63 \pm 7.10	8.16 \pm 0.12
PP/F2	18.17 \pm 0.67	9.95 \pm 0.34	270.53 \pm 5.78	7.83 \pm 0.32

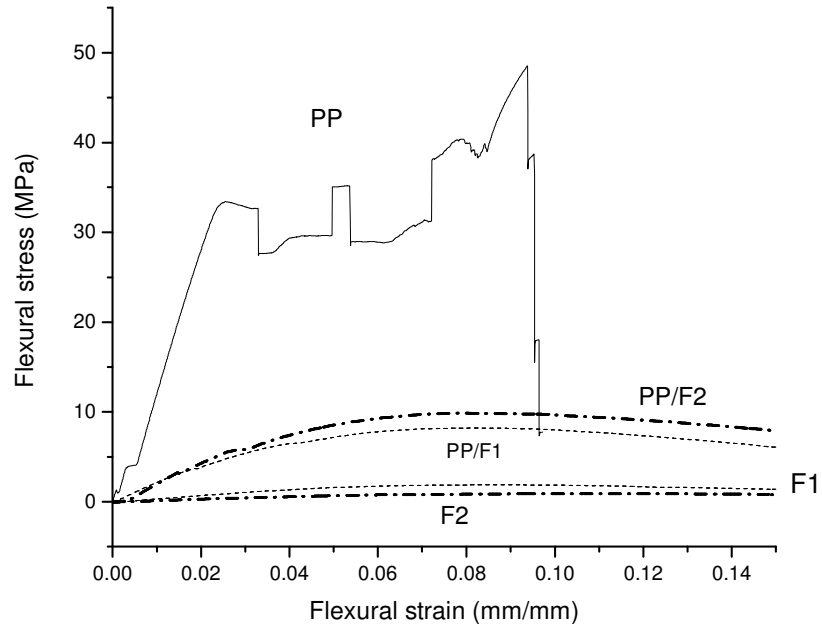


Figure 3.4. 3-point bending test stress-strain curves of PP, F1, F2, PP/F1 and PP/F2 samples.

Starkweather et al., [36] investigated the stiffness, tensile strength, and impact strength of unoriented Nylon 66 and Nylon 610 samples and observed that an increase in the degree of crystallization increases the tensile strength and stiffness while decreasing the impact strength. When PP is blended with elastomers, the toughness of the blend increases while a decrease in stiffness occurs [10, 26]. Houshyar and Shanks [37] studied the mechanical, thermal and structural properties of ethylene propylene elastomer added poly(propylene-co-ethylene) matrix having polypropylene fibers. They observed a decrease in flexural modulus as the elastomer content increased.

Blending PP with F1 and F2 gives a brittle to ductile transition in flexural properties; PP breaks in a brittle manner while PP/F1 and PP/F2 samples do not yet break at 15 % strain rate. The stiffness of PP/F1 and PP/F2 blends are lower than PP. The flexural moduli of PP/F1 and PP/F2, 218.63 MPa and 270.3 MPa respectively, are lower than the flexural modulus of PP which is 1713.93 MPa. The decrease of flexural modulus is a consequence of rubber toughening.

3.3.2. DSC Analysis

Thermal properties of samples were determined by differential scanning calorimetry (DSC) analysis. DSC measurements were done using TA Instrument QA2000 DSC at a heating rate of 5°C/min. First, temperature was brought to -90°C from room temperature; then, a heating ramp was applied from -90°C to 350°C, then a cooling ramp was applied from 350°C to -90°C under nitrogen atmosphere.

The experimental melting heat (ΔH_m) values were determined from the corresponding area under the melting peak. The overall crystallinity (X_c) was calculated as the ratio of experimental melting heat (ΔH_m) to melting heat of pure crystalline polypropylene material ($\Delta H_{m,c}$) using Equation 3.1 given below with the assumption that $\Delta H_{m,c}$ of pure polypropylene is 207.1 J/g [38]:

$$X_c = 100 \times \frac{\Delta H_m}{\Delta H_{m,c}} \dots\dots\dots (3.1)$$

Crystallinity of the polypropylene component of blends ($X_{c,m}$) was calculated by normalizing ΔH_m with the corresponding weight fraction of polypropylene in the blend. Figure 3.5 shows DSC thermograms of PP, F1 and PP/F1 samples while Figure 3.6 shows DSC thermograms of PP, F2, and PP/F2 samples during their heating and cooling scans.

Table 3.4 gives the thermal properties of samples obtained from the DSC analysis. The overall crystallinities of PP/F1 and PP/F2 samples are 18.68% and 19.18% respectively; while the crystallinity of PP samples is 36.62%. The crystallinity of polypropylene component did not change significantly.

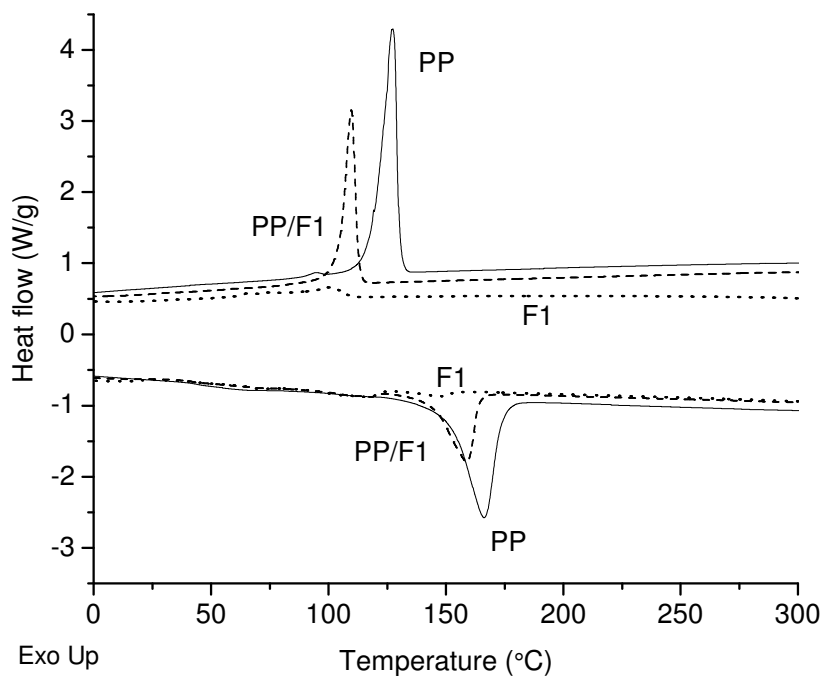


Figure 3.5. DSC thermograms of PP, F1 and PP/F1 samples.

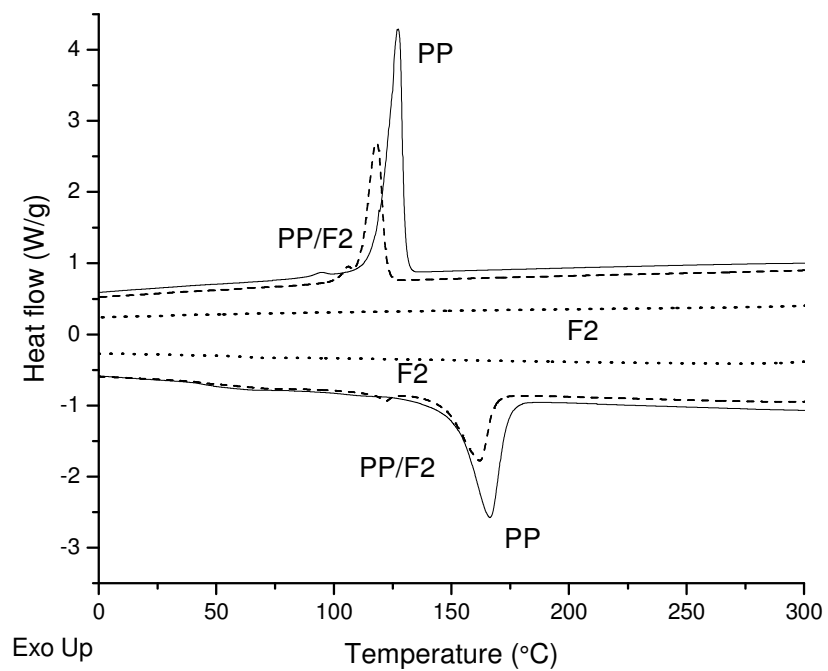


Figure 3.6. DSC thermograms of PP, F2 and PP/F2 samples.

Table 3.4. Thermal properties of PP, F1, F2, PP/F1 and PP/F2 samples obtained from DSC analysis.

Sample	ΔH_m (J/g)	X_c (%)	$X_{c,m}$ (%)
PP	75.,85	36.62	36.62
F1	7.92	–	–
F2	0.90	–	–
PP/F1	38.69	18.68	37.36
PP/F2	39.73	19.18	38.36

Blending of both F1 and F2 in polypropylene matrix decreased the overall crystallinity of the samples. The decrease in crystallinity had an effect on the increase of impact strength of PP/F1 and PP/F2 samples. The higher yield stress of PP and its brittle characteristic are due to the higher crystallinity of PP compared to PP/F1 and PP/F2 samples. These results are in agreement with the studies in the literature. Bessel et al., [39] synthesized Nylon 6 and studied the effect of structure on the mechanical properties of the molded polymer. They concluded that different annealing treatments resulted in different crystallinity; higher degree of crystallinity showed brittle failure, while samples having low crystallinity showed ductile behavior.

Starkweather and Brooks [40] worked on the tensile properties of injection molded Nylon 66 and proved that a big increase in yield stress occurs when crystallinity increases. Ohlberg et al., [41] investigated the effect of Ziegler type polyethylene crystallinity on impact strength and found out that impact strength decreases with increasing crystallinity. Hammer et al., [42] concluded that an increase in crystallinity gives higher modulus, higher yield strength and lower elongation at break.

3.3.3. SEM Analysis

The morphology of the blends was observed by SEM analysis. Blend specimens were etched in cyclohexane for 36 hours. The samples were then rinsed in pure water and left to dry for 48 hours. After gold sputtering, the phase morphology of the samples was observed in a ZEISS EVO 50 VP SEM instrument operating at 20 kV.

The SEM micrographs of PP/F1 and PP/F2 samples are given in Figures 3.7 and 3.8, respectively. The black holes represent elastomer particles which were dissolved in cyclohexane. Both Figure 7 and Figure 8 prove that elastomer particles are in roughly spherical shape and evenly distributed in the PP matrix.

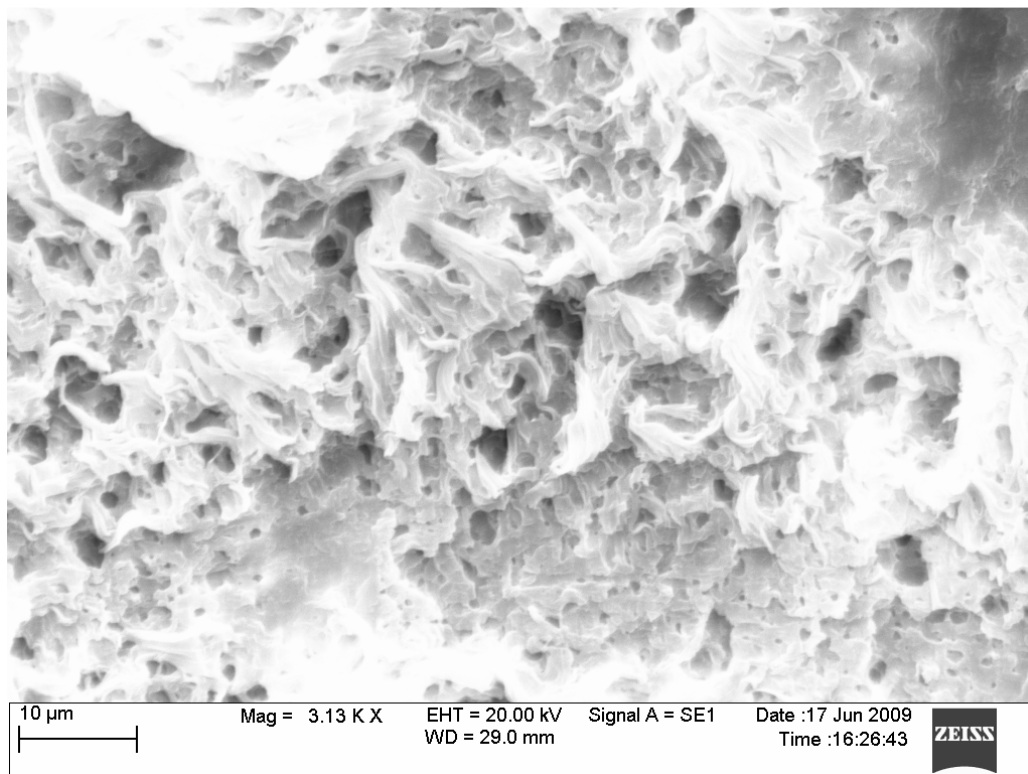


Figure 3.7. SEM micrograph of etched PP/F1 blend.

Even distribution and even shapes of elastomers have major effects on toughening of brittle polymeric matrices. Mechanical properties of polymer-rubber blends are mainly controlled by their morphology. For rubber toughened polymers, the shape, content, size, and size distribution of the dispersed phase particles have major effects on mechanical properties [14].

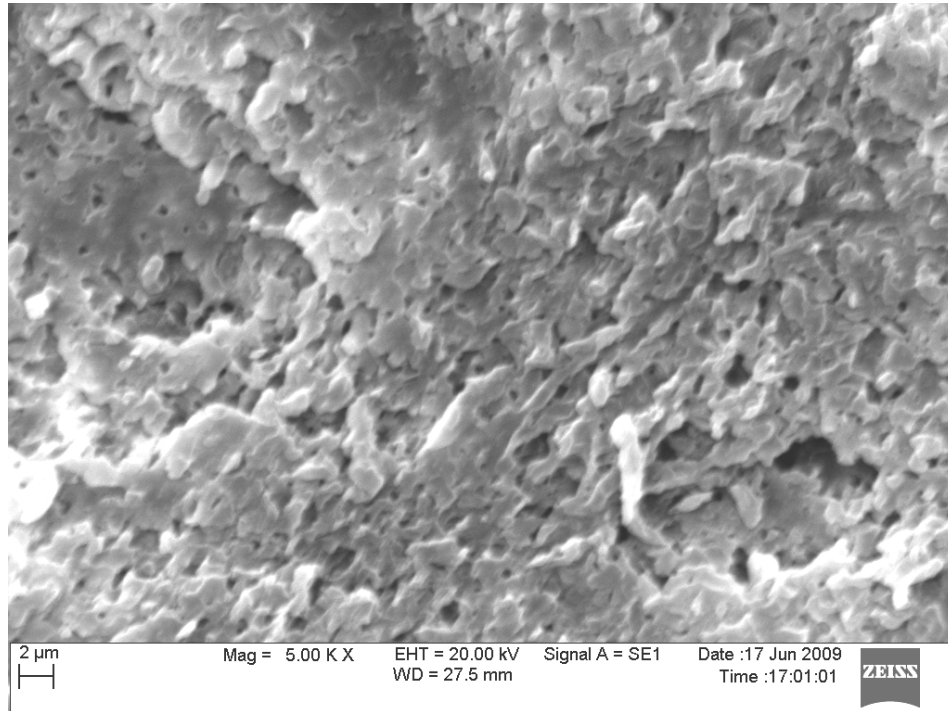


Figure 3.8. SEM micrograph of etched PP/F2 blend.

“Image J” program which is supplied by the National Institute of Health (NIH) at <http://rsb.info.nih.gov/ih-image/> website was used to determine the elastomer particle size distributions of F1 and F2 in samples PP/F1 and PP/F2, respectively. Particle size of F1 in PP/F1 samples is in the range of minimum 428.8 nm and maximum 3.8 μm with an average of 1566.37 nm in diameter (Figure 3.9). On the PP/F2 samples, F2 particle sizes vary between 643.6 nm and 2.1 μm with an average of 1028.68 nm in diameter (Figure 3.10).

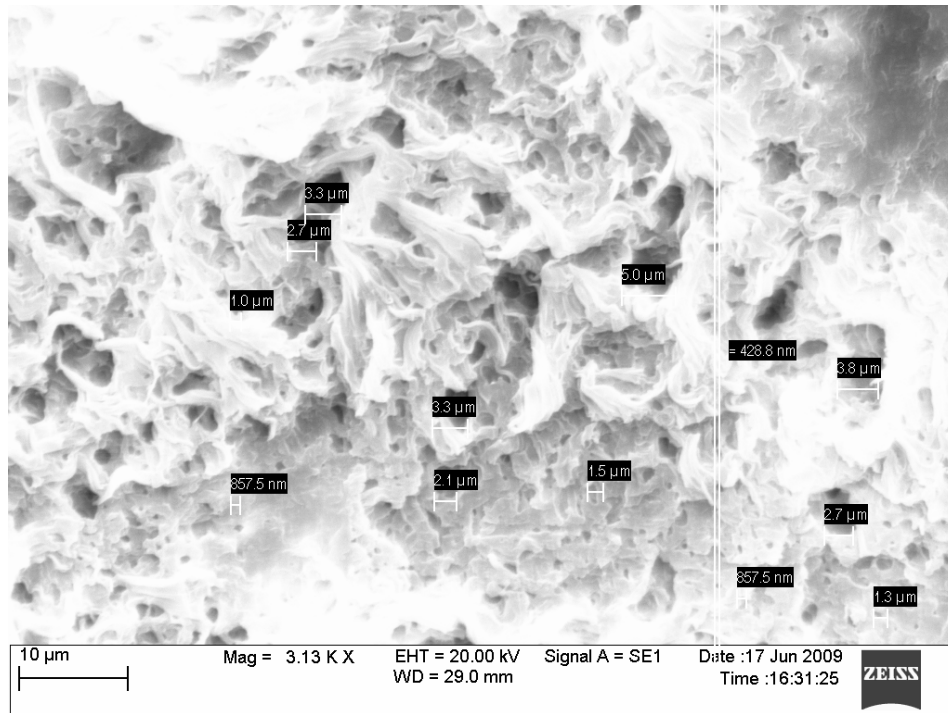


Figure 3.9. SEM micrograph of F1 particle sizes in etched PP/F1 blend.

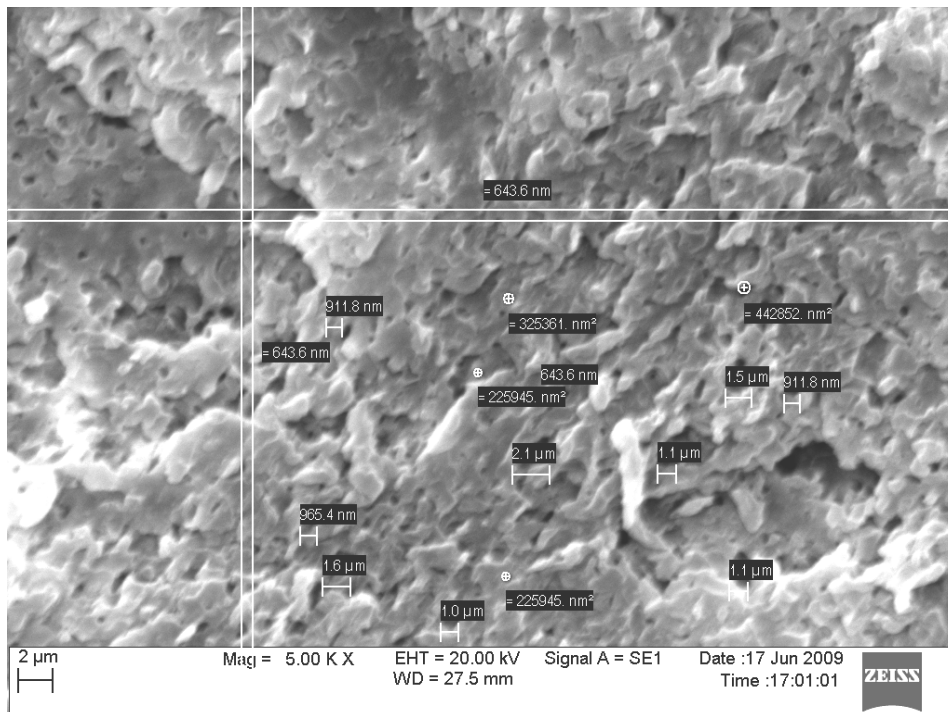


Figure 3.10. SEM micrograph of F2 particle sizes in etched PP/F2 blend.

The particle size distribution histograms of etched PP/F1 and PP/F2 samples are given in Figure 3.11 and Figure 3.12, respectively. F1 particles have larger diameters and a larger distribution range than the F2 particle distribution. Good particle size distribution is very important in having toughening results in blends. Size distribution of both PP/F1 and PP/F2 blends prove that a good distribution was achieved.

PP blends with smaller rubber particles are tougher and more ductile than blends with bigger rubber particles [25]. According to the cavitation theory, the dispersed rubber particles increase the fracture energy by increasing the total surface area [3]. F2 particles in PP/F2 samples are smaller than F1 particles in PP/F1 samples; therefore the bigger total surface area of PP/F2 samples compared to PP/F1 samples may have caused an increase in toughness.

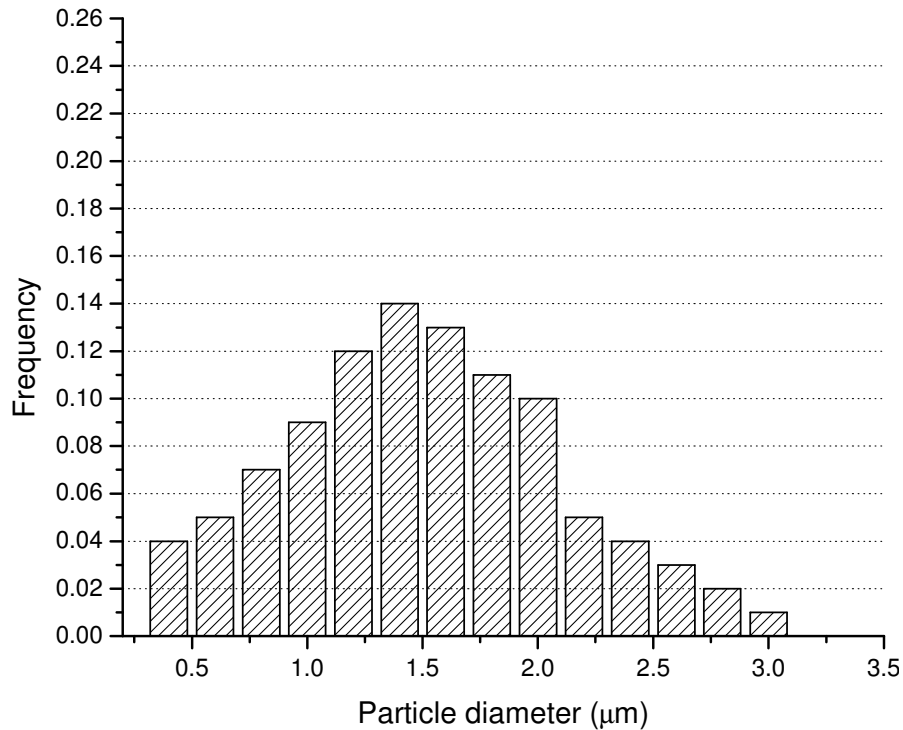


Figure 3.11. Histogram of particle diameter of F1 in etched PP/F1 blend.

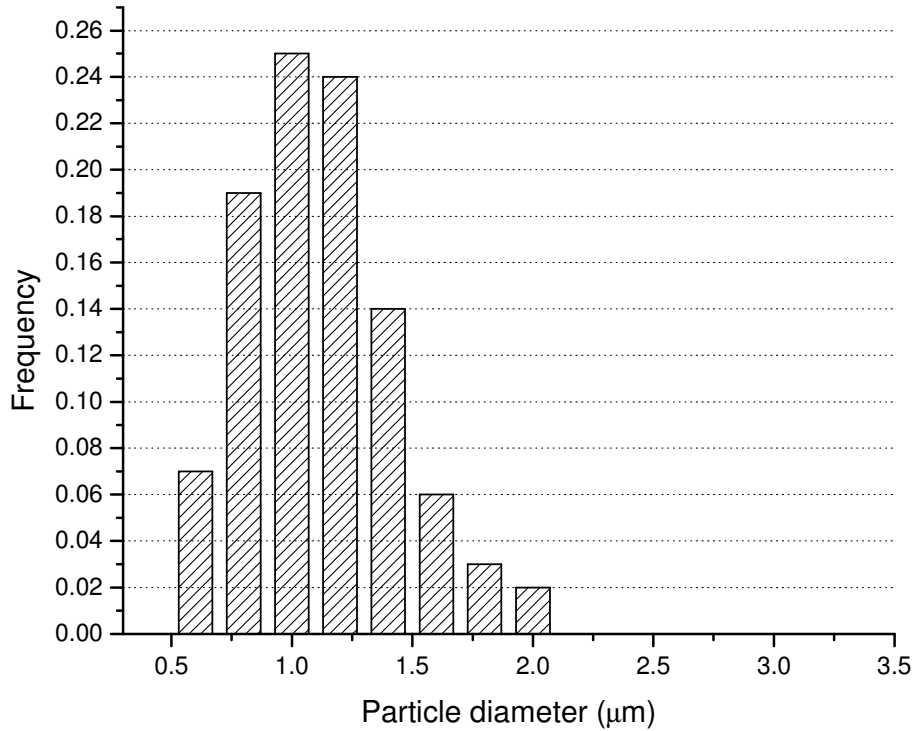


Figure 3.12. Histogram of particle diameter of F2 in etched PP/F2 blend.

3.4. Conclusions

The processing characteristics of PP/F1 and PP/F2 blends have been studied. Addition of thermoplastic elastomers F1 and F2 to PP decreased the yield stress of the blend and decreased its modulus. Toughening of polypropylene was achieved by blending of PP with both of the thermoplastic elastomers. Additional study may be conducted to investigate the suitability of PP/F1 and PP/F2 blends to extrude tougher fibers. Tensile tests show that brittle characteristics of PP turns to be ductile both in PP/F1 and PP/F2 blends.

3-point tests show that flexural strength is decreasing when PP is toughened with elastomers F1 and F2.

Impact tests give higher impact strength for elastomer blended PP. The brittle characteristic of PP turns to be ductile when both F1 and F2 are blended into PP.

DSC analysis shows the relation between crystallinity and toughness. PP blended with F1 and F2 elastomers give higher ductility and higher toughness while the overall crystallinity of blends decreases.

SEM analysis proves that both F1 and F2 elastomeric particles are evenly distributed in the PP matrix. Even distribution has a great effect on toughness increase in elastomer-polymer blends. SEM images also reveal that F2 particle sizes are smaller than F1 particle sizes.

Stiffness decrease is a sacrifice in rubber toughening. To obtain a good balance between pure PP and PP/elastomer blends, the addition of fillers such as CaCO₃ and silica nanoparticles to PP/elastomer blends may be helpful.

Acknowledgements

This research is supported by *U.S. Department of Commerce* (DOC-ITA-O8-TBD-E), which is appreciated. Special thanks go to Mr. *David Clark* for his help in operating the injection molding machine.

3.5. References

- [1] Karger-Kocsis, J., “*Structure and Morphology, Polypropylene Structure, Blends and Composites*”, 63-64, Chapman & Hall, Cambridge (1995).
- [2] Tortorella, N., and Beatty, C. L., Morphology and Mechanical Properties of Impact Modified Polypropylene Blends, *Polymer Engineering and Science*, **48**(11), 2098-2110 (2008).
- [3] Zabaleta, A., Gonzalez, L., Eguiazabal, J. I., and Nazabal, J., Rubber Toughening of Poly(ether imide) by Modification with Poly(butylenes terephthalate), *European Pol. Journal*, **45**(2), 466-473 (2009).

- [4] Perkins, W.G., Polymer Toughness and Impact Resistance, *Polymer Engineering and Science*, **39**(12), 2445-2460 (1999).
- [5] Yang, J., Zhang, Y., and Zhang, Y., Brittle-Ductile Transition of PP/POE Blends in Both Impact and High Speed Tensile Tests, *Polymer*, **44**(17), 5047-5052 (2003).
- [6] Fasce, L. A., Pettarin, V., Marano, C., Rink, M., and Frontini, P. M., Biaxial Yielding of Polypropylene/Elastomeric Polyolefin Blends: Effect of Elastomer Content and Thermal Annealing, *Polymer Engineering and Science*, **48**(7), 1414-1423 (2008).
- [7] Lee, H. Y., Kim, D. H., and Sun, Y., Effect of Octene Content in Poly(ethylene-co-1-octene) on the Properties of Poly(propylene)/Poly(ethylene-co-1-octene) Blends, *Journal of Applied Polymer Science*, **103**(2), 1133-1139 (2007).
- [8] Hristov, V., Lach, R., Krumova, M., and Grellmann, W., Fracture Toughness of Modified Polypropylene/poly(styrene-ran-butadiene) blends, *Polymer International*, **54**(12), 1632-1640 (2005).
- [9] Cook, R. F., Koester, K. J., and Macosko, C. W., Rheological and Mechanical Behaviour of Blends of Styrene-Butadiene Rubber with Polypropylene, *Polymer Engineering and Science*, **45**(11), 1487-1497 (2005).
- [10] Wang, W. Z., and Liu, T., Mechanical Properties and Morphologies of Polypropylene Composites Synergistically Filled by Styrene-Butadiene Rubber and Silica Nanoparticles, *Journal of Applied Polymer Science*, **109**(3), 1654-1660 (2008).
- [11] Zebarjad, S. M., Sajjadi, S. A., and Tahani, M., Modification of Fracture Toughness of Isotactic Polypropylene with a Combination of EPR and CaCO₃ Particles, *Journal of Materials Processing Technology*, **175**(1-3), 446-451 (2006).

- [12] Mighri, F., Huneault, M. A., Ajji, A., Ko, G. H., and Watanabe, F., Rheology of EPR/PP Blends, *Journal of Applied Polymer Science*, **82**(9), 2113-2127 (2001).
- [13] Yazdani-Pedram, M., Quijada, R., and Lopez-Manchado, M. A., Use of Monomethyl Itaconate Grafted Poly(propylene) (PP) and Ethylene Propylene Rubber (EPR) as Compatibilizers for PP/EPR Blends, *Macromol. Mater. Eng.*, **288**(11), 875-885 (2003).
- [14] Mae, H., Omiya, M., and Kishimoto, K., Material Ductility and Toughening Mechanism of Polypropylene Blended with Bimodal Distributed Particle Size of Styrene-Ethylene-Butadiene-Styrene Triblock Copolymer at High Strain Rate, *Journal of Applied Polymer Science*, **110**(6), 3941-3953 (2008).
- [15] Bassani A. and Pessan L. A., Toughening of Polypropylene with Styrene/Ethylene-Butylene/Styrene Tri-block Copolymer: Effects of Reactive and Nonreactive Compatibilization, *Journal of Applied Polymer Science*, **86**(14), 3466-3479 (2000).
- [16] Gupta A. K., and Purwar S. N., Crystallization of PP in PP/SEBS Blends and Its Correlation With Tensile Properties, *Journal of Applied Polymer Science*, **9**, 1595-1609 (1983).
- [17] Fu, Q., Wang, Y., Li, Q., and Zhang, G., Adding EPDM Rubber Makes Poly(propylene) Brittle, *Macromol. Mater. Eng.*, **287**(6), 391-394 (2002).
- [18] Da Costa, H. M., Ramos, V. D., and Rocha, M. C. G., Analysis of Thermal Properties and Impact Strength of PP/SRT, PP/EPDM and PP/SRT/EPDM Mixtures in Single Screw Extruder, *Polymer Testing*, **25**(4), 498-503 (2006).
- [19] Oksuz, M., and Eroglu, M., Effect of the Elastomer Type on the Microstructure and Mechanical Properties of Polypropylene, *Journal of Applied Polymer Science*, **98**(3), 1445-1450 (2005).

- [20] Jiang, W., Tjong, S. C. and Li, R. K. Y., Brittle-Tough Transition in PP/EPDM Blends: Effects of Interparticle Distance and Tensile Deformation Speed, *Polymer*, **41**(9), 3479-3482 (2000).
- [21] Gupta, N. K., Jain, A. K., Singhal, R. and Nagpal, A. K., Effect of Dynamic Crosslinking on Tensile Yield Behaviour of Polypropylene/Ethylene-Propylene-Diene Rubber Blends, *Journal of Applied Polymer Science*, **78**(12), 2104-2121 (2000).
- [22] Kim, J. Y., and Chun, B. C., Effect of High Density Polyethylene Addition and Testing Temperature on the Mechanical and Morphological Properties of Polypropylene/Ethylene-Propylene Diene Terpolymer Binary Blends, *Journal of Materials Science*, **35**(19), 4833-4840 (2000).
- [23] Kim, B. K., and Chui, C. H., Reactive Extrusion of Polyolefin Ternary Blends, *Journal of Applied Polymer Science*, **60**(12), 2199-2206 (1996).
- [24] Wang, Y., Wang, W., Peng, F., Liu, M., Zhao, Q., and Fe, P. F., Morphology of Nylon 1212 Toughened With a Maleated EPDM Rubber, *Polym. Int.*, **58**(2), 190-197 (2008).
- [25] Liang, J. Z., and Li, R. K. Y., Rubber Toughening in Polypropylene: A Review, *Journal of Applied Polymer Science*, **77**(2), 409-417 (1959).
- [26] Zhang, M., Li, Y., Zhang, X., Gao, J., Huang, F., Song, Z., Wei, G. and Qiao, Z., The Effect of Elastomeric Nano-particles on the Mechanical Properties and Crystallization Behaviour of Polypropylene, *Polymer*, **43**(19), 5133-5138 (2002).
- [27] Sun, D., Yuan, Q., and Jiang, W., Thermal Properties and Crystallization Behaviour of Ultrafine Fully-Vulcanized Powdered Rubber Particle Toughened Polypropylene, *Journal of Applied Polymer and Science*, **110**(3), 1318-1323 (2008).

- [28] George, S., Varughese, K. T., and Thomas, S., Thermal and Crystallization Behaviour of Isotactic Polypropylene/Nitrile Rubber Blends, *Polymer*, **41** (14), 5485-5503 (2000).
- [29] Barish, L., The Study of Cracking and Fracturing of Spherulitic Isotactic Polypropylene, *Journal of Applied Polymer Science*, **6**(24), 617-623 (1962).
- [30] D’Orazio, L., Mancarella, C., and Martuscelli, E., Polypropylene/Ethylene-co-Propylene Blends: Influence of Molecular Structure and Composition of EPR on Melt Rheology, Morphology and Impact Properties of Injection-Moulded Samples, *Polymer*, **32**(7), 1186-1194 (1991).
- [31] D’Orazio, L., Mancarella, C., Martuscelli, E., and Sticotti, G., Polypropylene/Ethylene-co-Propylene Blends: Influence of Molecular Structure of EPR and Composition on Phase Structure of Isothermally Crystallized Samples, *Journal of Material Science*, **26**(15), 4033-4047 (1991).
- [32] D’Orazio, L., Mancarella, C., Martuscelli, E., and Sticotti, G., Melt rheology, Phase Structure and Impact Properties of Injection-Moulded Samples of Isotactic Polypropylene/Ethylene-Propylene Copolymer (iPP/EPR) Blends: Influence of Molecular Structure of EPR Copolymers, *Polymer*, **34**(17), 3671-3681 (1993).
- [33] D’Orazio, L., Mancarella, C., Martuscelli, E., and Sticotti, G., Thermoplastic Elastomers From iPP/EPR Blends: Crystallization and Phase Structure Development, *Journal of Applied Polymer Science*, **53**(4), 387-404 (1994).
- [34] D’Orazio L., Mancarella C., Martuscelli E., Cecchin G. and Corrieri R., Isotactic Polypropylene/Ethylene-co-Propylene Blends: Effects of the Copolymer Microstructure and Content on Rheology, Morphology and Properties of Injection Moulded Samples, *Polymer*, **40**(10): 2745-2757. (1999).

- [35] Inoue, T., Selective Crosslinking in Polymer Blends. II. Its Effect on Impact Strength and Other Mechanical Properties of Polypropylene/Unsaturated Elastomer Blends, *Journal of Applied Polymer Science*, **54**(6), 722-733, (1994).
- [36] Starkweather, H. W., Moore, G. E., Hansen, J. E., Roder, T. M., and Brooks, R. E., Effect of Crystallinity on the Properties of Nylons, *Journal of Polymer Science*, **21**(98), 189-204 (1956).
- [37] Houshyar, S., and Shanks, R. A., Mechanical and Thermal Properties of Toughened Polypropylene Composites, *Journal of Applied Polymer Science*, **105**(2), 390-397 (2007).
- [38] Wunderlich, B., "Thermal Analysis", Academic Press, New York, 1990.
- [39] Bessel, T. J., Hull, D., and Shortall, J. B., The Effect of Polymerization Conditions and Crystallinity on the Mechanical Properties and Fracture of Spherulitic Nylon 6, *Journal of Material Science*, **10**(7), 1127-1136 (1975).
- [40] Starkweather, H. W., and Brooks, R. E., Effect of Spherulites on the Mechanical Properties of Nylon 66, *Journal of Applied Polymer Science*, **1**(2), 236-239 (1959).
- [41] Ohlberg, S. M., Roth, J., and Raff, R. A. V., Relationship Between Impact Strength and Spherulite Growth in Linear Polyurethane, *J. of Applied Polymer Science*, **1**(1), 114-120 (1959).
- [42] Hammer, C. F., Koch, T. A., and Whitney, J. F., Fine Structure of Acetal Resins and Its Effect on Mechanical Properties, *Journal of Applied Polymer Science*, **1**(2), 169-178 (1959).

CHAPTER 4

FIBER AND NANOCCLAY REINFORCED PP COMPOSITES

4.1. Materials used

In this study, polypropylene (PP) matrix is reinforced with glass fibers, carbon fibers, nanoclay at several ratios. Compatibilizer is used to increase bonding for nanoclay.

4.1.1. Polypropylene (PP)

Matrix in a composite keeps fibers in their locations and in a variety of orientations. Matrix has several functions such as transferring load between fibers, protecting fibers from environmental damages such as humidity, temperature and breakage [1]. In this study polypropylene (PP) is used as the matrix material. Chemical structure of polypropylene is shown in Figure 4.1. Polypropylene whose IUPAC name is poly(propene) does not take moisture and is extremely resistant to chemicals (acids, alkalis, bleaches, solvents), and to mildew. Polypropylene has high strength; and resiliency so it is used in carpet production. It may be used for weight reduction as it has a low density [2].

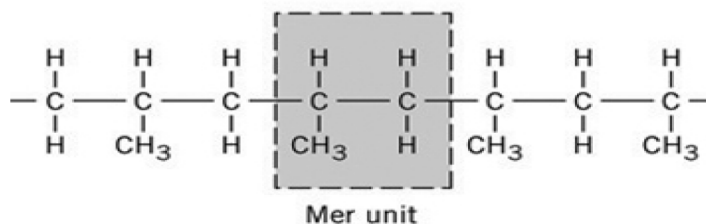


Figure 4.1. Repeating unit of polypropylene [3].

Polypropylene copolymer (PP) from Premier Plastic Resins (30 Melt Copolymer Natural Polypropylene) having a melt flow rate (MFR) of 34g/10 min at 230°C, and a density of 0.910 g/cm³ was used in this study.

4.1.2. Glass fibers

Glass is made up of silicon, boron and phosphorus combined with oxygen, sulfur and selenium; when additives are added to glass, it is possible to form glass fibers. Glass fibers have different classes such as A-glass, E-glass, C-glass, S-2 glass, D-glass, R-glass and low K glass fibers, hollow glass fibers and Te glass fibers [4]. Glass fibers are produced by extruding molten glass from a die having desired shape and size. The properties of the glass used for making glass fibers and the glass fiber produced are very similar. But glass fibers have their weavability property since their small diameter (5-20 µm) gives flexibility to their structure [5].

Glass fibers have high tensile strength which exceeds strength to weight ratio of steel wire, they have moisture resistance, they are insulative and they are durable to thermal environments. Due to their inorganic structure, glass fibers are resistant to heat and fire. As they don't have an organic structure they have high chemical resistance to most chemicals. [4].

In this study, glass fibers used are in filament form, are supplied from Multi-End Roving Company and they are of E-glass type. The properties of glass fibers are given in Table 4.1.

Table 4.1. Properties of glass and carbon fibers used.

Material	Fiber length	Tensile Strength (MPa)	Tensile Modulus (GPa)	Density (g/cm³)	Diameter (µm)
E-Glass fibers	5-6 mm	1380	55.2	2.12	13
Carbon fibers	6 mm	4344	225	1.82	7

4.1.3. Carbon fibers

Carbon fibers are described as ‘fibers containing at least 90% carbon’. At the end of the 19th century, Thomas Edison and Joseph Swan invented a light bulb using carbon fiber produced from carbonizing cotton and bamboo. Currently high performance carbon fibers are produced from mostly polyacrylonitrile (PAN). Production of carbon fibers may be rayon-based, and pitch-based: gas-phase-grown carbon fibers are used as well [6].

Carbon fiber production has three main steps. The first step is the stretching process. PAN is firstly stretched and oxidized at air in 300°C. In the second step, the stretched PAN is carbonized at about 1000°C under inert atmosphere, which is usually nitrogen, for a few hours. The carbonization of PAN is illustrated in Figure 4.2.

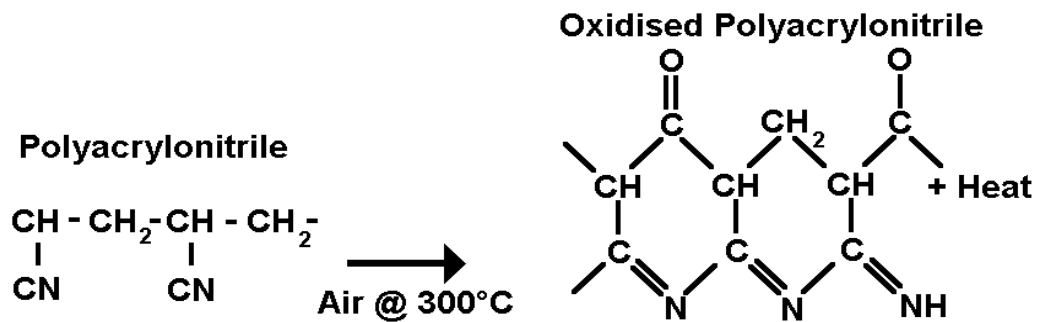


Figure 4.2. Carbonization step for producing carbon fibers [6].

The last step is the treatment at high temperatures between 1500-3000°C and it is called graphitization (Figure 4.3).

For this study, carbon fibers are in bundle form at 6mm length and are bought from Toho Tenax. The properties of carbon fibers are given in Table 4.1.

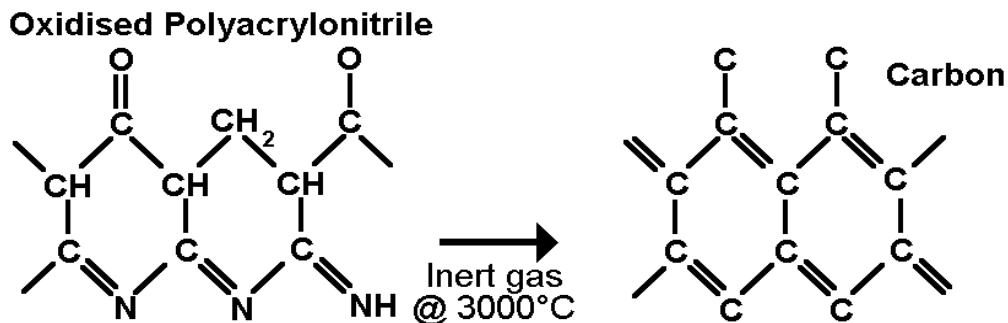


Figure 4.3. Graphitization step for producing carbon fibers [6].

4.1.4. Nanoclay

In this study, Nanofil 919® is used as nanoclay. Chemical structure of Nanofil 919®, which has an average particle size of 35 μm , is given in Figure 4.4.

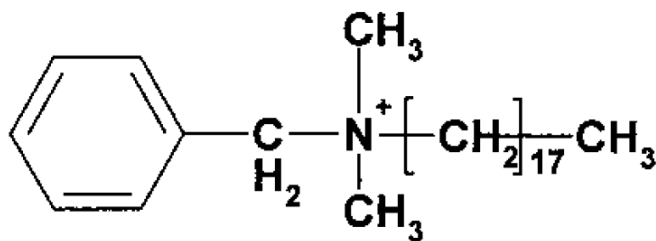


Figure 4.4. Chemical structure of Nanofil 919® [7].

Nanofil 919® is a commercial organophilic montmorillonite nanoclay produced by Sud Chemie. Nanofil 919® is modified with dimethyl, benzyl hydrogenated tallow, quaternary ammonium ion. Its silicate layers have a length of approximately 200nm and a thickness of 1nm with a cation exchange of 75 mequiv/100 g [8].

4.1.5. Compatibilizer

Intercalation or exfoliation is not enough for obtaining optimum interaction; high affinity between nanoclay (organic modifier) and polymer chains is needed. This affinity is very low when polymer matrix is a non-polar polymer such as polyolefins [9].

The addition of small amount of polar groups such as compatibilizers to nonpolar polyolefin matrices enables silicate layer exfoliation in polyolefins [10].

Especially maleic anhydride (MA) modified PP is used as a compatibilizer, but as it is only grafted to the end of main PP chain, its improvement is limited. Other compatibilizers are glycidyl methacrylate (GMA) grafted PP and acrylic acid (AA) grafted PP [11].

Fusabond® P613 is used as a compatibilizer in PP and nanoclay blends. Fusabond® P613 is an anhydride modified polypropylene (PP-g-maleic anhydride) produced by DuPont which has a melt index of 120 g/10 min; its melting point is 162°C [12].

4.2. Machines Used

The machine brands, models and the purpose they are used for are given in Table 4.2.

Table 4.2. Machines used for the manufacturing and testing of samples.

Purpose	Machine Brand and Model
Sample production	Battenfeld EM 50/300 injection molding machine
Tensile testing (ASTM D638-03)	Instron 5565 Universal Tester
Impact testing (ASTM D3763-06)	Instron DynaTup 8250
Three point bending (flexural) testing (ASTM D790-07)	Instron 5565 Universal Tester

In this study, mainly four machines are used. Injection molding machine is used to produce the samples, Instron 5565 Universal Tester is used for tensile tests and three point bending tests and Instron DynaTup 8250 is used for impact testing.

4.2.1. Injection Molding Machine EM 50/300 Battenfeld

In injection molding machine (IMM), polymer pellets are fed through a hopper to the barrel. Polymer receives conductive heat from the heated wall of the barrel and frictional heat from the rotation of a screw. The heated polymer melts and is pushed through the nozzle with the reciprocating screw. The melt is pushed to the tip and forms a reservoir melted plastic ready to be injected into the mold cavities. The nozzle moves in forward position, injects the melt and as cavities are filled, the nozzle moves backward. The mold is cooled through cooling channels. As the part cools, clamping unit is released and movable platen moves away from the stationary platen; the solidified part leaves the mold by the force of pushing pins [13]. Schematic of an IMM is given in Figure 4.5 [14]. Injection molding machine consists of two main parts: injection unit and clamping unit [15].

Injection unit consists of drive system, feed hopper, injection reciprocating screw, barrel and injection cylinder and nozzle. The drive system may be hydraulic, electric or hybrid driven.

The hopper feeds polymer pellets with gravity to the barrel-screw assembly, but there are IMM's having automatic feeding systems to the hopper. The reciprocating screw compresses, helps melting polymer and transports the melt. In thermoplastics IMM's, the reciprocating screw's outer diameter stays constant but the distance between screw and walls gets smaller from feeding zone to the metering zone.

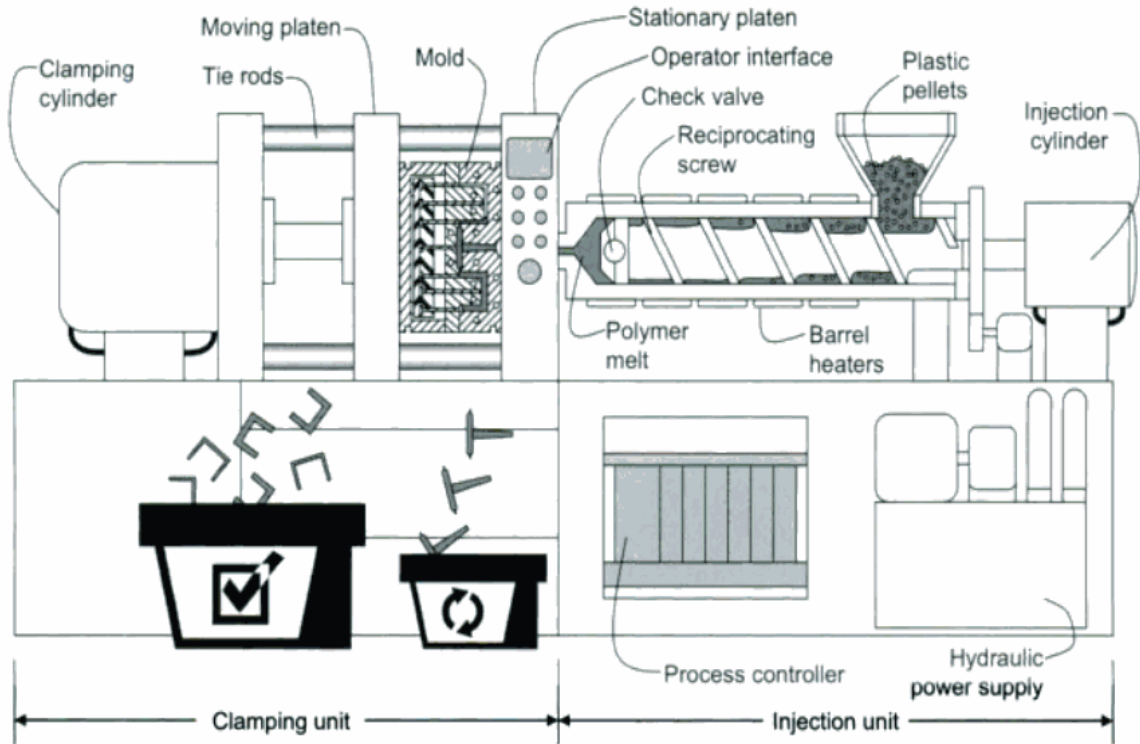


Figure 4.5. Injection molding machine [14].

Due to increasing channel depth from hopper to nozzle, the polymer melt is compressed which produces viscous (shear) heat that helps with melting the polymer. Heater band regions outside the barrel help with keeping the barrel at desired temperature. There may be three or more heater sets and their temperatures may be the same or different. The screw has 3 regions: feeding zone, compressing zone and metering zone [15]. The nozzle connects the barrel and sprue. Temperature of the nozzle should be at the polymer melting temperature or below it. The barrel supports the reciprocating screw and is heated by sensors electrically. The sensors are used in both increasing and decreasing the temperature to keep the barrel in desired temperature. The barrel is in full forward position during injection and the nozzle seals into the sprue. After injection is finished, the polymer melt inside the barrel should be purged to avoid solidifying

inside the barrel. When purging, the barrel is backed to let the purging polymer melt come out of the nozzle [16].

Clamping unit consists of mold system (sprue, mold cavities, ejector pins, cooling channels, molding plates) and clamping system (clamping cylinder and tie bar). Stationary and moving platens, molding plates including mold cavities, sprue, ejector pins and cooling channels make the mold system which shapes up the part. The mold is a part where heat exchange occurs in order to solidify the molten polymer into the final product: the volume of the melt decreases as it cools. Cooling channels are located in the mold: a cooling liquid such as water passes through the cooling channels to regulate temperature over the mold and shape the product. Clamping system opens and closes the mold, supports the mold structure and gives enough force to prevent the mold from opening when injecting the melt polymer. There are control units for processing parameters such as temperature, pressure, injection speed, screw speed, and screw position [17].

Polymers are compressible and they have lower density at higher temperature ranges. To keep the melt polymer at the same volume, pressure is applied to the polymer in the mold cavity until the polymer cools and the part is produced. For fiber reinforced polymer production during injection molding, the applied pressure is essential. Fiber-reinforced polymers have lower overall shrinkage, lower injection-pressure sensitivity and lower in-flow shrinkage but they may have higher warping and higher cross-flow shrinkage compared to pure polymers [4].

Shear rates and velocity profiles in injection molding show differences in the shell and core structure. Figure 4.6 shows shear rate and velocity profiles for nonisothermal flow during injection molding process. Figure 4.7 shows fountain flow in injection molding, which affects the orientation of fibers in a composite.

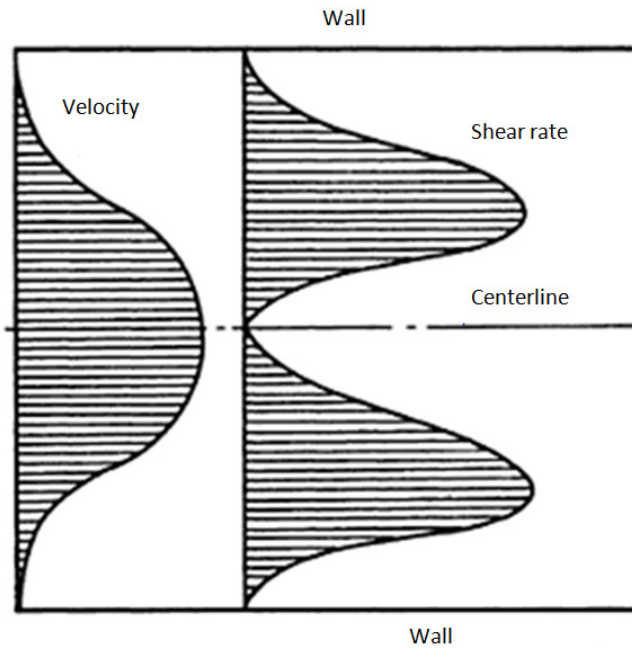


Figure 4.6. Shear rate and velocity profiles for nonisothermal flow during injection molding process [4].

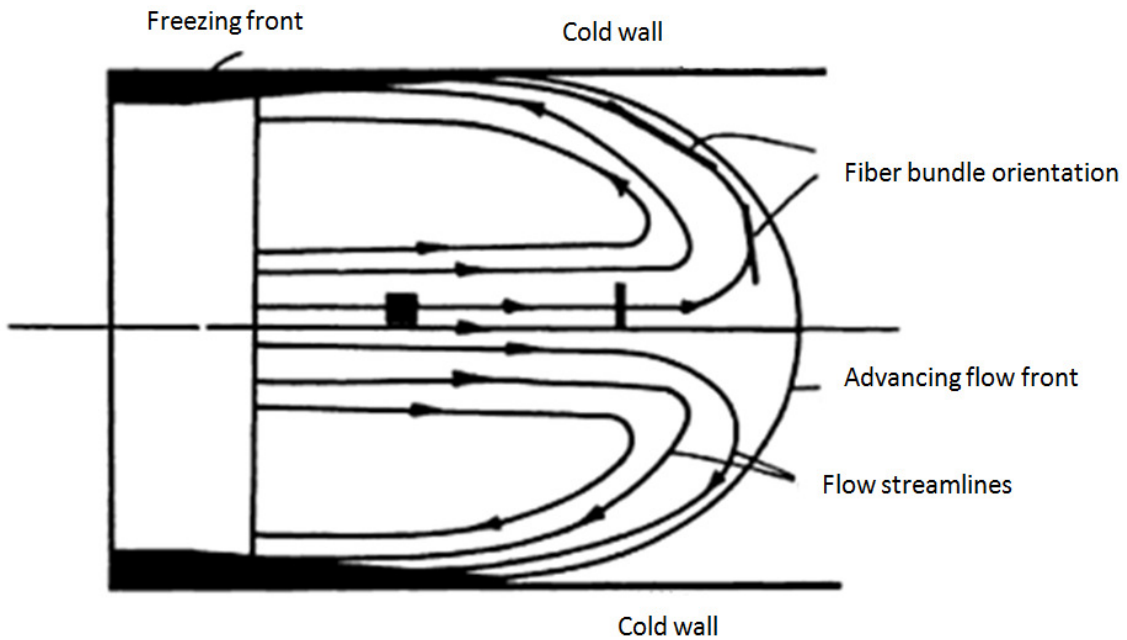


Figure 4.7. Fountain flow in injection molding [4].

4.2.1.1. Operation of the EM 50/300 Battenfeld IMM

The samples were injection molded using EM 50/300 Battenfeld injection molding machine shown in Figure 4.8. The machine's software makes it possible to monitor and control the parameters of production. Some preparation steps should be done before running IMM.



Figure 4.8. Injection molding machine used to produce samples.

The polymer pellets to be used in production are filled in the hopper. The hopper is positioned just above the barrel. It should be noted that the hopper should not be in its forward position, as in the forward position all the pellets would flow to the front of the machine. The forward position is used to empty the remaining pellets after production.

As the feeding system of the EM 50/300 Battenfeld model is gravity-fed, polymer pellets are filled into the hopper manually. The lid of the hopper is opened before feeding and closed after feeding. Excess temperature should be avoided; otherwise the polymer pellets will melt before entering the barrel and get stuck on the hopper forming a neck.

The main switch of the machine is located at the backside. To have appropriate cooling, water is fed to the cooling system. After starting the machine, it takes 3-4 minutes for the screen to start showing data, then; operation of the machine can be started using the control panel. The control panel consists of a monitoring screen and a key panel shown in Figure 4.9. Items of the control panel are listed in Table 4.3.

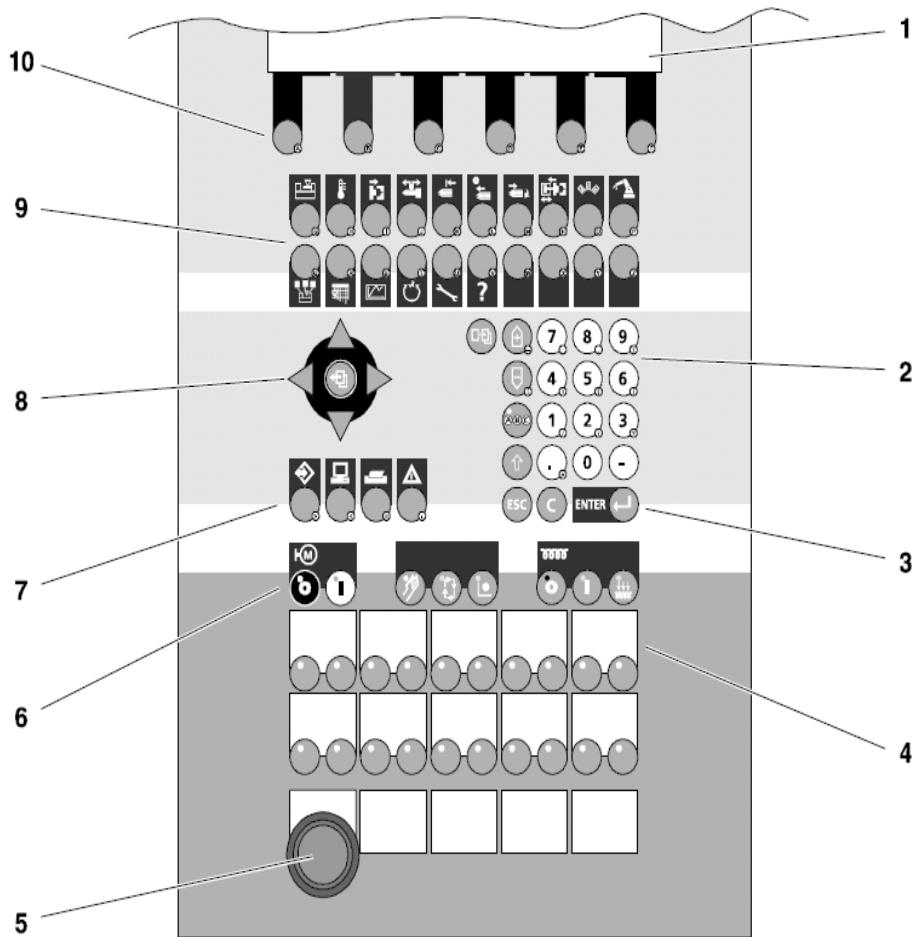


Figure 4.9. Control panel of the machine [18].

When operating the IMM, the first step is starting the motor by pressing the “drive” key, and then switching on the drive by clicking the start button on the drive key.

If the emergency stop button is pushed the machine will not start, therefore it is important to release all emergency stop buttons. The machine will not work if any of the safety gates are open or are not closed properly. For this reason all of the four safety gates need to be closed.

The red triangle on the top bar of the control panel indicates that the interrupt list has to be cleared from alarms. Press the “alarm” key to see alarms on the interrupt list. The interrupt list will list all the current alarms.

Table 4.3. Parts of the control panel.

Number	Item
1	Monitoring screen
2	Numerical keys
3	“Enter” key
4	Function keys
5	Emergency stop key
6	Function keys
7	Function keys
8	Cursor keys
9	Function keys
10	Soft keys

Figure 4.10 shows the appearance of the interrupt list and some alarm messages. If the meaning of the message is not clear, the meaning of the alarm messages can be found from the alarm list given in the manual of the machine. For example alarm 210, purge guard limit switching monitoring is an alarm for unopened power supply.

The password entrance and preparations of the machine have to be done in the manual mode. For this reason, the “mode” key is pressed and the manual mode button on Table 4.4 should be pushed.

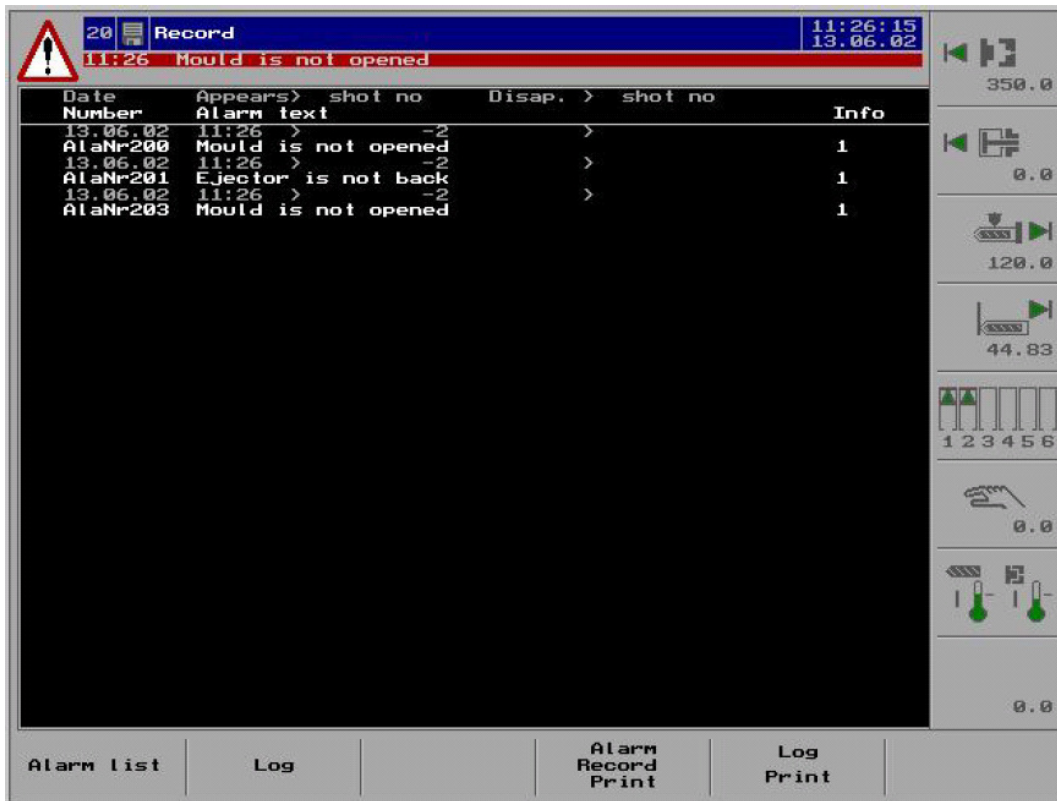








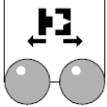
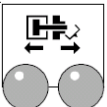
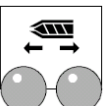
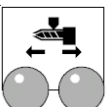

Figure 4.10. Appearance of the interrupt list of the Battenfeld EM 50/300 IMM [18].

To see the logon screen shown in Figure 4.11, the “machine in general” key is pressed. The password is entered on the logon screen. Going down in the menu with cursor arrow keys, the “Enter” key is pressed twice.

The password is entered again to confirm, and enter key should be pressed. If the password is accepted, the “User level 20” information will appear on the upper bar of the screen as information.

Heating is the main source for melting the polymer. To start the heating of the barrel, press the “heating” key and switch on the heating, then, barrel heating will start. The temperature of the barrel is controlled with sensors and data of temperature are sent to the control panel.

Table 4.4. Symbols of the most widely used keys on the Unilog [18].

Symbol	Name	Function
	“drive” key	Drive stop (with stop button) Drive start (with start button)
	“alarm” key	Lists the interrupt list
	“mode” key	Shifts to manual mode. Shifts to automatic mode. Shifts to setting (override) mode.
	“machine in general” key	Shows the logon screen.
	“enter” key	Accepts the data entered such as password and temperature values.
	“heating” key	Stops heating. Starts heating. Decreases temperature.
	“mold” key	Opens mold. Closes mold.
	“ejector” key	Forward button starts ejecting. Backward button stops ejecting.
	“injection/metering” key	Forward button starts injecting. Backward button enables metering.
	“barrel” key	Moves barrel forward. Moves barrel backward.
	“temperature control zone” key	Shows the temperature screen.

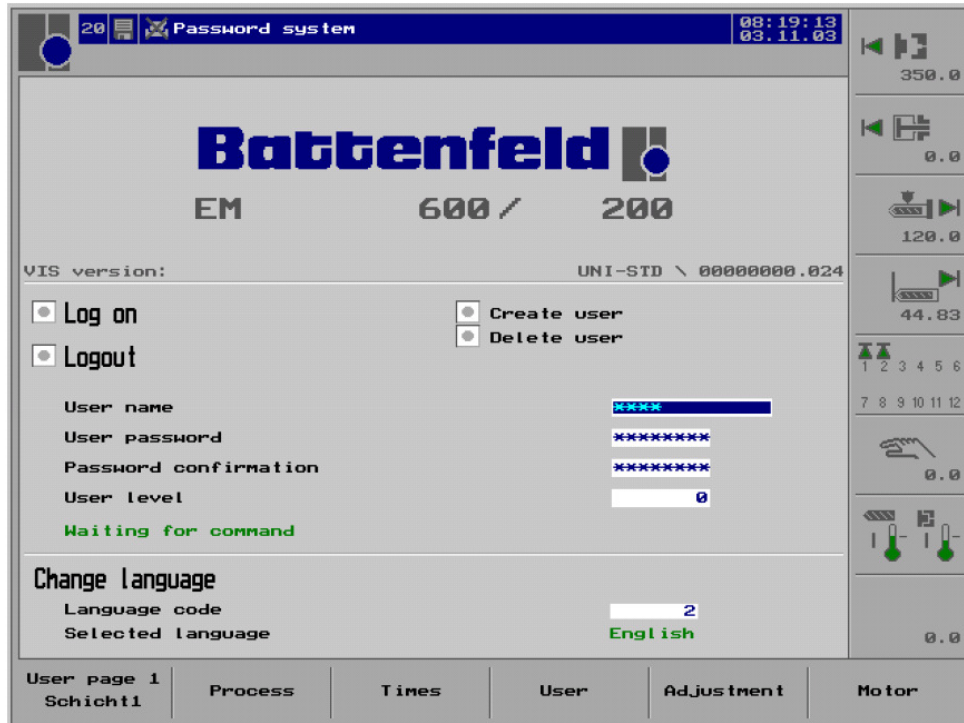


Figure 4.11. Logon panel of the IMM [18].

The mold is one of the most expensive parts of IMMs. It is important to have the mold open when starting to operate. Otherwise, the mold may be damaged by application of heavy pressure. To fully open the mold, “mold” key is pressed and its open button is hit.

To make sure that the polymer is not wasted before the desired temperature is obtained along the IMM, the ejector has to be in back position. “Ejector” key and its backward button should be pressed to have the ejector at the back position.

The injection unit and the nozzle have to be in the back position before starting the injection procedure. “Injection/metering” key, and its back button need to be pressed to have the nozzle at the back position.

To have the screw at the back position, the “barrel” key and its backward button need to be pressed. The barrel should move to the very back position.

On the main menu it is necessary to enter the desired values of volume flow (Q), volume of melt (V) and pressure (P) during the injection molding process.

The temperature range along the IMM is a very important issue to have flawless products. Suggested temperature values are given in the manual for specific polymers. However, the suitable temperature range from barrel to nozzle will be based on experience or may be found during production trials. “Temperature control zone” key need to be pushed to enter the desired temperature values for production; followed by hitting the “enter” key.

Especially if the temperature of the nozzle is at least 10°C or more, it is suggested to have zero melt pressure at the beginning of the production [18]. To make the melt pressure zero, the “machine in general” button is pushed. Then the “Zeroing the melt pressure” icon on the menu of this button is clicked.

Once the temperature range for production is entered into the program, it will take time for the machine to achieve the desired temperature values. At least 30 minutes warming time should be considered for the production. Temperature may be controlled from the “temperature control zone” button.

Once the temperature rises to the desired values, the “automatic mode” key is pressed. The cycle of the machine has steps of taking the screw forward, injecting, closing the mold, cooling the mold and opening the mold. It is very important to have the operator watching the production and attending the machine even in the automatic mode. The production in the automatic mode may encounter problems such as high temperature, high pressure, lack of cooling water, sample locked in the mold or other mechanical problems. Therefore, the operator has to be very careful. If a sample is not released by the mold, then the machine is set to override mode from the automatic mode. The mold is opened using the open button of the “mold key”;

then the “ejector” key is pushed forward to release the part from the mold. The “ejector” key is taken to back position so the ejector part will not be damaged during the injection. Before switching to automatic mode, the mold is opened fully, and the machine is set to automatic mode again by hitting the “automatic mode” key.

Online monitoring is one of the benefits of the software. On the main menu, it is possible to view the real values of volume flow (Q), volume of melt (V) and pressure (P) along the injection molding machine. Therefore, it is possible to decide if more polymer should be added or the pressure should be changed. In Figure 4.12, the main menu showing real data for the machine during production is shown. Even though in the figure only three points are selected to observe the real data, it is possible to select more points, up to eight. The delta values are the values entered for volume flow (Q), volume of melt (V) and pressure (P) by the user for production.

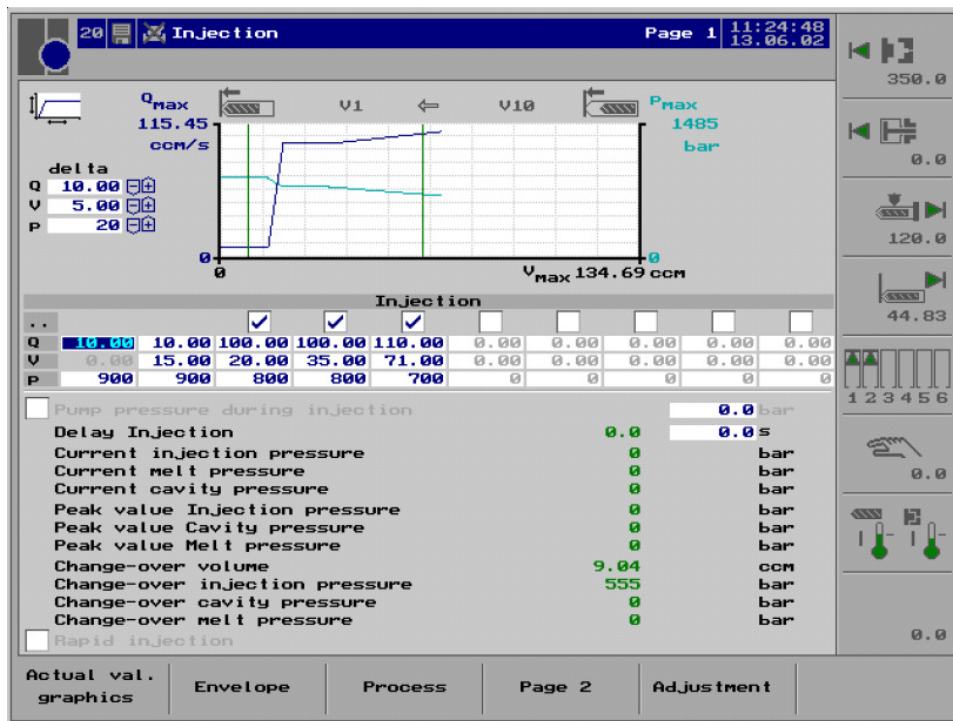


Figure 4.12. Main menu showing real data for the machine during production [18].

When production is finished, the machine should be shut down properly following these steps:

- Press “mode” key and hit the manual mode button.
- Press the “mold” key and open the mold.
- Press the “ejector” key and push the backward button.
- Press the “barrel” key and move the barrel backward.

The melt inside the barrel should be emptied before the machine cools down. If any melt remains in the machine after operating, the screw may be damaged and the subsequent production batch may be polluted by the remaining polymer. To collect the remaining polymer, after pressing the “injection/metering” key, a container is placed to collect the residual polymer melt; the “barrel” key forward button is pushed to start injecting the residual polymer melt inside the barrel.

Emptying the remaining polymer melt is useful for protecting the screw. Purging is the only way to make sure that the barrel is completely cleaned. To purge the machine, purging material or high density polyethylene is used. Purging is done using the “injection/metering” key forward button.

If any melt residue is left on the nozzle, it will clog the nozzle when it solidifies. To protect the nozzle, the tip of the nozzle should be cleaned with a cloth carefully avoiding the high temperature.

To close the machine, first, the heating should be stopped. Press the “heating” key and stop heating. Even though it is possible to shut down the machine without stopping the drive, this may cause damage to the fuse of the machine. Therefore, it is important to stop the drive by pushing the “drive” key and hitting the stop drive button.

It is important to close the cooling water supply not to cause any flood in the production area. The last steps required are switching off the main switch of the machine and switching off the power supply.

4.2.2. Instron 5565 Universal Tester

Instron 5565 Universal Tester is used for both tensile testing and three point bending testing. This machine is capable of applying either tensile forces or compressive forces. During tensile testing, the load cell and the crosshead speed are very important. For this reason, they should be chosen according to the standard that is used. Before starting tensile testing, it is crucial to balance the load to zero and to reset the extension.

In three point bending tests, the distance between the support beams and the crosshead speeds are very important and should be chosen according to the standard used.

4.2.3. Instron DynaTup 8250

Instron DynaTup 8250 is an impact machine with a hemispherical impactor head at 12.70 mm diameter. The impactor is made of stainless steel that has a compressive stiffness value of 60.92 N/mm. The impactor is dropped from a certain height and at a certain velocity onto the sample. For this reason, before testing, a velocity testing should be conducted. The sample should be clamped very carefully such that it does not move during the test. The drop height is very important for testing. The sensors built in the dart send data to the computer of the machine. As the sensors start to gather data when they reach the flag sensor, the flag sensor has to be adjusted according to the sample thickness for not losing any data.

Impact tests are carried out to determine the toughness of samples. The program gives either impact velocity-time or load-deflection graphs according to the user's needs. The impact velocity is the velocity of the crosshead at the point of contact. Some results that can be obtained from the impact tester are impact energy, impact velocity, energy to maximum load, total energy, deflection at maximum load, total deflection, total time, and yield and failure point.

4.3. Sample preparation

Carbon fibers purchased from Toho Tenax were in bundle form. Bundles were opened using pressurized air (Figure 4.13).

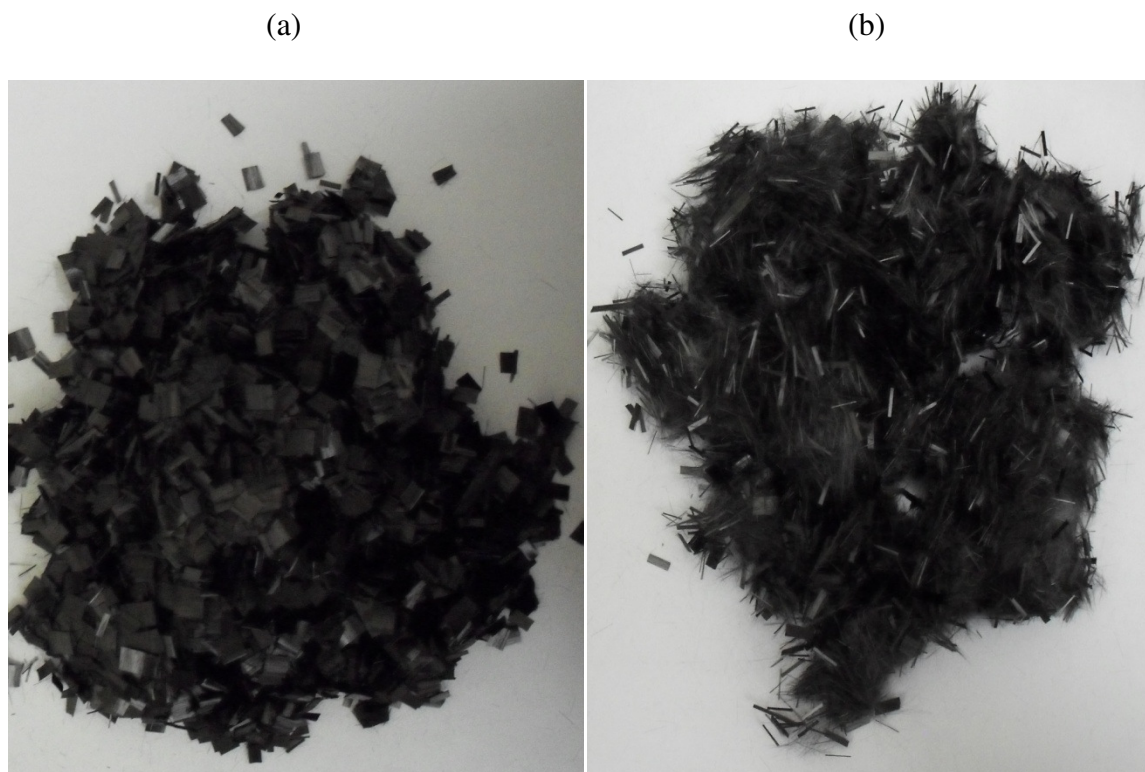


Figure 4.13. Carbon fibers in bundle form (a) and opened fibers using pressurized air (b).

The pellets used in blends were dried in a vacuum oven at 100°C overnight. The blends were prepared by in-situ mixing using an EM 50/300 Battenfeld injection molding machine, with

a 190-192-192-190-190°C temperature profile from nozzle to barrel and at 50°C mold temperature. Pressure values were 383 bars for injection pressure, and 364 bars for melt pressure. Processing time was 30 sec; injection time was 4-5 seconds and cooling time was 26 seconds. The distance between screw tip and mold was set to 53 mm.

The samples were injected into a mold to produce impact (ASTM D3763-06), tensile (ASTM D638-03), and 3-point bending (ASTM D790) testing bars. An average value of at least five measurements was reported for the test results.

The sample codes and blend compositions for each sample are listed in Table 4.5.

Table 4.5. Sample codes and blend compositions.

Sample Code	PP (wt %)	Glass fiber (wt %)	Carbon fiber (wt %)	Nanoclay (wt %)	Compatibilizer (wt %)
PP	100	–	–	–	–
GF1	99	1	–	–	–
GF4	96	4	–	–	–
GF7	93	7	–	–	–
C1	99	1	–	–	–
C4	96	4	–	–	–
C7	93	7	–	–	–
NN1	99	1	–	–	–
NN4	96	4	–	–	–
NN7	93	7	–	–	–
CMP-NN1	79	–	–	1	20
CMP-NN4	76	–	–	4	20
CMP-NN7	73	–	50	7	20

4.4. Tests

4.4.1. Tensile strength

To determine the fracture and tensile strength of the materials, tensile testing is done according to the ASTM D638-03 standard test. Tensile test results are given in Table 4.6; tensile graphs are given in Figure 4.26 -4.29.

Table 4.6. Results of the tensile tests (mean \pm standard deviation).

Sample Code	Tensile stress at Maximum Load (MPa)	Tensile strain at Maximum Load (%)	Energy at Maximum Load (J)	Elastic Modulus (MPa)
PP	18.64 \pm 8.79	2.2 \pm 0.45	0.36 \pm 0.06	1226.32 \pm 4.13
GF1	19.60 \pm 0.20	1.11 \pm 0.05	0.74 \pm 0.09	3361.89 \pm 12.26
GF4	23.23 \pm 0.42	1.80 \pm 0.17	1.62 \pm 0.20	2753.77 \pm 164.88
GF7	24.30 \pm 0.15	2.42 \pm 0.04	2.55 \pm 0.05	2468.51 \pm 83.72
C1	23.90 \pm 0.16	1.85 \pm 0.01	1.67 \pm 0.01	2516.92 \pm 49.66
C4	24.55 \pm 0.30	2.2 \pm 0.05	2.09 \pm 0.08	2251.45 \pm 23.33
C7	24.92 \pm 0.95	1.76 \pm 0.18	1.69 \pm 0.68	2123.03 \pm 117.52
NN1	23.33 \pm 0.16	2.41 \pm 0.12	2.30 \pm 0.12	2139.69 \pm 88.25
NN4	22.09 \pm 0.35	2.18 \pm 0.12	1.93 \pm 0.14	2203.48 \pm 130.48
NN7	19.95 \pm 0.70	1.95 \pm 0.70	1.59 \pm 0.12	2350.86 \pm 90.76
CMP-NN1	22.78 \pm 0.17	2.22 \pm 0.05	2.16 \pm 0.05	2418.53 \pm 67.10
CMP-NN4	23.59 \pm 0.12	2.36 \pm 0.04	2.39 \pm 0.06	2371.75 \pm 11.29
CMP-NN7	24.86 \pm 0.07	2.60 \pm 0.10	2.80 \pm 0.11	2199.47 \pm 86.07

Figure 3.3 shows the brittle characteristic of PP. Improvement in tensile strength is observed with reinforcements of carbon fiber, glass fiber and nanoclay-compatibilizer system. Figure 4.14 shows the tensile graph of the glass fiber reinforced samples and Figure 4.15 shows the tensile graph of the carbon fiber reinforced samples. For nanoclay reinforced samples, as

nanoclay is not dispersed evenly and tends to aggregate within the sample, tensile strength improvement is not achieved.

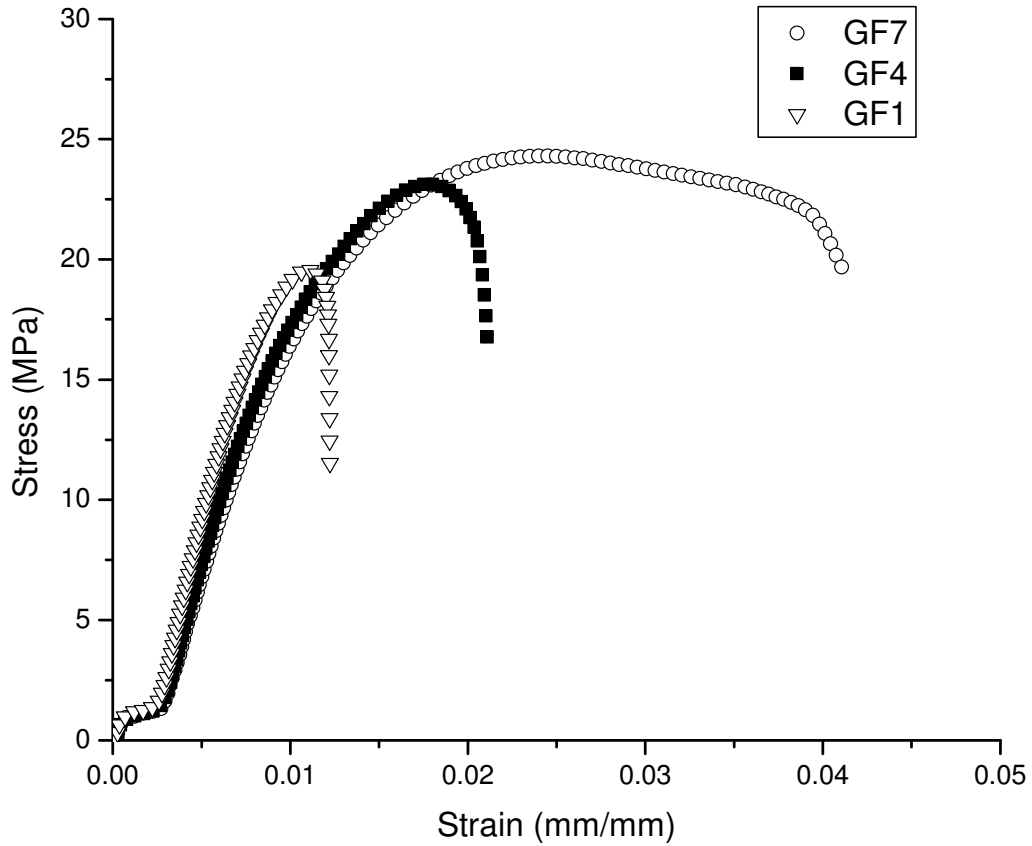


Figure 4.14. Tensile graph of glass fiber reinforced samples.

Figure 4.16 shows the tensile graph of NN1 sample while the tensile graph of NN4 and NN7 samples are given in Figure 4.17. Figure 4.18 shows the stress-strain graph of nanoclay and compatibilizer reinforced samples. Figure 4.18 proves that tensile property improvement is achieved when nanoclay is embedded in PP in the presence of compatibilizer.

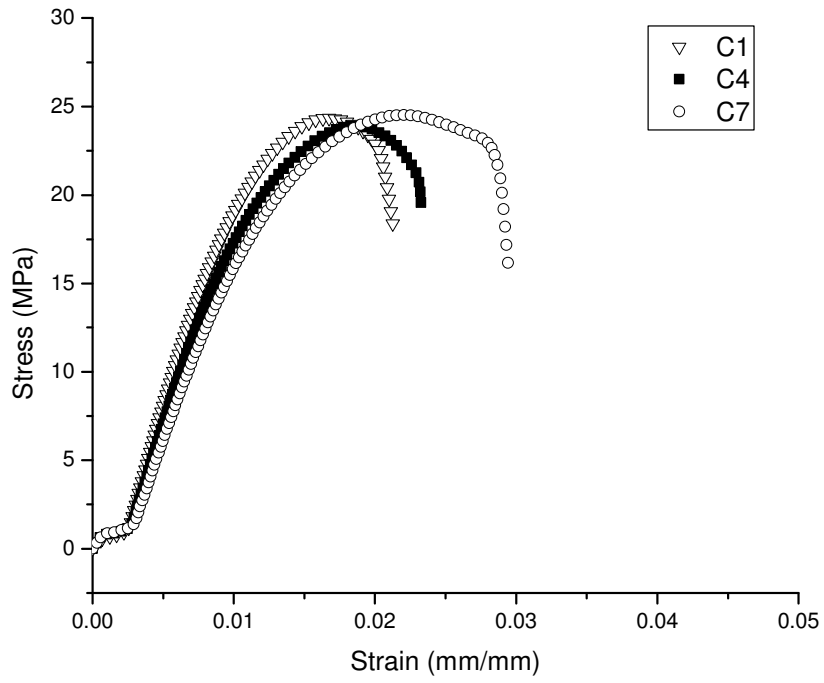


Figure 4.15. Tensile graph of carbon fiber reinforced samples.

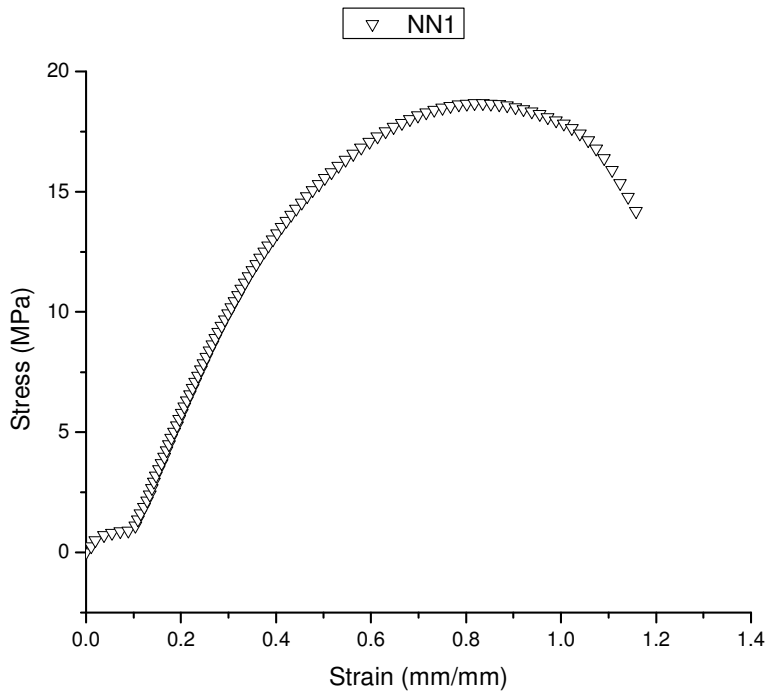


Figure 4.16. Tensile graph of NN1.

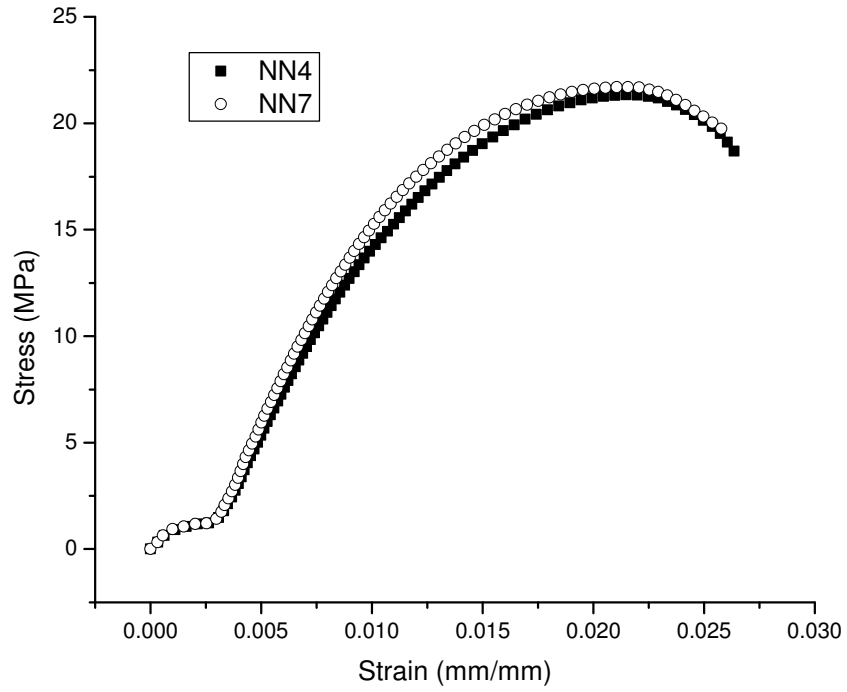


Figure 4.17. Tensile graph of NN4 and NN7.

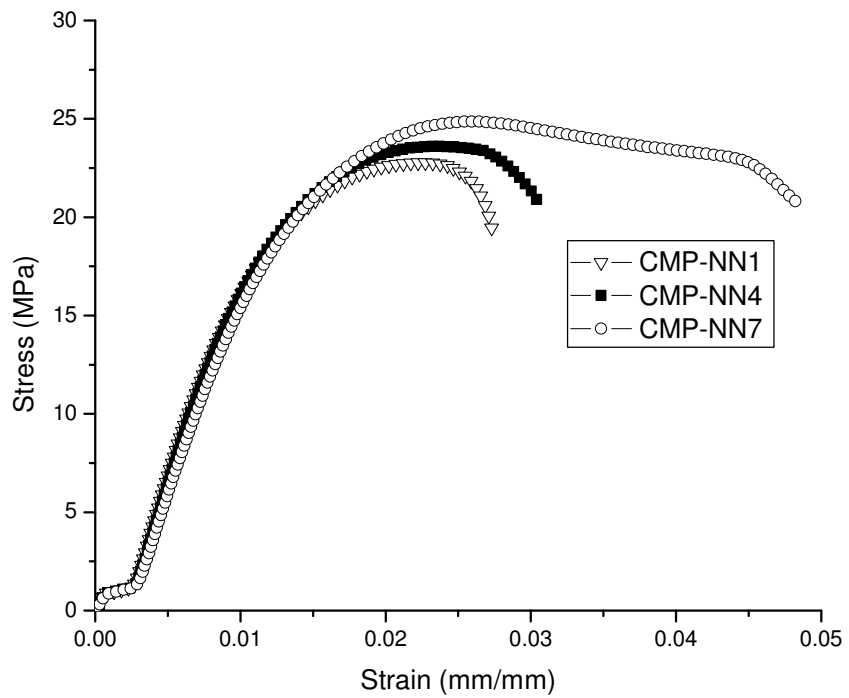


Figure 4.18. Tensile graph of nanoclay and compatibilizer reinforced samples.

4.4.1.1. SEM Analysis of the Samples

The tension fractured cross sections of the samples C1, C4, C7, GF1, GF4, GF7, NN1, NN4, NN7, CMP-NN1, CMP-NN4 and CMP-NN7 are given in Figures 4.19-4.30, respectively.

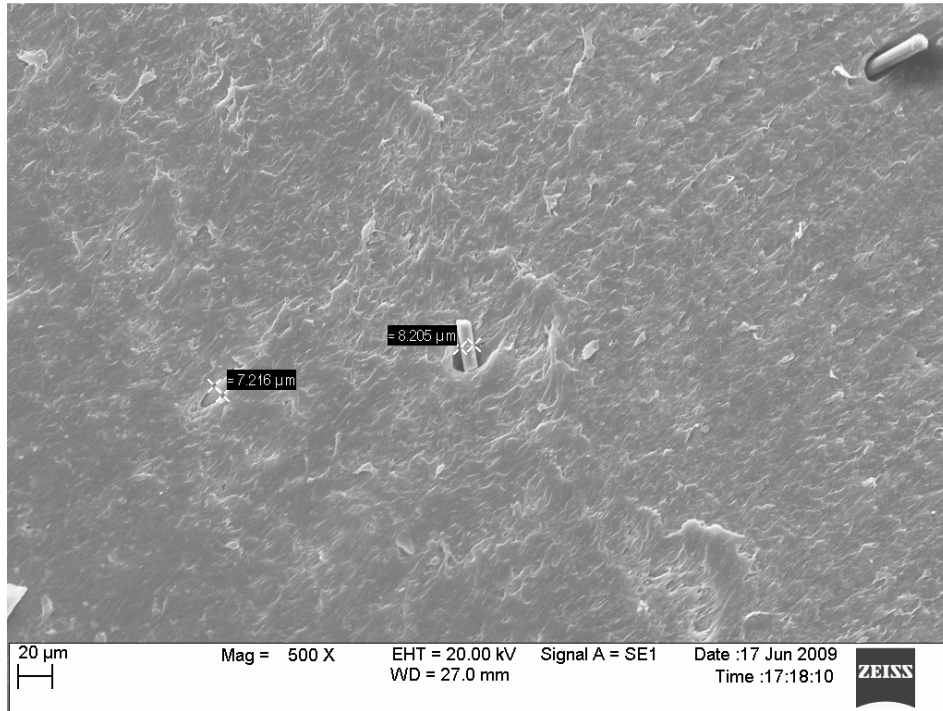


Figure 4.19. SEM micrograph of C1.

SEM analysis of fractured surfaces gives information about the diameter of fibers and fiber orientation in the composite. The cross sectional areas give an approximation of the orientation of fibers. However, to get more precise orientation information, longitudinal images need to be analyzed since the probability of error is higher when analyzing diameters compared to when analyzing fiber lengths for getting information about fiber orientation degrees [19]. Figure 4.19, Figure 4.20 and Figure 4.21 show that the carbon fiber

reinforcements are in micron scale and there is a void in the interphase of polypropylene matrix and carbon fiber.

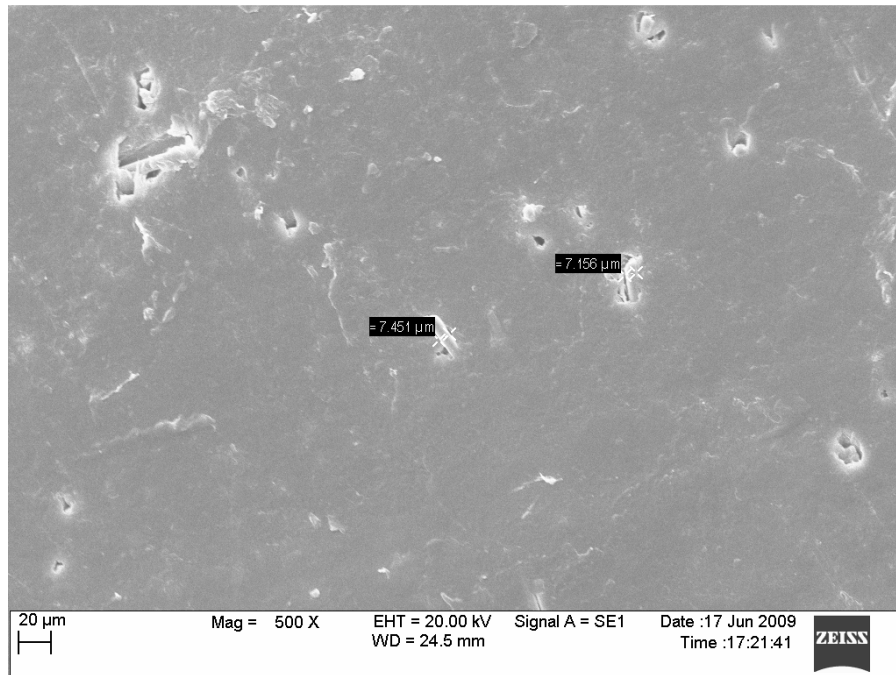


Figure 4.20. SEM micrograph of C4.

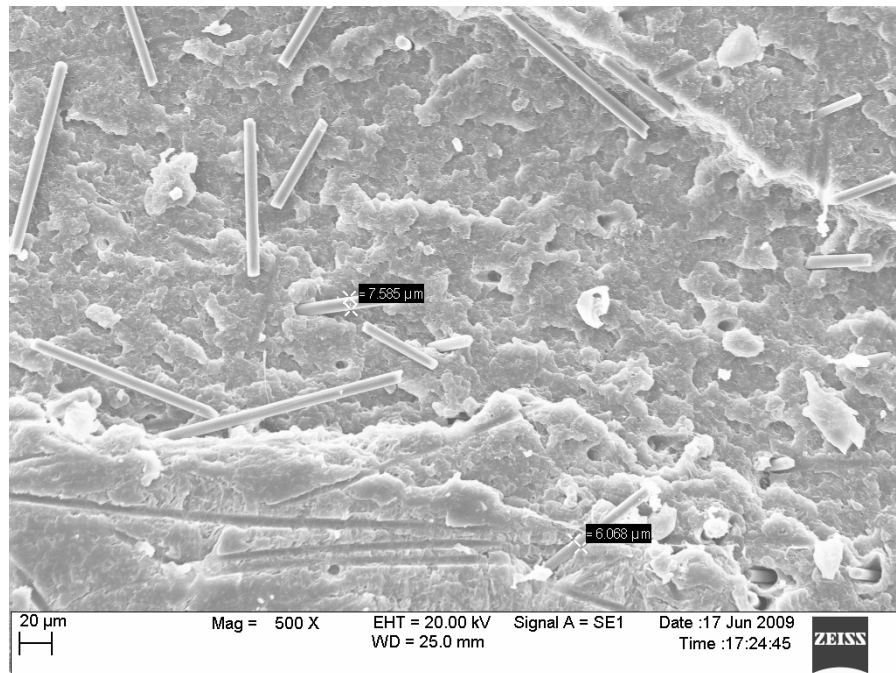


Figure 4.21. SEM micrograph of C7.

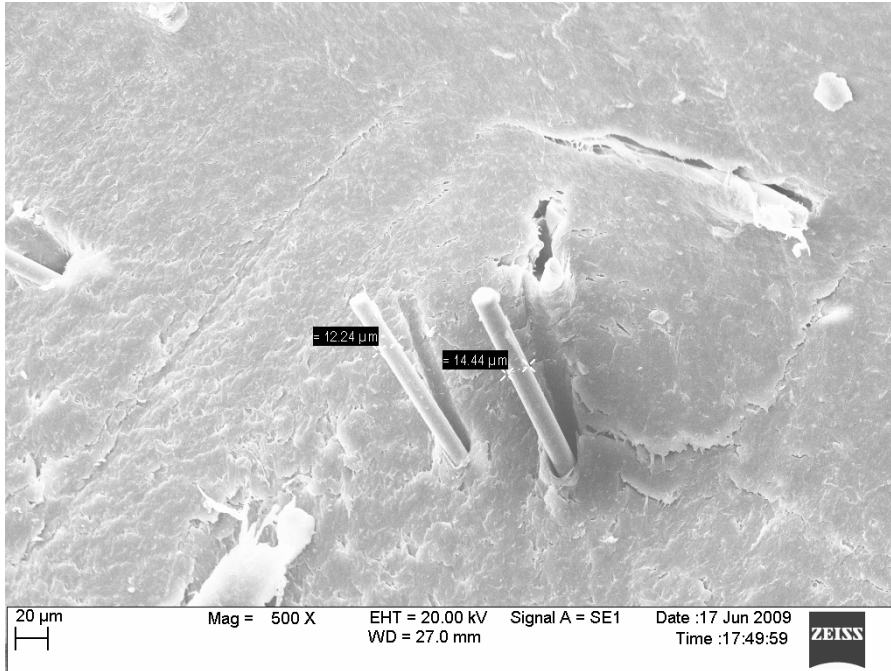


Figure 4.22. SEM micrograph of GF1.

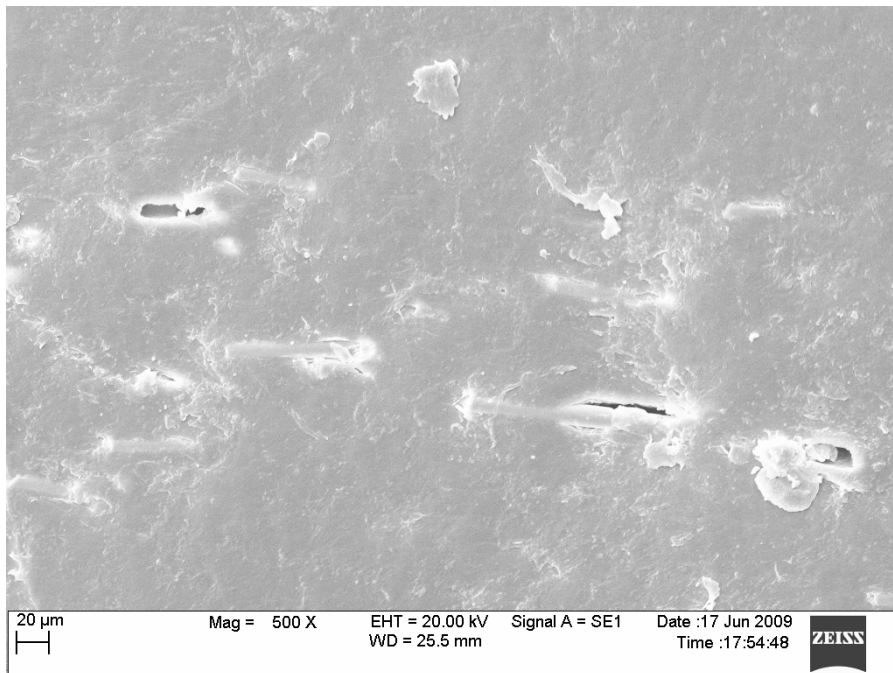


Figure 4.23. SEM micrograph of GF4.

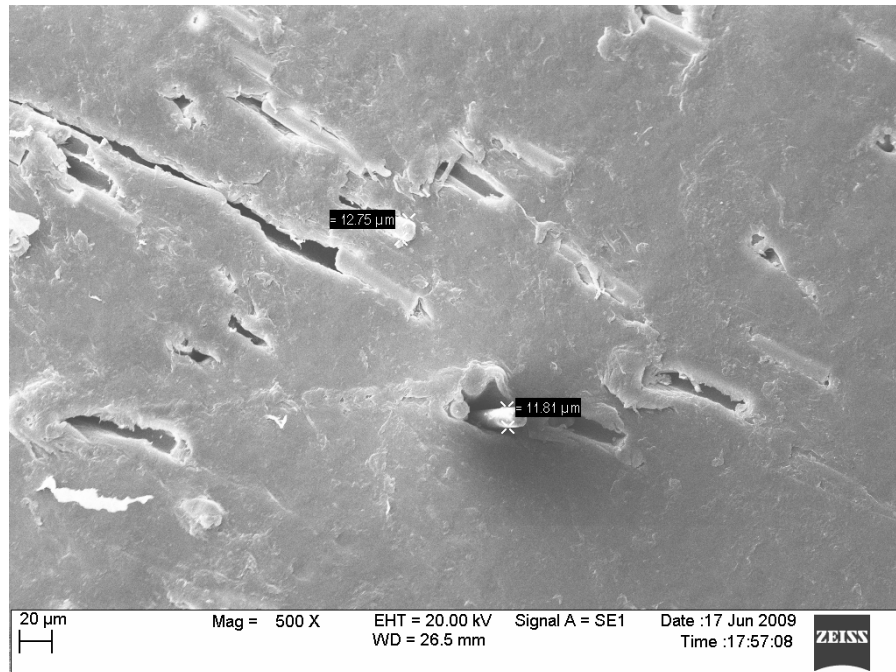


Figure 4.24. SEM micrograph of GF7.

Figure 4.22, Figure 4.23 and Figure 4.24 show that the glass fiber reinforcements are in micron scale, they are aligned both parallel and vertical to the flow direction and there is a void in the interphase of polypropylene matrix and glass fiber.

Figure 4.25, Figure 4.26 and Figure 4.27 show that nanoclay particles are aggregating in the polypropylene matrix. The tensile properties of nanoclay reinforced samples are not showing any increase, as nanoclay particles are acting as defects within the samples.

To have a better nanoclay distribution, samples having compatibilizer and nanoclay reinforcement are produced. Figures 4.28-30 prove that nanoclay has better distribution when compatibilizer is added to the polypropylene.

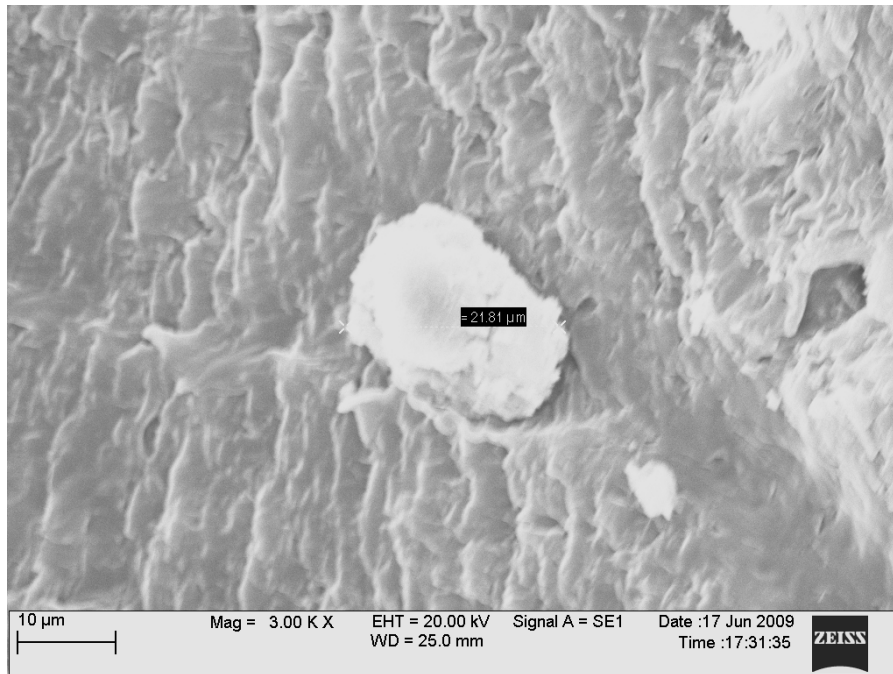


Figure 4.25. SEM micrograph of NN1.

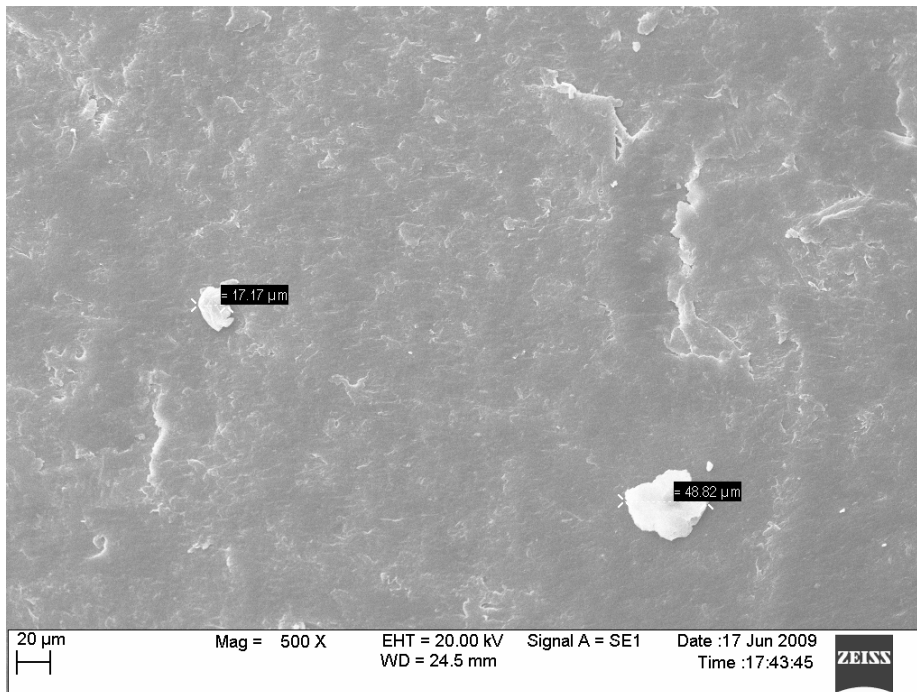


Figure 4.26. SEM micrograph of NN4.

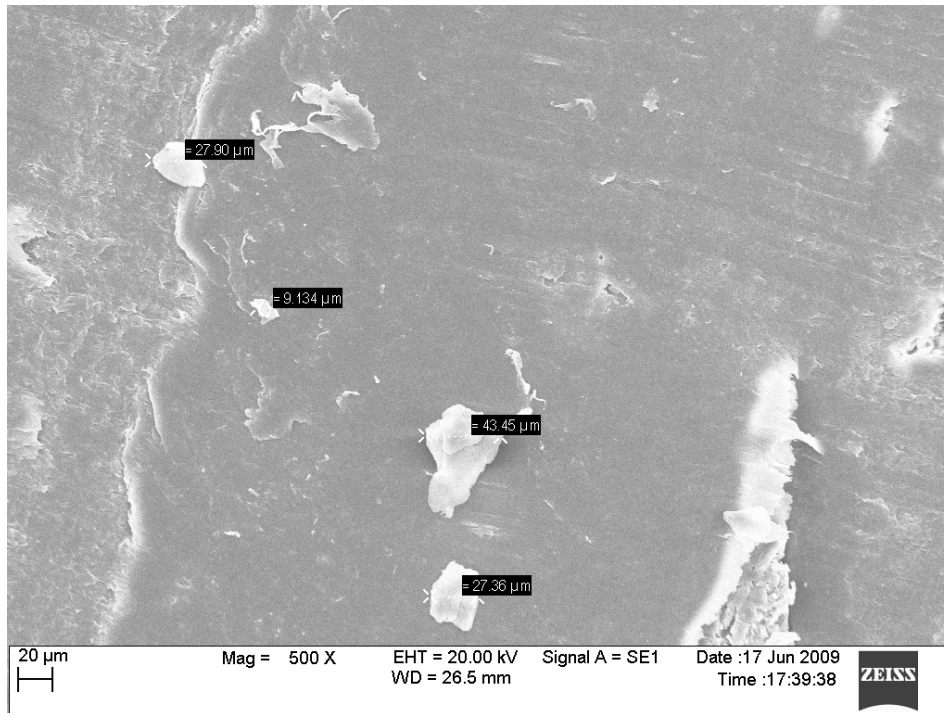


Figure 4.27. SEM micrograph of NN7.

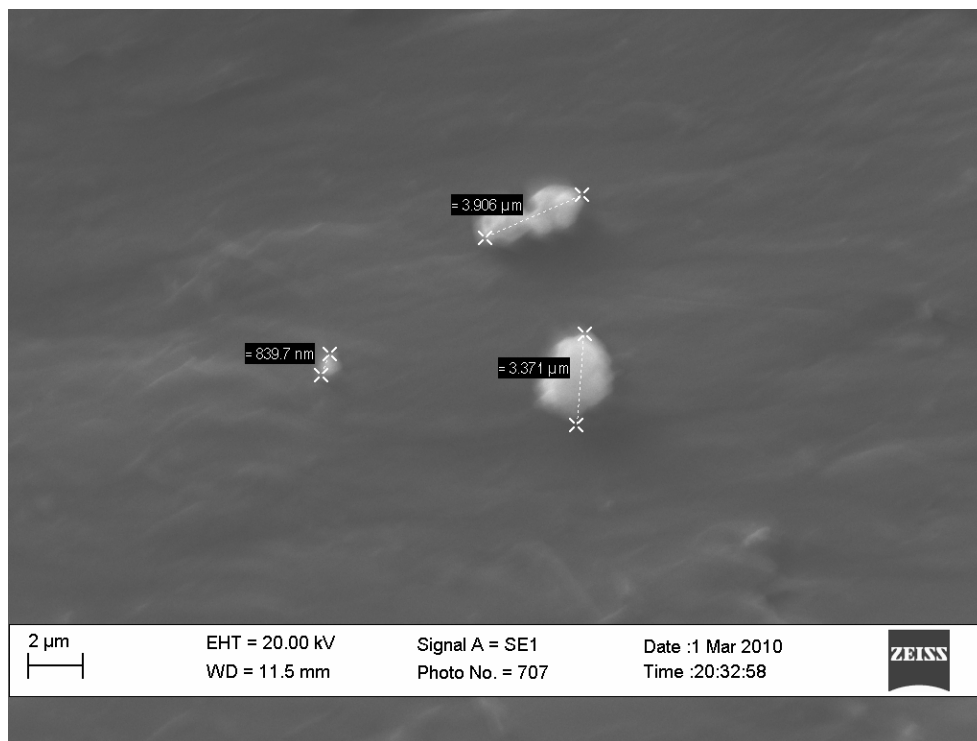


Figure 4.28. SEM micrograph of CMP-NN1.

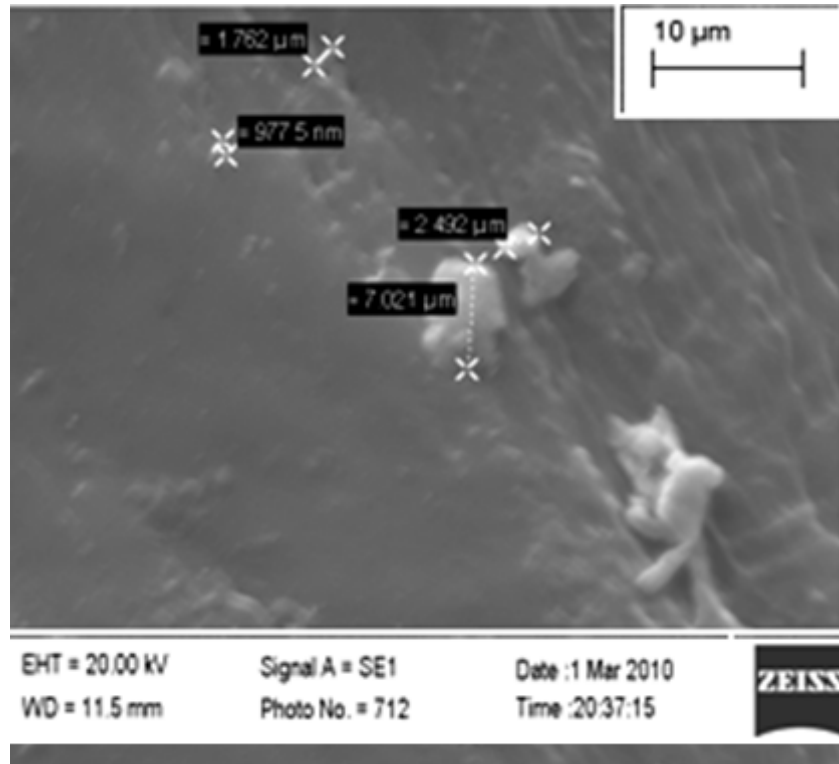


Figure 4.29. SEM micrograph of CMP-NN4.

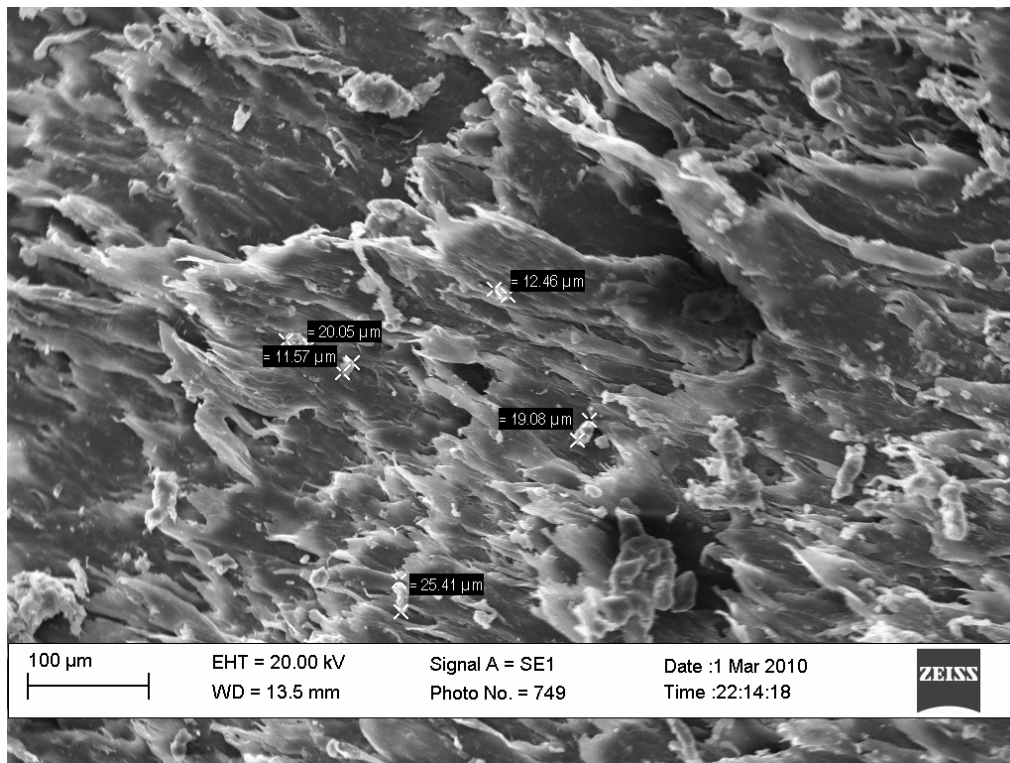


Figure 4.30. SEM micrograph of CMP-NN7.

4.4.2. Impact strength

Impact of a material can be improved by optimizing its crystallinity ratio, by blending a rubbery phase into the matrix, or by addition of a fibrous or non-fibrous reinforcer to the matrix. The impact strength may be determined using pendulum tests, falling weight tests, tensile impact tests, or tensile elongation tests. The area under the stress-strain curve of each test gives the toughness; but each test gives different values as they have different mechanisms [14].

To evaluate the toughness of the reinforced samples, impact tests were done according to the ASTM D3763-06 using falling weight. Impact energy values are given in Table 4.7.

Table 4.7. Results of the impact tests for pure polypropylene and glass fiber, carbon fiber and nanoclay reinforced polypropylene samples (mean \pm standard deviation).

Sample Code	Impact Energy (J)
PP	0.42 \pm 0.03
GF1	0.83 \pm 0.08
GF4	1.62 \pm 0.2
GF7	2.32 \pm 0.65
C1	2.35 \pm 0.24
C4	2.57 \pm 0.50
C7	3.18 \pm 0.37
NN1	3.70 \pm 0.69
NN4	2.88 \pm 0.55
NN7	2.33 \pm 0.76
CMP-NN1	3.00 \pm 0.44
CMP-NN4	3.72 \pm 0.72
CMP-NN7	4.93 \pm 0.69

Areas under load-deflection curves given in Figures 4.31-4.33-4.35-4.37-4.39-4.41 and 4.43 show that the total energy values are close to each other. This proves that, frictional energy is neglectable. Load-deflection graphs for impact tests show that all the samples had a brittle behavior and so their fracture process can be characterized as cracking.

Velocity drop in velocity-time curves given in Figures 4.32-4.34-4.36-4.38-4.40-4.42 and 4.44 show higher drops in samples having lower impact strength values. The energy turned into impact energy causes velocity drop, samples showing more velocity drop have lower impact strength values. PP sample has the lowest impact strength value among the samples, it exhibits the highest velocity drop from 4.3 m/s to 3.8 m/s.

Glass and carbon fiber reinforcements improved the impact strength values of pure PP. When the contributions of glass fibers and carbon fibers are compared, carbon fibers show more improvement in the impact strength of the sample. This difference may be caused by the brittle characteristic of glass fibers since they have low loop and knot strength of glass fibers.

Nanoclay reinforcement improves the impact strength of samples. The addition of compatibilizer to nanoclay reinforcement enhances the improvement in impact strength. This increase may be due to the stronger bonds formed between PP macromolecules and nanoclay particles in the presence of compatibilizer.

The increase of reinforcement weight percentage causes more improvement in impact strength of glass fiber, carbon fiber and nanoclay reinforced samples (Table 4.7). The weight percentages of reinforcements are in the low weight percentage range. To see the contribution of reinforcement weight percentages and determine if there is a maximum weight percentage value for impact strength improvement, samples having high weight percentages may be produced and tested.

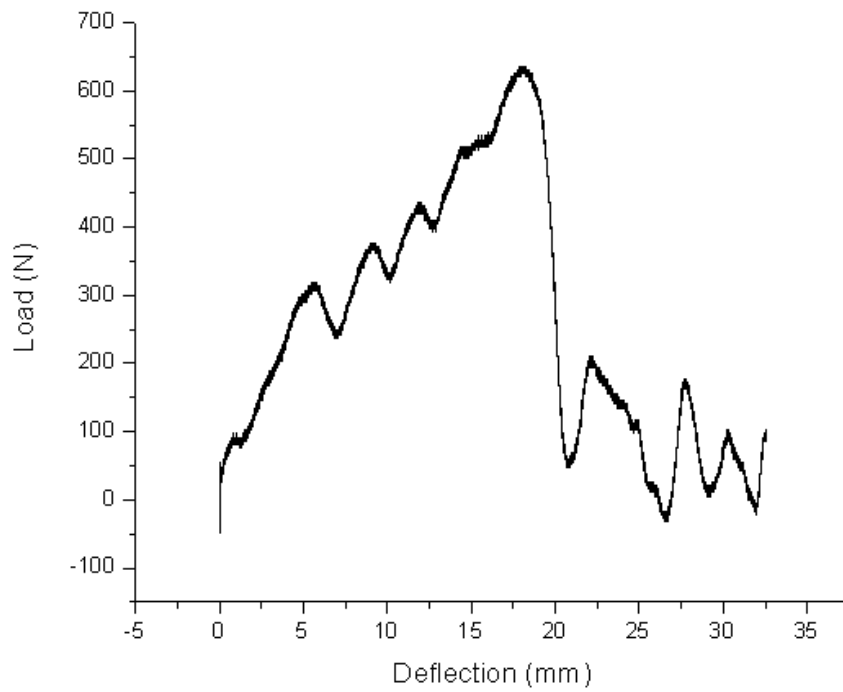


Figure 4.31. Load-deformation graph of PP.

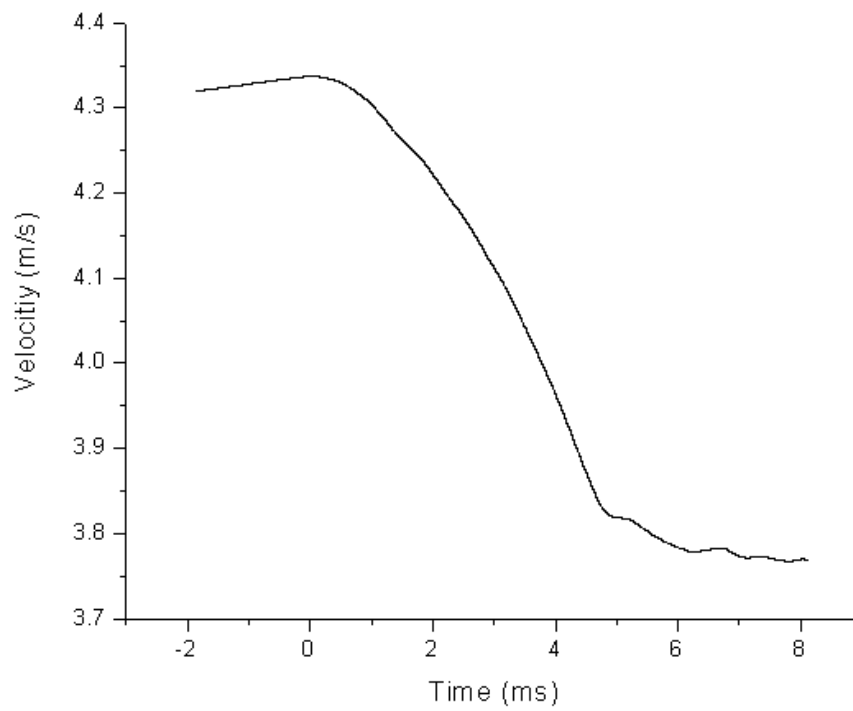


Figure 4.32. Velocity-time graph of PP.

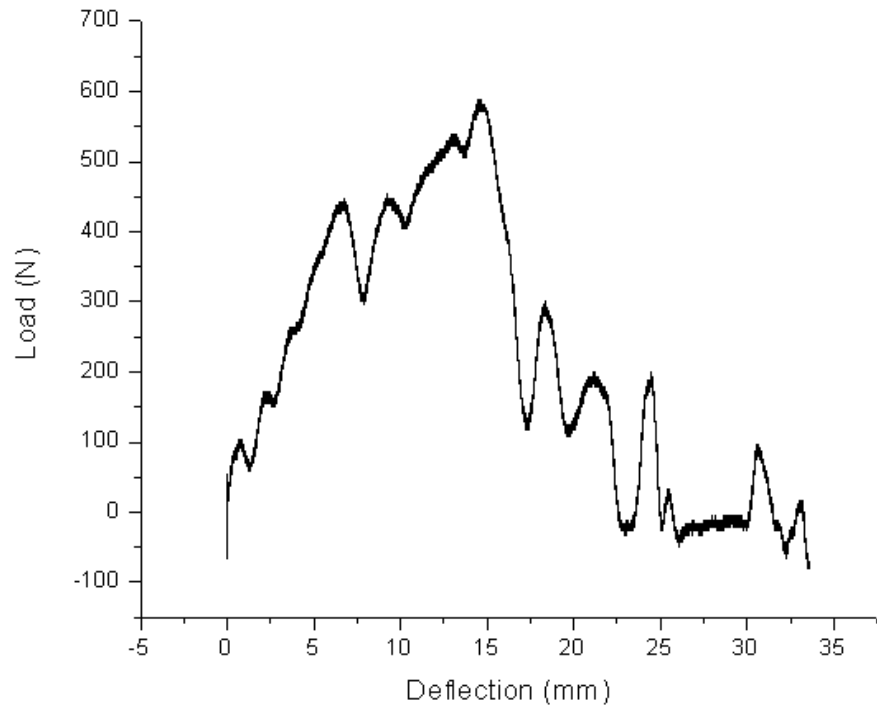


Figure 4.33. Load-deformation graph of GF1.

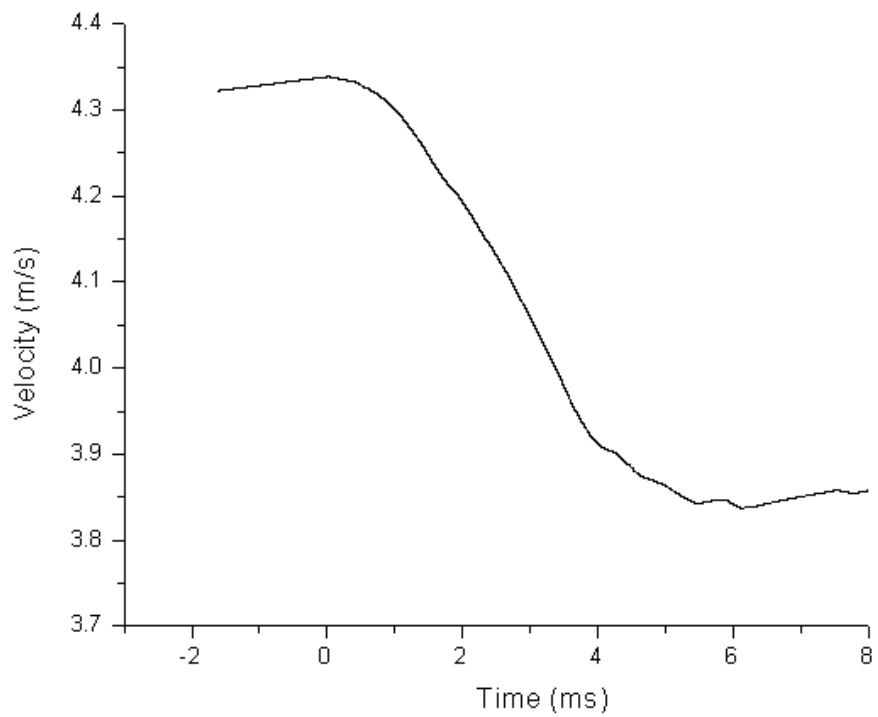


Figure 4.34. Velocity-time graph of GF1.

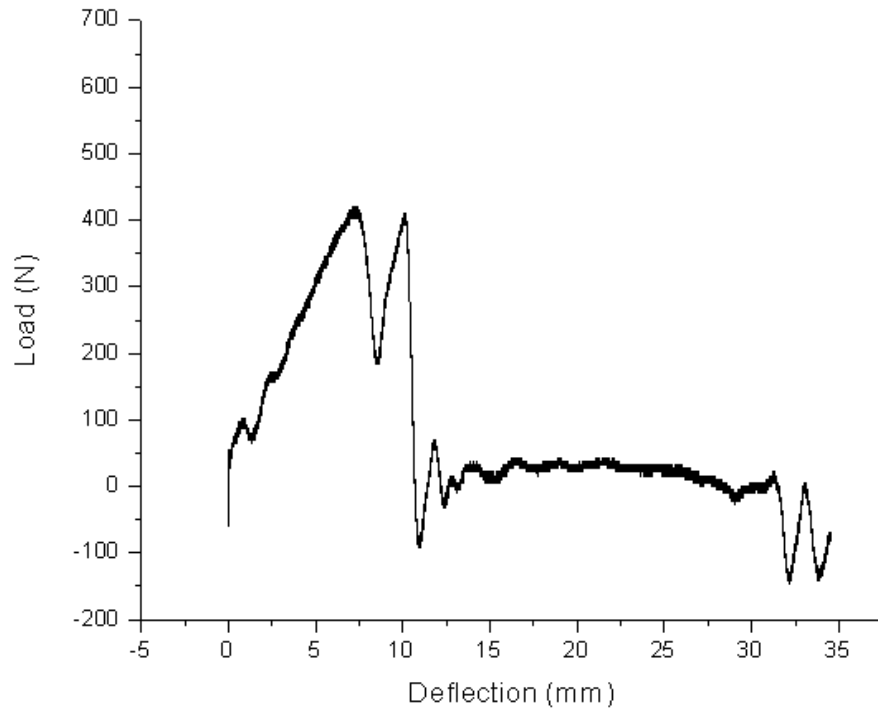


Figure 4.35. Load-deformation graph of GF4.

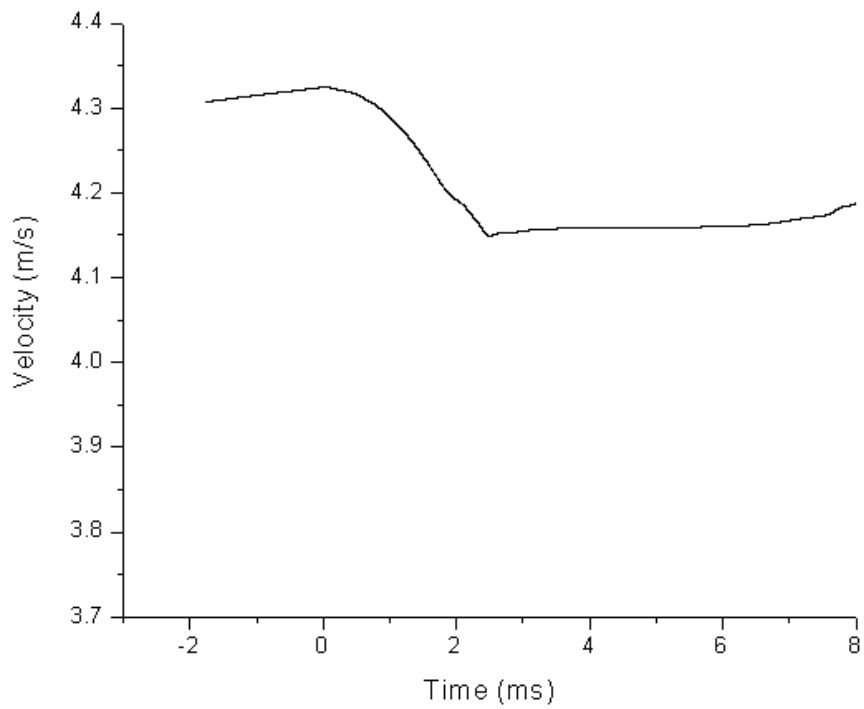


Figure 4.36. Velocity-time graph of GF4.

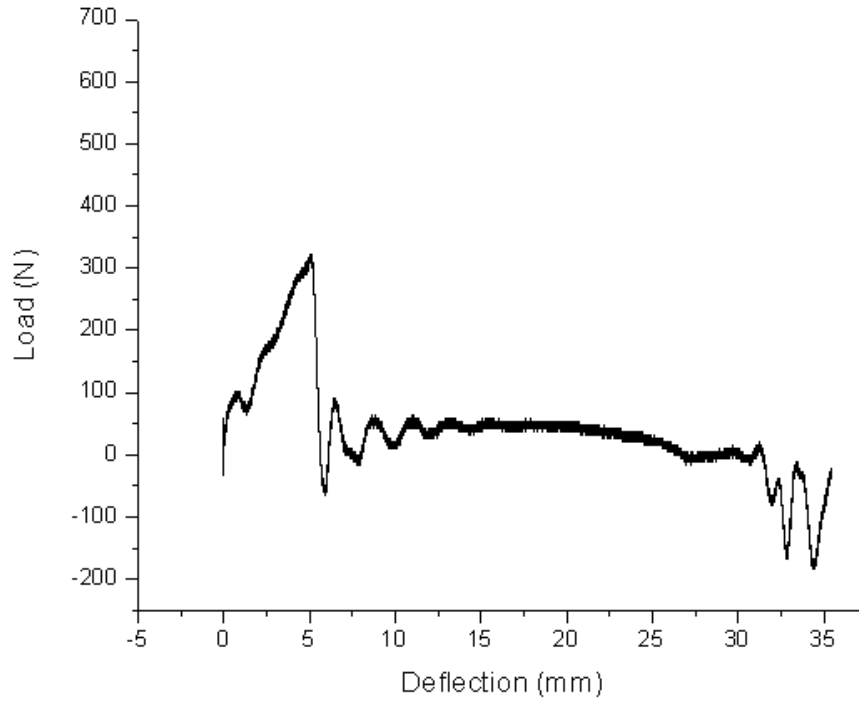


Figure 4.37. Load-deformation graph of GF7.

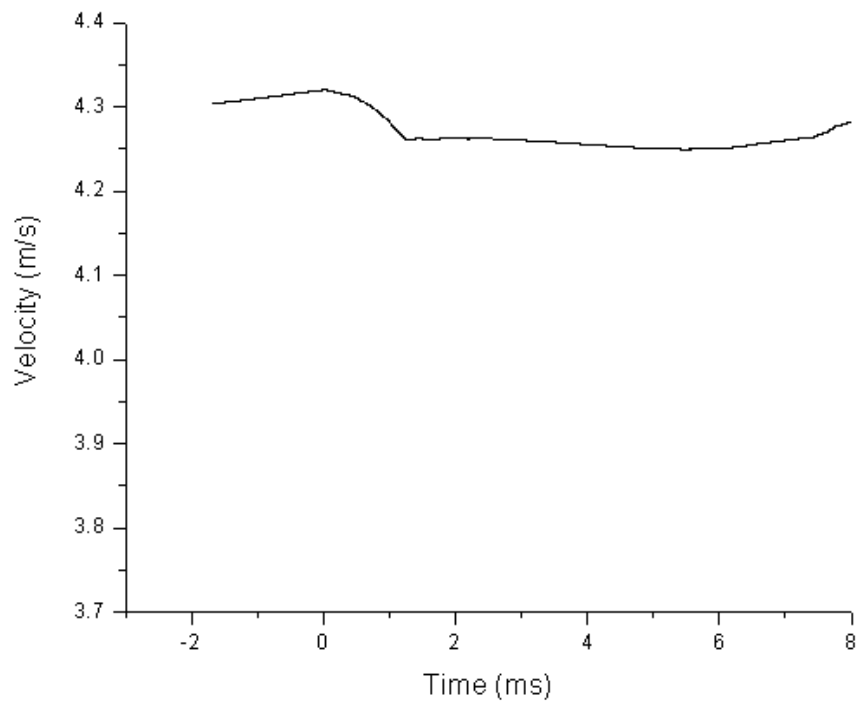


Figure 4.38. Velocity-time graph of GF7.

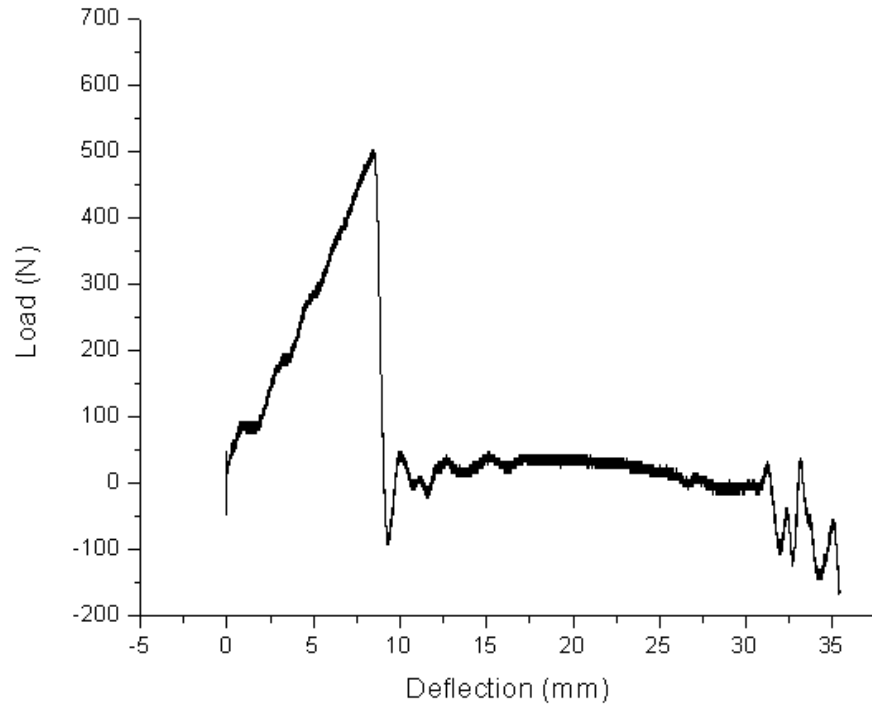


Figure 4.39. Load-deformation graph of C1.

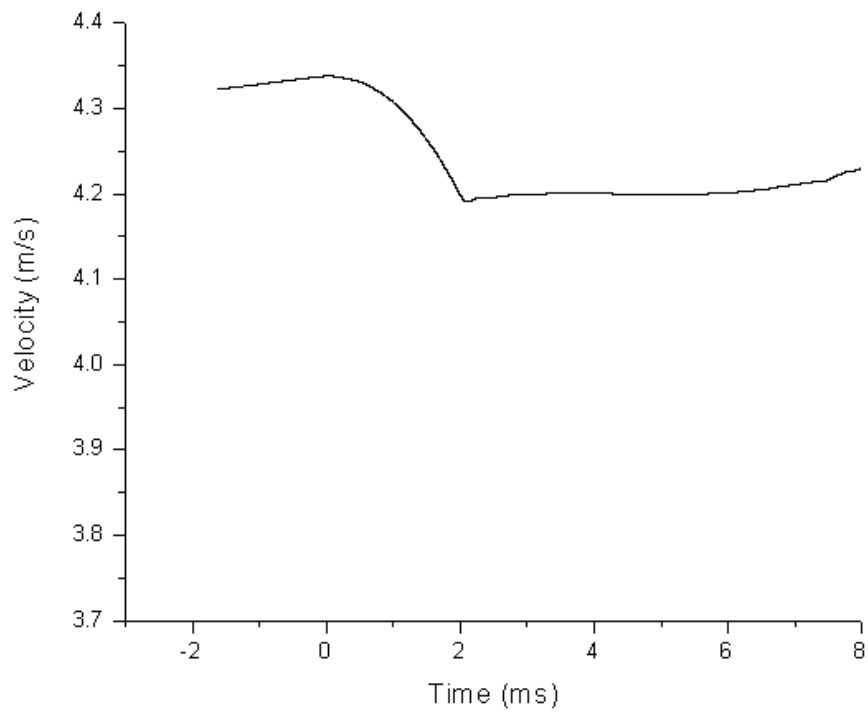


Figure 4.40. Velocity-time graph of C1.

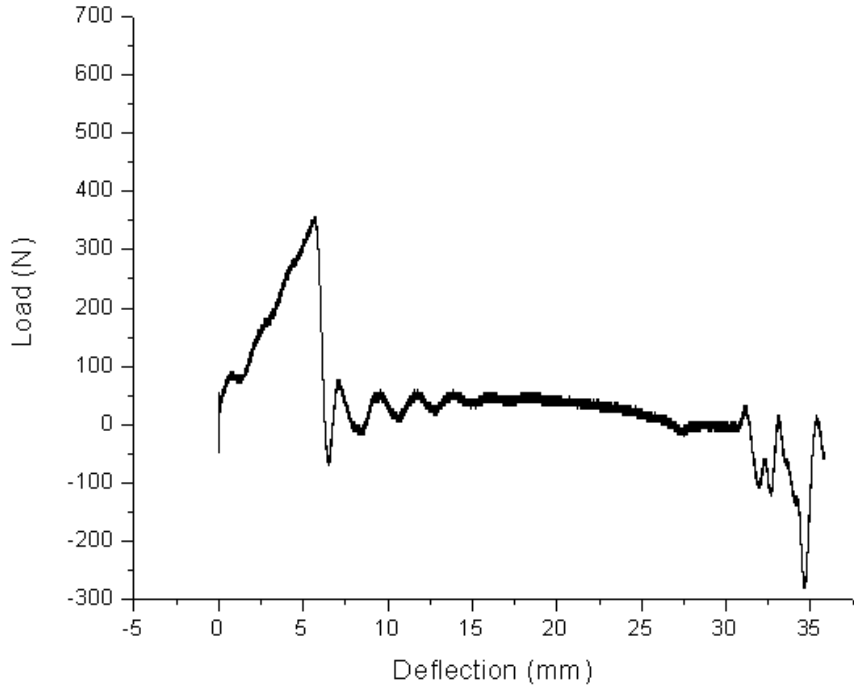


Figure 4.41. Load-deformation graph of C4.

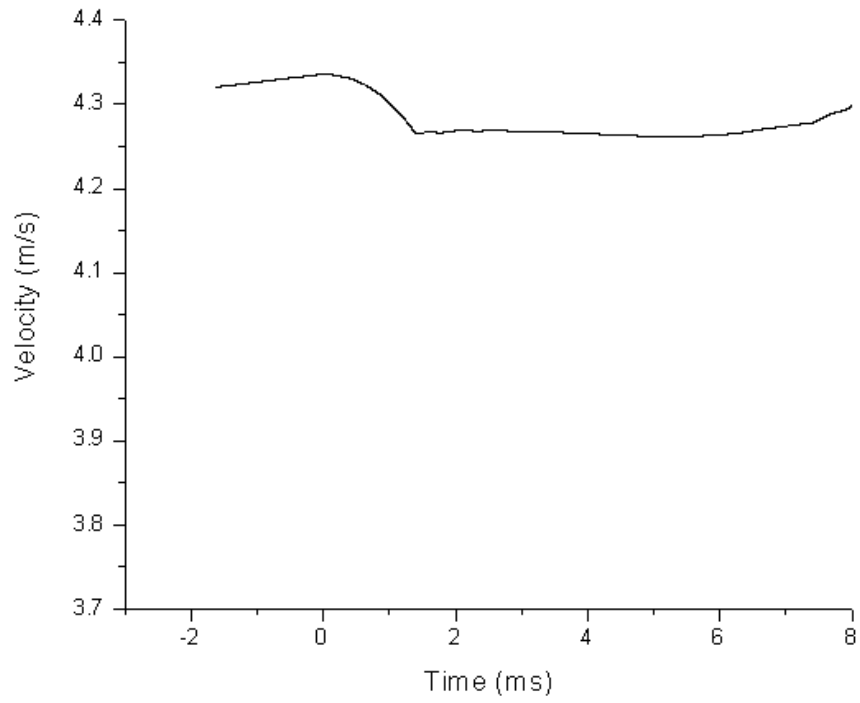


Figure 4.42. Velocity-time graph of C4.

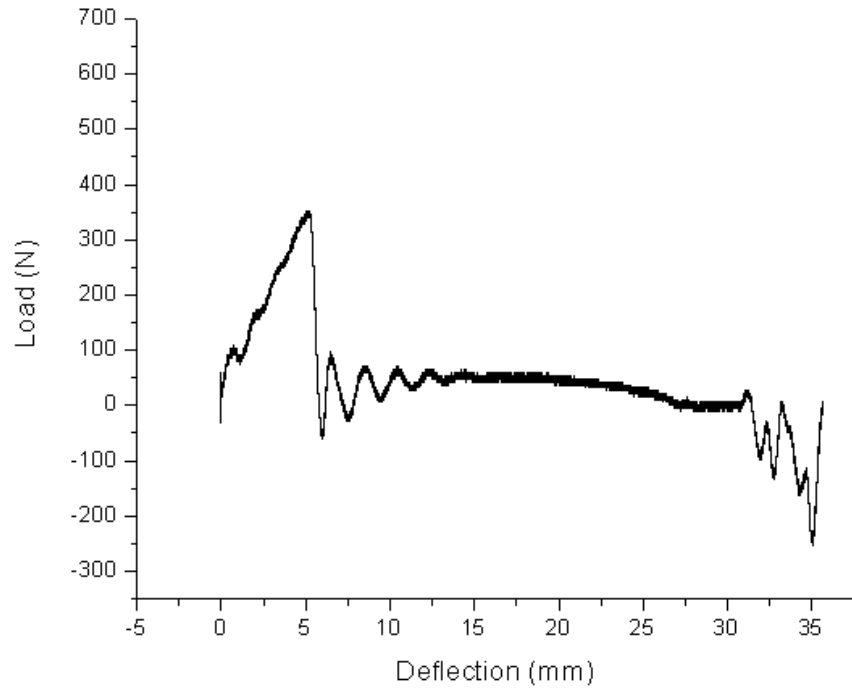


Figure 4.43. Load-deformation graph of C7.

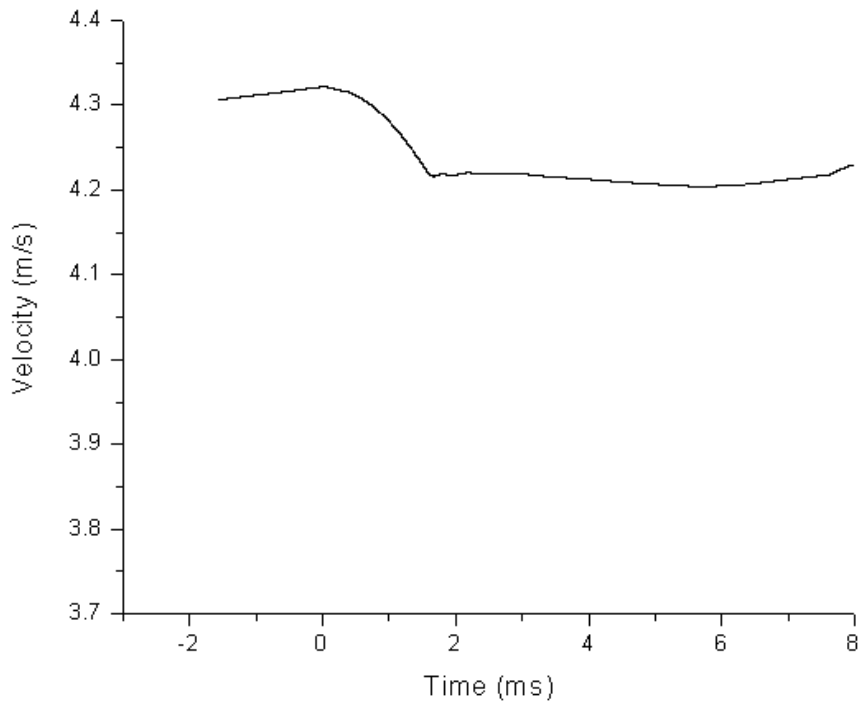


Figure 4.44. Velocity-time graph of C7.

4.4.3. Flexural strength

Materials can be strong in the longitudinal direction but they may be brittle to loads in the transverse direction. Three-point bending tests (3PB) were conducted to determine the flexural properties of the samples according to the ASTM D790-07; mean values of five specimens are obtained.

Test result values for pure polypropylene and PP reinforced with glass fibers, carbon fibers and nanoclay are given in Table 4.8.

Table 4.8. Three point bending test results for pure polypropylene and glass fiber, carbon fiber and nanoclay reinforced polypropylene (mean \pm standard deviation).

Sample Code	Maximum Load (N)	Maximum Stress (MPa)	Flexural modulus (MPa)	Flexural strain at Maximum Flexural stress (%)
PP	82.43 \pm 2.37	49.59 \pm 0.61	1713.93 \pm 48.11	9.56 \pm 0.22
GF1	55.51 \pm 0.56	34.17 \pm 0.44	987.04 \pm 33.87	6.77 \pm 0.13
GF4	58.95 \pm 1.51	36.41 \pm 0.91	1237.92 \pm 114.38	6.29 \pm 0.78
GF7	65.19 \pm 3.06	39.97 \pm 1.98	1603.94 \pm 110.08	9.18 \pm 1.07
C1	55.77 \pm 1.17	34.16 \pm 0.73	1002.47 \pm 40.87	6.72 \pm 0.07
C4	61.93 \pm 3.80	38.68 \pm 2.60	1785.27 \pm 137.52	8.81 \pm 1.04
C7	62.88 \pm 0.68	39.22 \pm 0.77	2018.75 \pm 168.03	9.48 \pm 0.15
NN1	52.23 \pm 0.58	31.67 \pm 0.41	997.66 \pm 29.68	6.38 \pm 0.51
NN4	50.65 \pm 0.65	30.79 \pm 0.45	985.48 \pm 75.20	5.83 \pm 0.53
NN7	50.09 \pm 0.99	30.48 \pm 0.60	975.15 \pm 26.93	5.88 \pm 0.24

Three point bending stress-strain graph of pure polypropylene is given in Figure 4.45. The results with glass fibers, carbon fibers and nanoclay reinforcement are shown in Figures 4.46-4.47, respectively.

Figure 4.45 shows the brittle behavior of PP samples in flexural testing. The brittle behavior of PP turns to be ductile when glass fibers, carbon fibers and nanoclay particles are added in PP. The addition of reinforcement causes a sacrifice in flexural strength. Even though pure PP sample has the highest flexural strength value among samples, increase in reinforcement gives an improvement in flexural strength. Pure PP samples break between 9-11 % strain rates while glass fiber, carbon fiber and nanoclay reinforced samples do not break even at 15 % strain rates. According to the ASTM D790-07 standard, if samples are not breaking test is stopped at 15 % strain rate. Additional testing may be conducted over 15 % strain rates to determine whether samples show breakage during flexural testing.

Figures 4.46, 4.47 and 4.48 show that increase of weight percentages of glass fiber, carbon fiber and nanoclay reinforcements increase the flexural strength of samples. The increase in weight percentages of carbon fibers and glass fibers give more improvement in the flexural strength values of samples compared to nanoclay reinforcement.

The stress-strain curves obtained during flexural strength testing have characteristic shapes which are ‘fingerproof’ graphs for each sample. The stress-strain curves of samples are getting more obvious as reinforcement weight increases (Figure 4.46-4.47). Compared to glass fiber and carbon fiber reinforced samples, nanoclay reinforcement shows a smoother stress-strain curve and this smooth characteristic remains smooth when reinforcement weight percentage is increased (Figure 4.48).

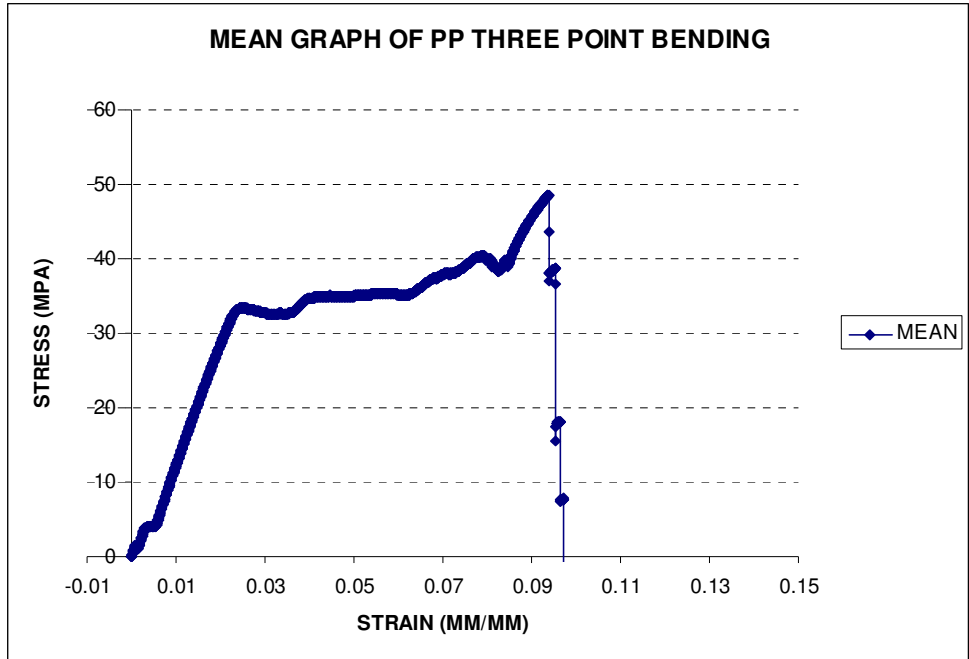


Figure 4.45. Three point bending graph for pure polypropylene.

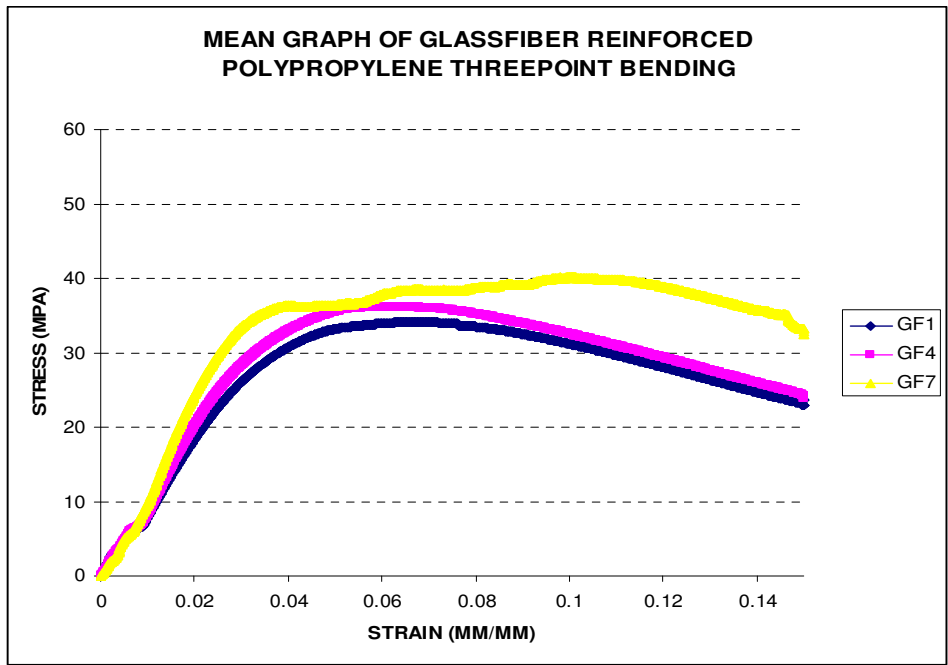


Figure 4.46. Three point bending results for glass fiber reinforced PP.

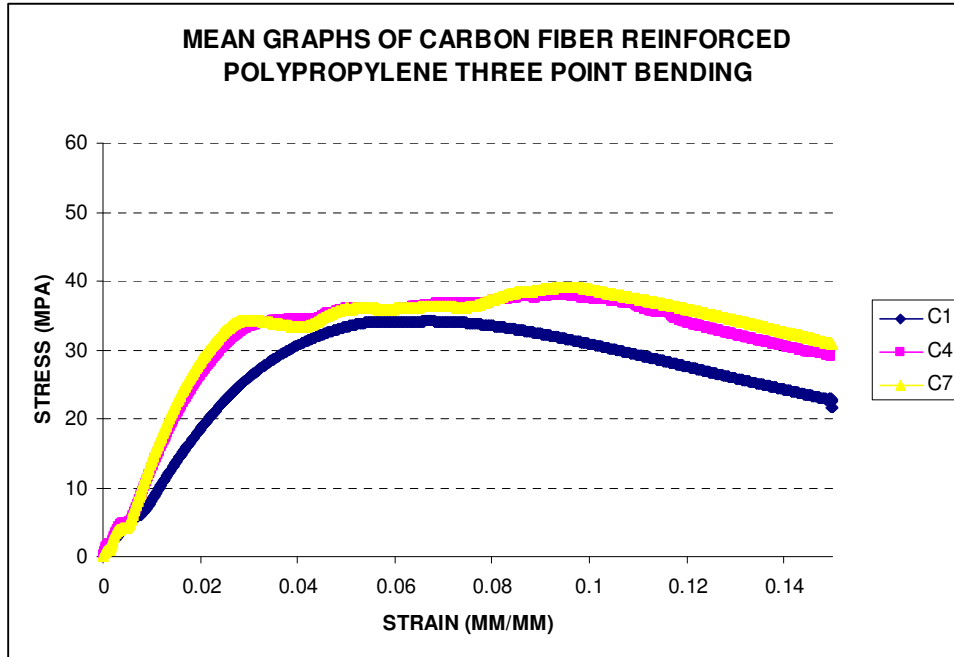


Figure 4.47. Three point bending results for carbon fiber reinforced PP.

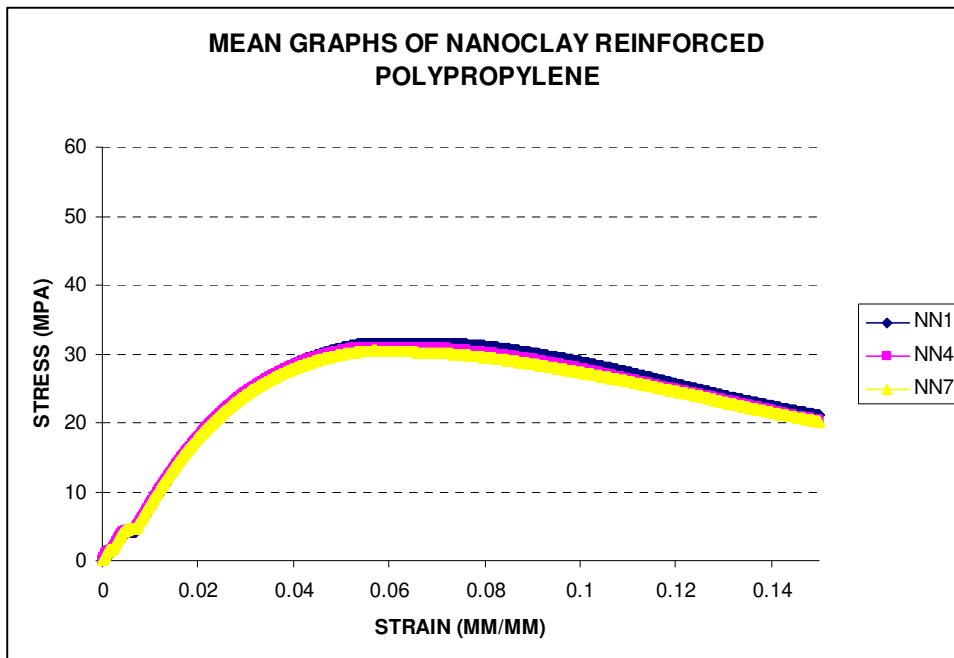


Figure 4.48. Three point bending results for nanoclay reinforced PP.

4.5. References

- [1] Mallick, P. K., "Fiber Reinforced Composites Materials, Manufacturing and Design", CRC Press, 240-361 (1993).
- [2] Adanur, S., "Wellington Sears Handbook of Industrial Textiles", Technomic Publishing Co, 36-47 (1995).
- [3] http://cheserver.ent.ohiou.edu/ChE231DR/Chapter_04_outline.pdf, access date 03.05.2010.
- [4] Peters, S. T., "Handbook of Composites", Chapman & Hall, 525-555 (1998).
- [5] Bunsell, A.R., and Berger, M.H., "Fine Ceramic Fibers", CRC Press, 1-2 (1999).
- [6] <http://www.geocities.com/vpkelly.geo>, access date 03.01.2010.
- [7] Scarfato, M. P., Scatteia, L., Costa, G., and Acierno, D., Effect of the Organoclay Structure on Morphology and Rheological Response of PBT Nanocomposites, *Macromol. Symp.*, **228**, 125-137 (2005).
- [8] Solar, L., Nohales, A., Munoz-Espi, R., Lopez, D., and Gomez, C. M., Viscoelastic Behavior of Epoxy Prepolymer/ Organophilic Montmorillonite Dispersions, *Journal of Polymer Science: Part B: Polymer Physics*, **46**, 1837-1844 (2008).
- [9] Pascual, J., Fages, E., Fenollar, O., Garcia, D., and Balart, R., Influence of the Compatibilizer/Nanoclay Ratio on Final Properties of Polypropylene Matrix Modified With Montmorillonite-Based Organoclay, *Polym. Bull.*, **62**, 367-380 (2009).
- [10] Hasegawa, N., and Usuki, A., Silicate Layer Exfoliation in Polyolefin/Clay Nanocomposites Based on Maleic Anhydride Modified Polyolefins and Organophilic Clay, *Journal of Applied Polymer Science*, **93**, 460-470 (2004).
- [11] Lopez-Quintanilla, M. L., Sanchez-Valdes, S., Ramos de Valle, L. F., and Medellin-Rodriguez, F.J., Effect of Some Compatibilizing Agents on Clay Dispersion of

Polypropylene-Clay Nanocomposites, *Journal of Applied Polymer Science*, **100**, 4748-4756 (2006).

[12] http://www2.dupont.com/Fusabond/en_US/assets/downloads/fusabond_p613.pdf, access date 04.01.2009.

[13] http://enr.bd.psu.edu/pkoch/plasticdesign/IM_Thermoplastic.htm, access date 04.01.2009.

[14] Kazmer, D., Injection Mold Design Engineering, Hanser Verlag, 2-3 (2007).

[15] http://plastics.inwiki.org/Injection_molding_machine, access date 04.01.2009.

[16] Chanda, M., Roy, S. K., *Plastics Technology Handbook, Injection Molding of Thermosetting Resins*, 2-21 (1993).

[17] http://www.scudc.scu.edu/cmdoc/dg_doc/develop/process/control/b1000002.htm, access date 04.01.2009.

[18] Manual for operating instructions injection molding machine EM 50/300 Battenfeld.

[19] Fu, S. Y., and Lauke, B., Effects of Fiber Length and Fiber Orientation Distributions on the Tensile Strength of Short-Fiber-Reinforced Polymers, *Composites Science and Technology*, **56**, 1179-1190 (1996).

CHAPTER 5

MODEL DEVELOPMENT

5.1. Objective

The objective of this study is to model the tensile strength, flexural strength and impact strength of carbon fiber, and glass fiber reinforced polymeric materials. Testing the product and repeating the production until desired properties are achieved is a time, money and effort consuming process. Reinforcement of polymer matrices has attracted a lot of attention because their applications in sectors such as automotive and aerospace are very important. For this reason, models predicting their final properties are being developed. Knowledge of the final mechanical properties of polymer matrices reinforced with fibers is essential to improve performance, prevent failure and reduce production costs.

Kalaitzidou et al., (2007) tested the flexural and tensile properties of polypropylene nanocomposites and FRCs and compared their experimental data to Halpin Tsai and Tandon Wang models. They concluded that the difference was caused by reinforcing efficiency and fiber alignment [1].

Fu et al. (2001) tested PP reinforced with glass fibers and carbon fibers and compared the results to a modified rule of mixture, in which they used two correction factors. As a result, they found good relationship for tensile strength results [2].

Mohsen et al., (2008) compared the tensile properties of nanosized and micron-sized CaCO₃/PA66 composites using Rule of Mixtures, Guth, Nicolais-Narkis, Hashin-Shtrikman and Halpin Tsai equations. They concluded that these model results are lower than calculated values [3].

Beckermann and Pickering (2009) studied the strength prediction of hemp fiber reinforced PP composites using Rule of Mixtures and Bowyer-Bader models. They found the experimental tensile strength to be one third of the theoretical result of the Bowyer-Bader model. They concluded that this difference was caused by the random orientation of fibers [4].

5.2. Approach

Usually modeling is done assuming perfect interfacial strength between matrix and reinforcer ; in this study, interfacial shear strength is one of the parameters that is examined too. The factors affecting the properties of reinforced polymers are [5]:

- 1- Particle size, particle size distribution, and reinforcer content
- 2- Particle shape and surface structure
- 3- Mechanical properties of the reinforcer
- 4- Method used to produce the composite
- 5- Bond strength between reinforce and polymer
- 6- Mechanical properties of the polymer matrix.

In this study, modeling of fiber reinforced polypropylene samples is based on the parameters listed in Table 5.1. The effect of each parameter on the product properties is examined and the affecting parameters are included in the models.

Table 5.1. Parameters to be included in modeling.

Number	Parameter
1	fiber content vol %
2	matrix content vol %
3	void content vol %
4	total surface area (m ²)
5	IFSS (interfacial shear strength)
6	fiber orientation
7	fiber length

5.3. Factors affecting the mechanical properties of IMPM

5.3.1. Fiber length and diameter

During injection molding process, the shear stresses formed by the ram break the fibers and result in a fiber length distribution with an asymmetric character. The mechanical properties are related to this distribution [6].

Fiber lengths are determined by image analysis and optical microscopy on fiber samples removed from the molded samples after high temperature ashing. Measurement of fiber orientation is carried out on cross sections of molded tensile bars which were cut parallel to the flow direction. Fiber diameters are based on the values given by the manufacturers; these values are given in Table 4.1 in Chapter 4.

Fibers obtained from ashed samples were analysed using SEM and optical microscopy. Long fibers were hard to analyse using SEM so these fibers were examined using optical microscope. Fiber length distributions are graphed from shortest to longest fibers using at least 100 fiber length values for each sample. The graphs for samples GF1, GF4 and GF7 are given in

Figure 5.1, Figure 5.2 and Figure 5.3, respectively; the graphs of samples C1, C4 and C7 are given in Figure 5.4, Figure 5.5 and Figure 5.6, respectively.

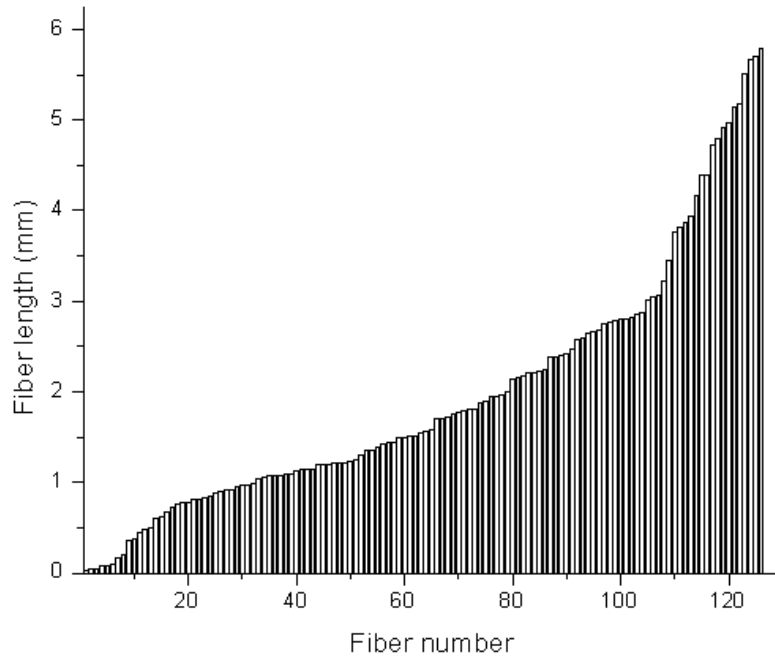


Figure 5.1. Fiber length distribution of GF1.

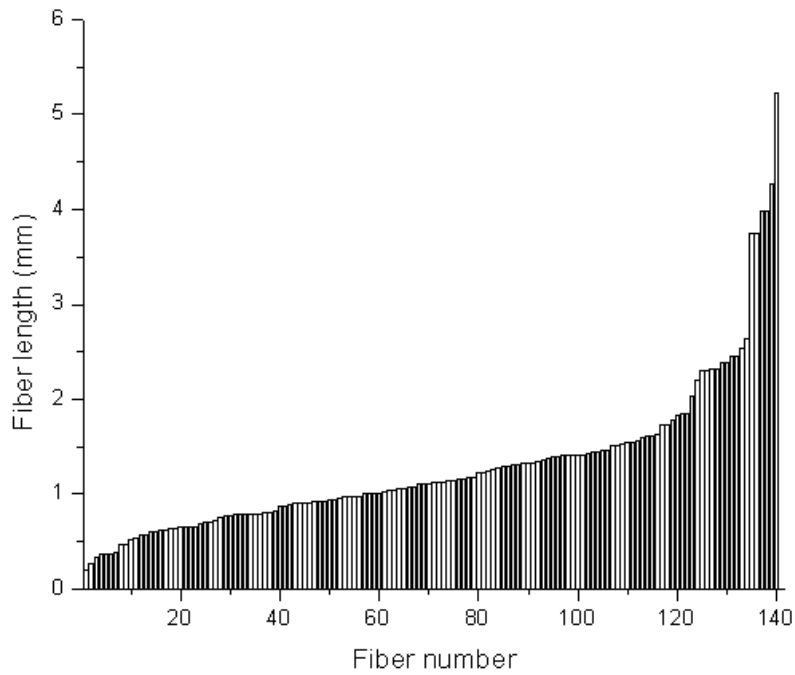


Figure 5.2. Fiber length distribution of GF4.

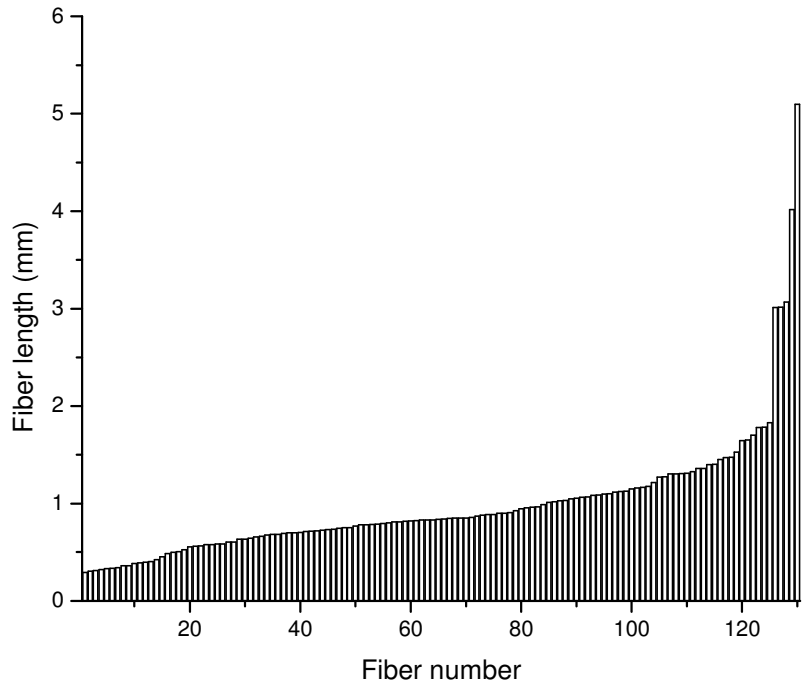


Figure 5.3. Fiber length distribution of GF7.

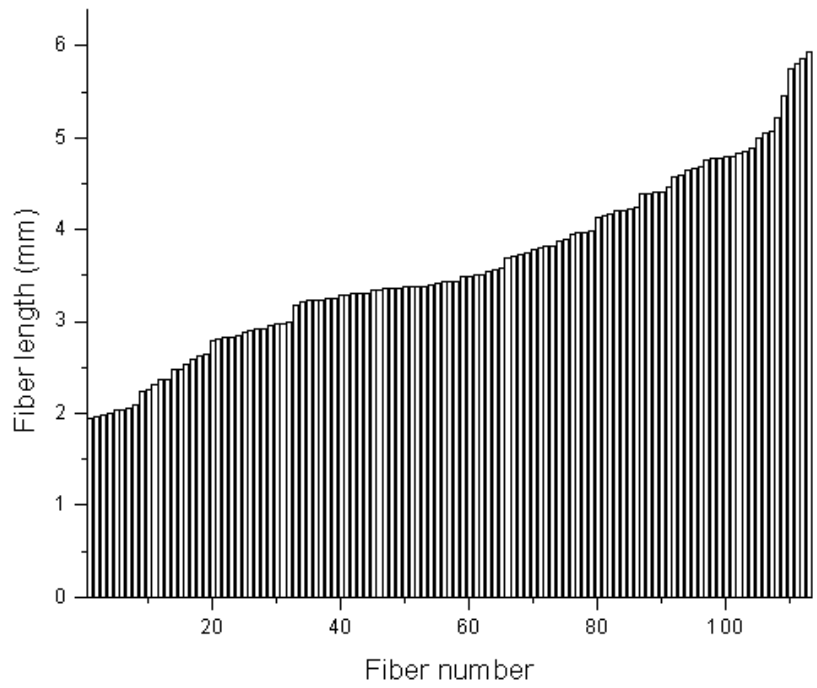


Figure 5.4. Fiber length distribution of C1.

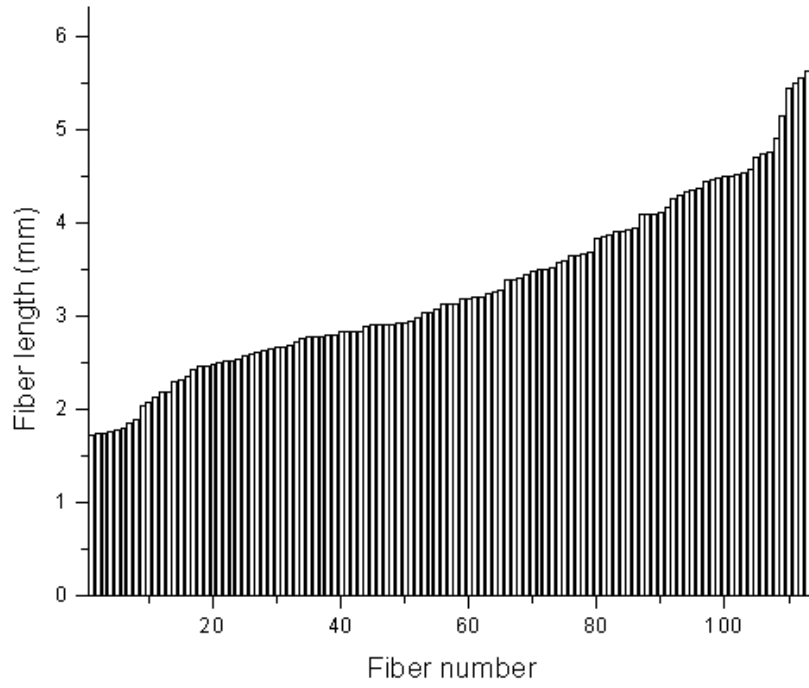


Figure 5.5. Fiber length distribution of C4.

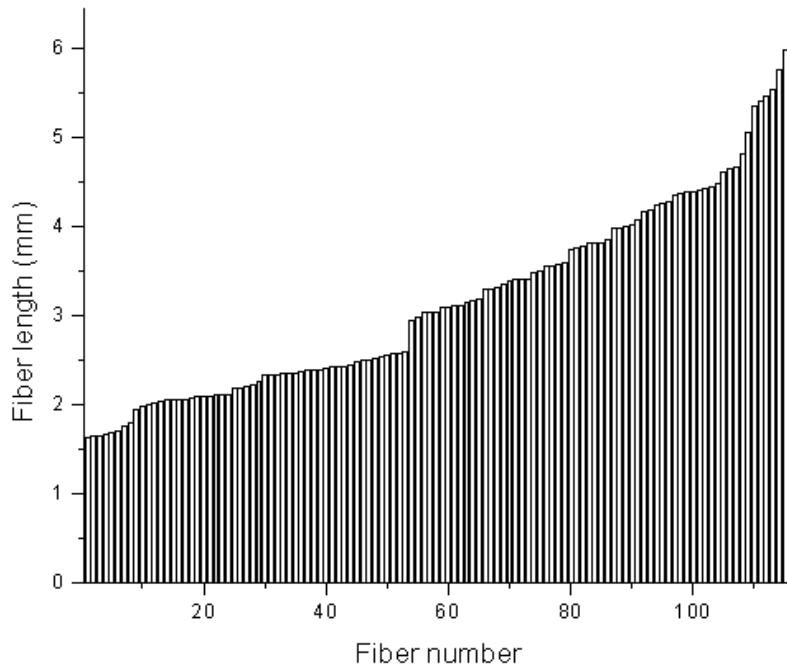


Figure 5.6. Fiber length distribution of C7.

Fiber length distribution mean values ‘ l_m ’ are given in Table 5.2, which shows that mean length values are decrease as fiber weight percent in the sample increases. The interaction between fibers may have caused fiber breakage during the injection molding process: the more fibers there are, the more breakage occurs due to increased interaction between individual fibers in the polymer melt. When the mean values of each fiber type are compared, it is observed that the mean length values of glass fibers are smaller than the mean length values of carbon fibers. This may be due to the low loop and knot strength of glass fibers.

Table 5.2. Fiber length distribution mean values ‘ l_m ’ (mean \pm standard deviation).

Sample	Fiber type	Fiber wt%	Fiber length mean value ‘l_m’ (mm)
GF1	Glass fiber	1	1.987 \pm 1.425
GF4	Glass fiber	4	1.292 \pm 0.803
GF7	Glass fiber	7	1.007 \pm 0.532
C1	Carbon fiber	1	3.607 \pm 0.943
C4	Carbon fiber	4	3.321 \pm 0.957
C7	Carbon fiber	7	3.166 \pm 1.089

5.3.1.1. Critical length

An important parameter when dealing with discontinuous fibers is the critical length ‘ l_c ’. When using fibers shorter than this critical length, the full strength of the fiber cannot be obtained in the finished composite. Equation 5.1 gives the formula for critical length ‘ l_c ’:

$$l_c = \frac{\sigma_t \times d}{2 \times \tau} \dots\dots\dots (5.1)$$

where: σ_t : Fiber tensile strength (MPa)

d : Fiber diameter (mm)

τ : Interfacial shear stress at the boundary of fiber and matrix (MPa)

The critical length values for the E-glass fiber/PP and carbon fiber/PP systems are given in Table 5.3.

Table 5.3. Calculated critical length ' l_c ' values for the fibers used.

Fiber	Matrix	l_c (mm)
E-glass fiber	Polypropylene	1.565
Carbon fiber	Polypropylene	0.973

Fiber breakage failure mode depends on whether the fiber mean length is larger or smaller than the critical length in a composite.

Comparing the mean fiber length values given in Table 5.2 and the critical length values given in Table 5.3, it is observed that in GF4 and GF7 samples; the mean fiber length is smaller than the critical fiber length, but in the remaining GF1, C1, C4 and C7 samples, the mean fiber length is larger than the critical fiber length. This indicates that, in GF4 and GF7 samples, failure due to fiber pull out is more likely than failure due to fiber breakage.

Fractured surfaces in tensile tests of samples GF1, GF4, GF7, C1, C4 and C5 are given in Figures 5.7-5.12, respectively. Figure 5.8 and Figure 5.9 show that the failure of GF4 and GF7 samples are based on pulled out. The failure of C1 samples shown in Figure 5.10, and failure of C4 samples shown in Figure 5.11 prove that the failure is based on fiber breakage. The failure of C7 samples (Figure 5.12) is caused by both fiber pull out and fiber breakage. In Figure 5.7, broken glass fibers are visible; as the mean fiber length is bigger than the critical fiber length in GF1 samples, this is an expected result for the failure type.

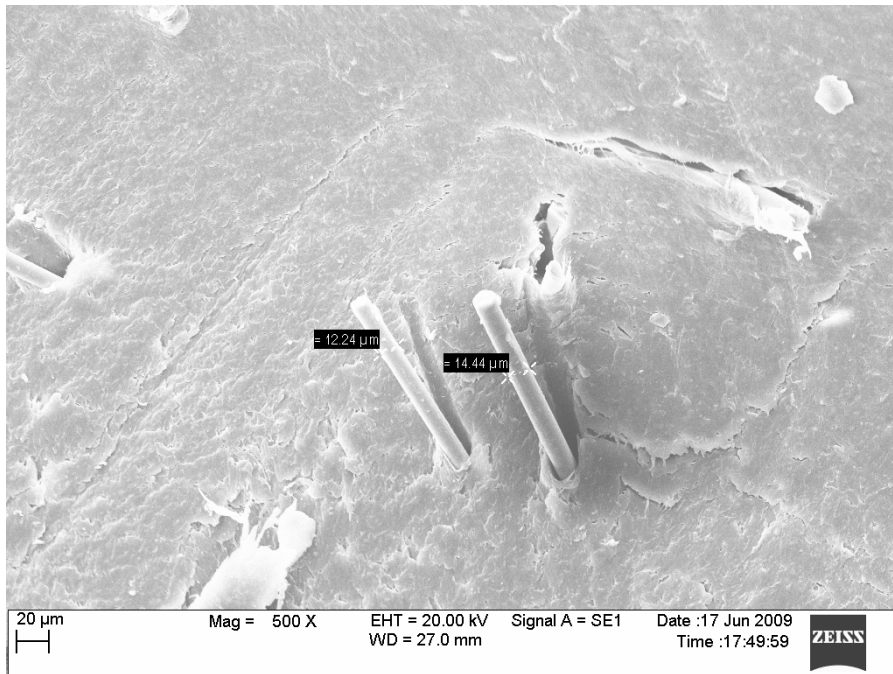


Figure 5.7. SEM micrograph of GF1.

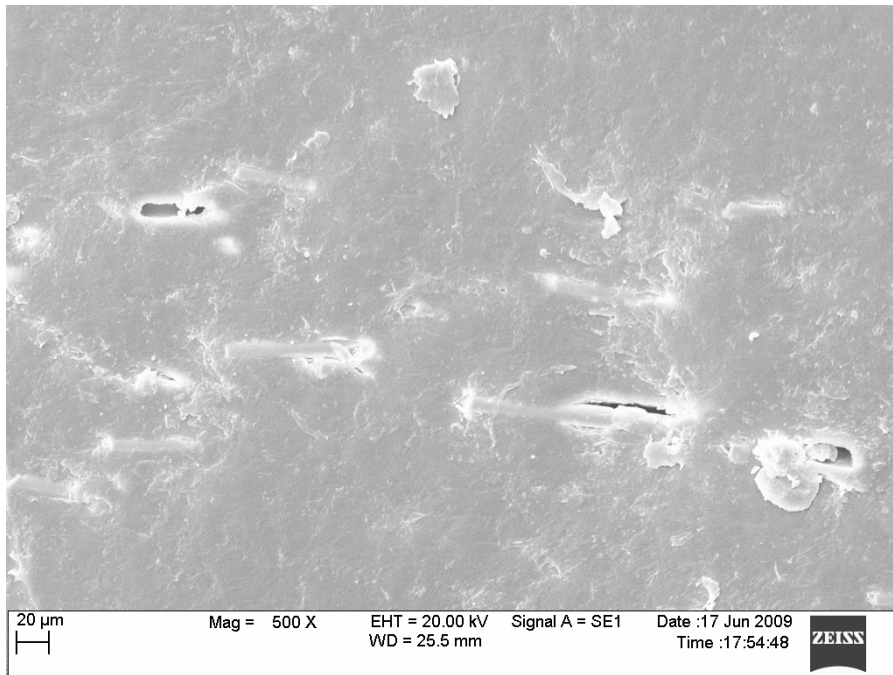


Figure 5.8. SEM micrograph of GF4.

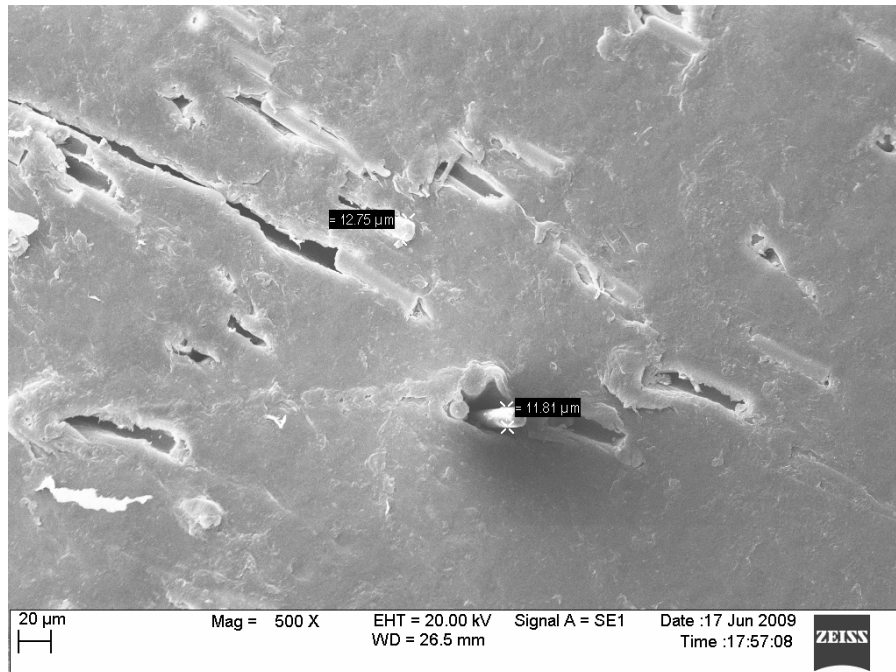


Figure 5.9. SEM micrograph of GF7.

Figures 5.7 - 5.9 show that the glass fibers are in micron scale, they are aligned both parallel and vertical to the flow direction and there is a void at the interphase of polypropylene matrix and glass fiber.

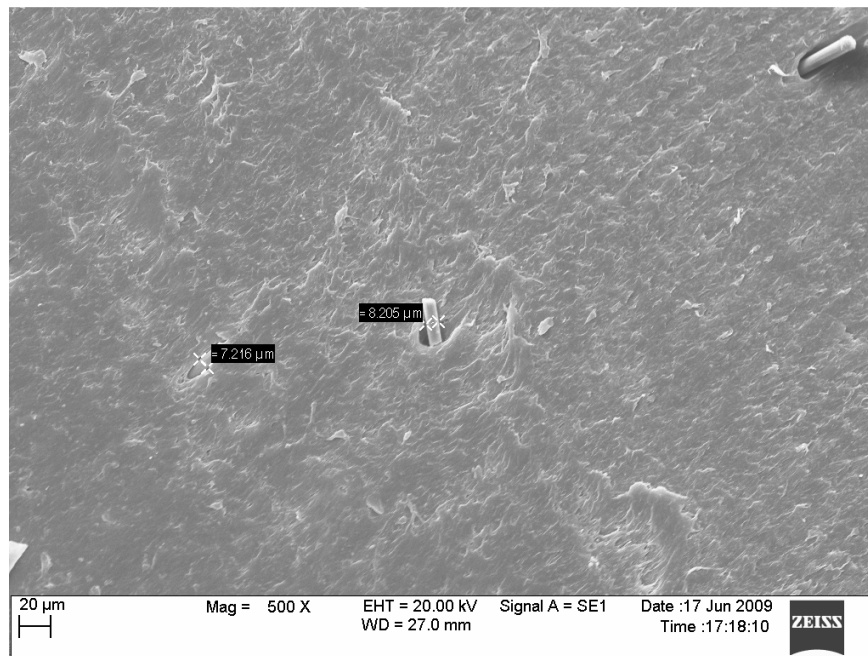


Figure 5.10. SEM micrograph of C1.

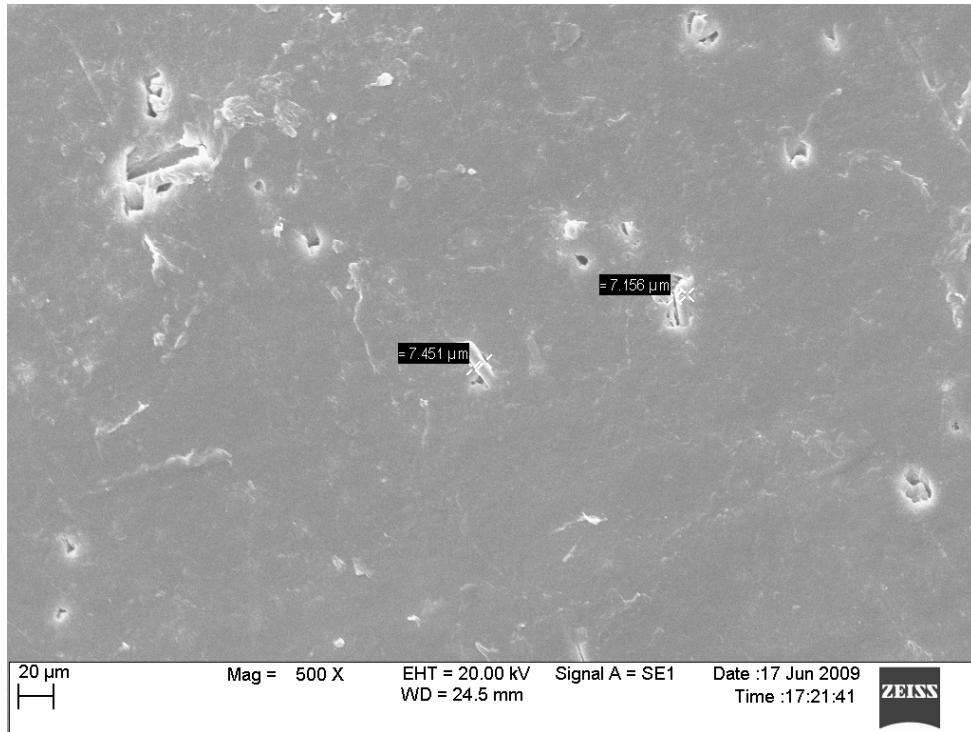


Figure 5.11. SEM micrograph of C4.

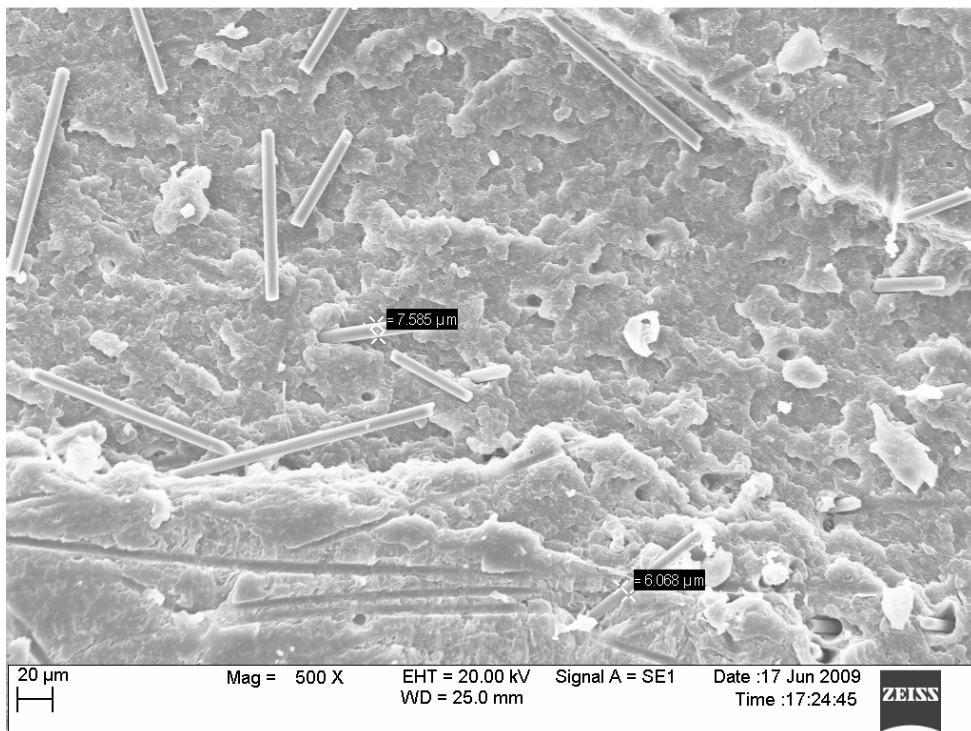


Figure 5.12. SEM micrograph of C7.

Figures 5.10 - 5.12 show that the carbon fibers are in micron scale and there is a void at the interphase of polypropylene matrix and carbon fiber.

5.3.2. Void volume

The volume of the test samples was calculated after careful measurements of their dimensions with a micrometer several times.

The samples were weighed on an electronic balance and then each sample was ashed in furnace at 500°C for 10 minutes to remove the matrix from the fibers. The remaining fibers were filtered in distilled water using a Whatman Grade 5, filter paper. After drying the fiber weight was measured. The following equations are used:

$$W_{sample} = W_m + W_f \dots\dots\dots (5.2)$$

$$V_{sample} = V_m + V_f + V_{void} \dots\dots\dots (5.3)$$

Fiber, matrix and void volumes were calculated according to the following equations.

$$V_f = \frac{W_f}{d_f} \dots\dots\dots (5.4)$$

$$V_m = \frac{W_{sample} - W_f}{d_m} \dots\dots\dots (5.5)$$

$$V_{void} = V_{sample} - (V_f + V_m) \dots\dots\dots (5.6)$$

where: W: weight

V: Volume

Subscripts:

m: Matrix

f: Fiber

The fiber volume, matrix volume and void volume of the samples are given in Table 5.4.

Table 5.4. The fiber volume, matrix volume and void volume of pure polypropylene and glass fiber, carbon fiber and nanoclay reinforced polypropylene (mean \pm standard deviation).

Sample code	Fiber vol %	Matrix vol %	Void vol %
GF1	2.91 \pm 0.07	93.26 \pm 0.68	3.83 \pm 0.62
GF4	3.69 \pm 0.18	93.12 \pm 0.17	3.19 \pm 0.34
GF7	4.59 \pm 0.75	92.97 \pm 0.79	2.43 \pm 0.36
C1	0.45 \pm 0.29	95.51 \pm 1.37	4.04 \pm 0.94
C4	0.78 \pm 0.17	95.37 \pm 0.51	3.85 \pm 0.18
C7	1.23 \pm 0.19	95.23 \pm 1.28	3.54 \pm 0.21

5.3.3. Fiber orientation degree (FOD)

Orientations of fibers are changing continuously during injection molding due to the fountain flow in the barrel. For this reason, different fiber orientations are observed throughout the molded sample. The fiber orientations are related to the size (length and diameter) of fibers, volume of fibers, flow behavior of the melt, mold cavity and conditions used in process [6].

Fiber orientation is defined as the degree between the flow direction and fiber direction. In this study fiber orientation degrees (FOD) are obtained using SEM analysis. Figures 5.13-5.15 show some fiber orientation degrees of GF1, GF4 and GF7 samples.

Samples were cut parallel to the flow direction and examined in SEM; for each sample, approximately 100 fibers were measured.

FOD distributions of samples GF1, GF4, GF7, C1, C4 and C7 are given in Figures 5.16 - 5.21 respectively.

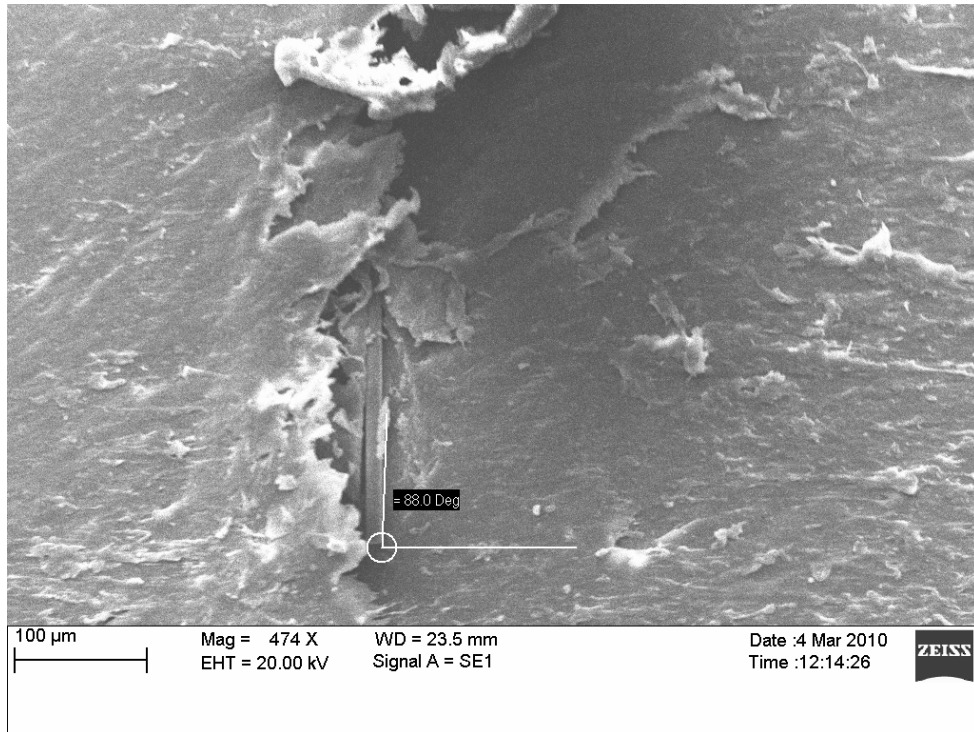


Figure 5.13. SEM micrograph of a fiber orientation angle of GF1.

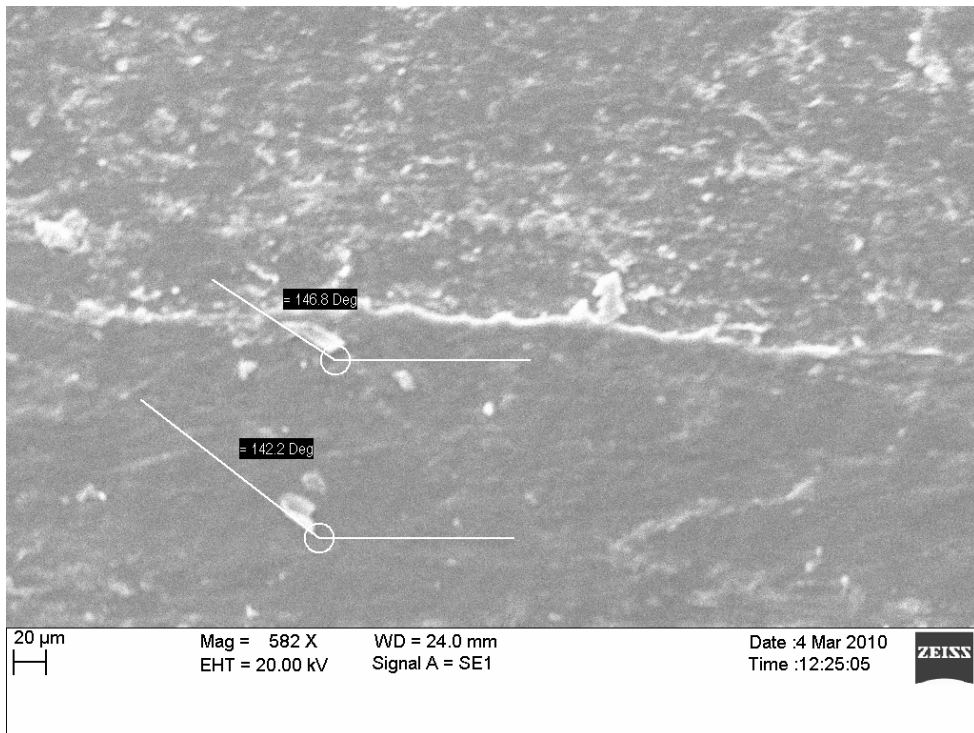


Figure 5.14. SEM micrograph of a fiber orientation angle of GF4.

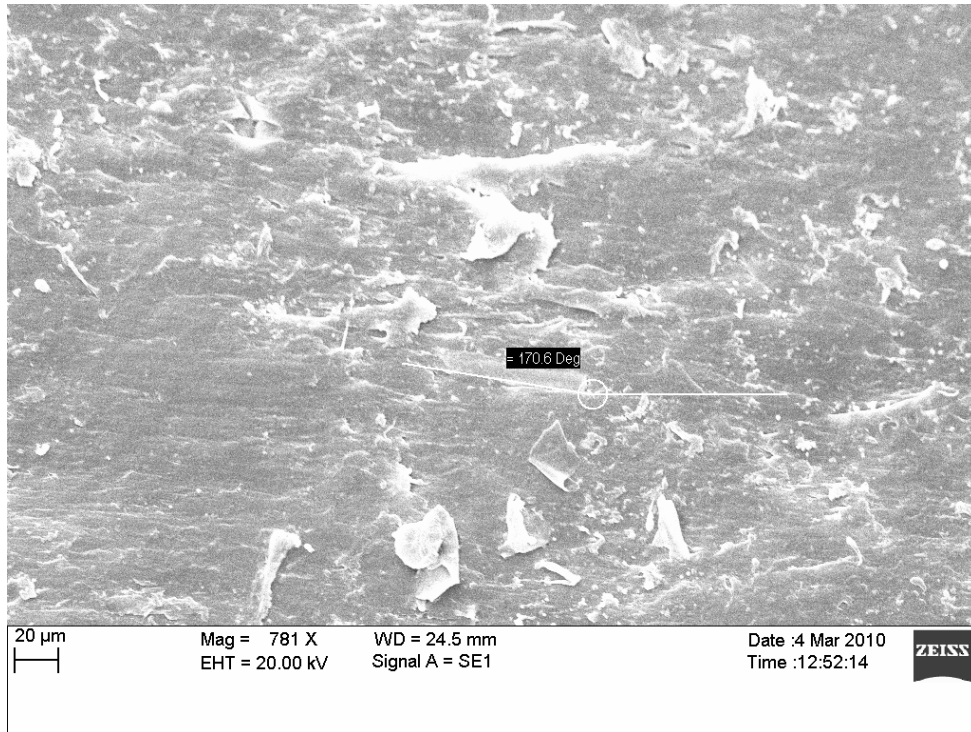


Figure 5.15. SEM micrograph of a fiber orientation angle of GF7.

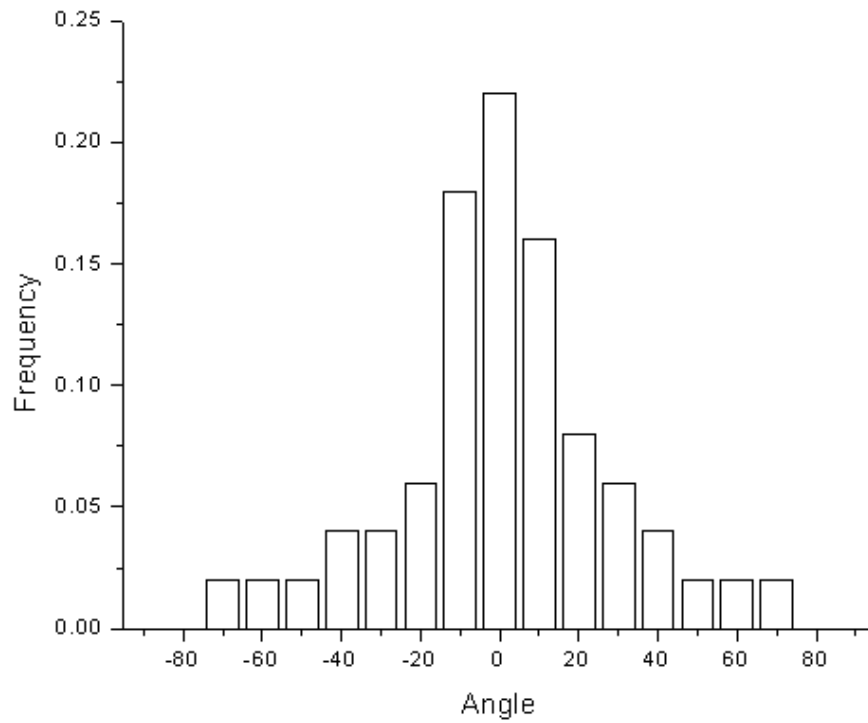


Figure 5.16. FOD for dogbone shaped GF1

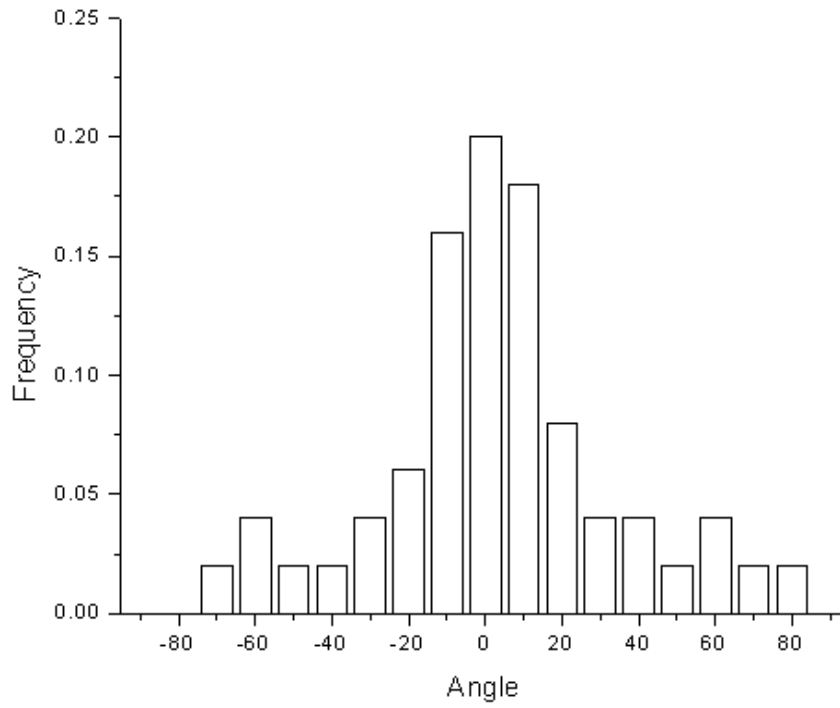


Figure 5.17. FOD for dogbone shaped GF4

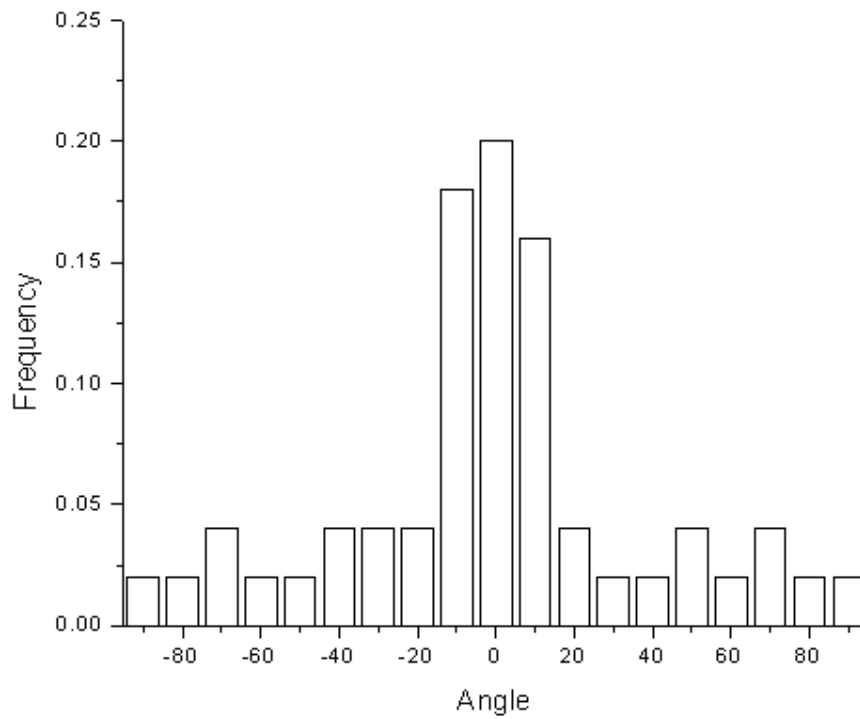


Figure 5.18. FOD for dogbone shaped GF7

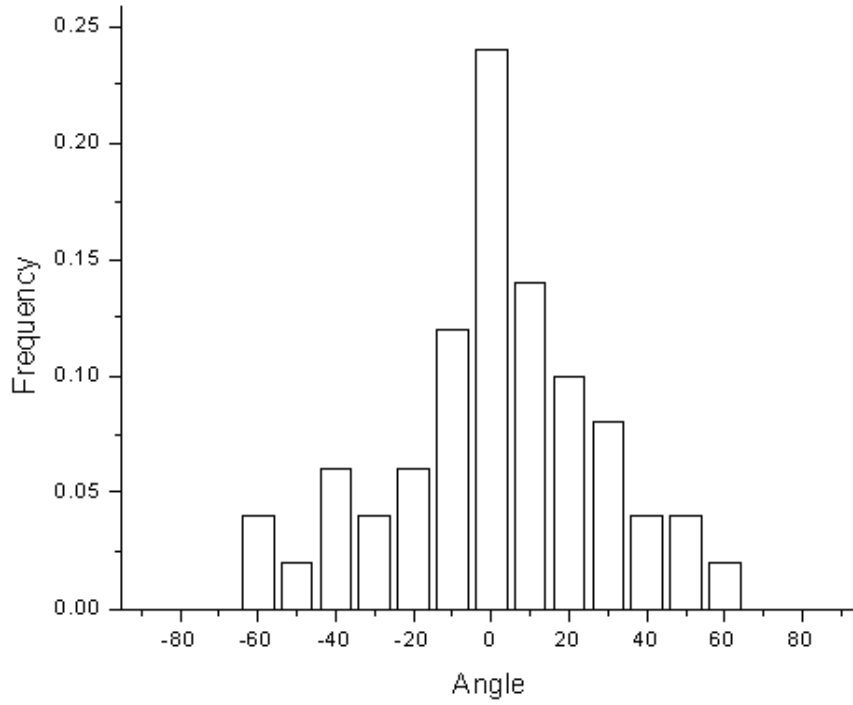


Figure 5.19. FOD for dogbone shaped C1

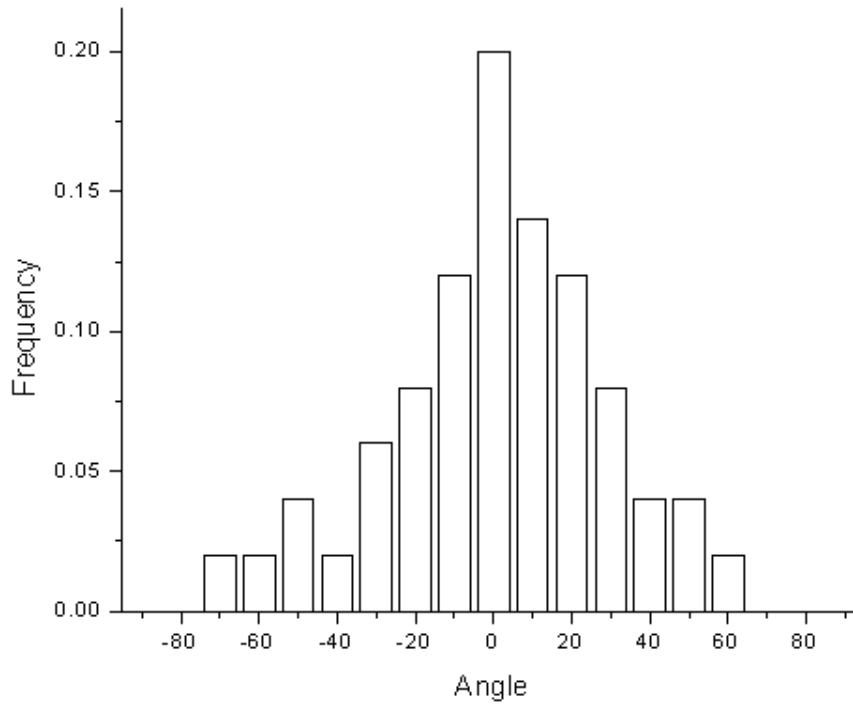


Figure 5.20. FOD for dogbone shaped C4

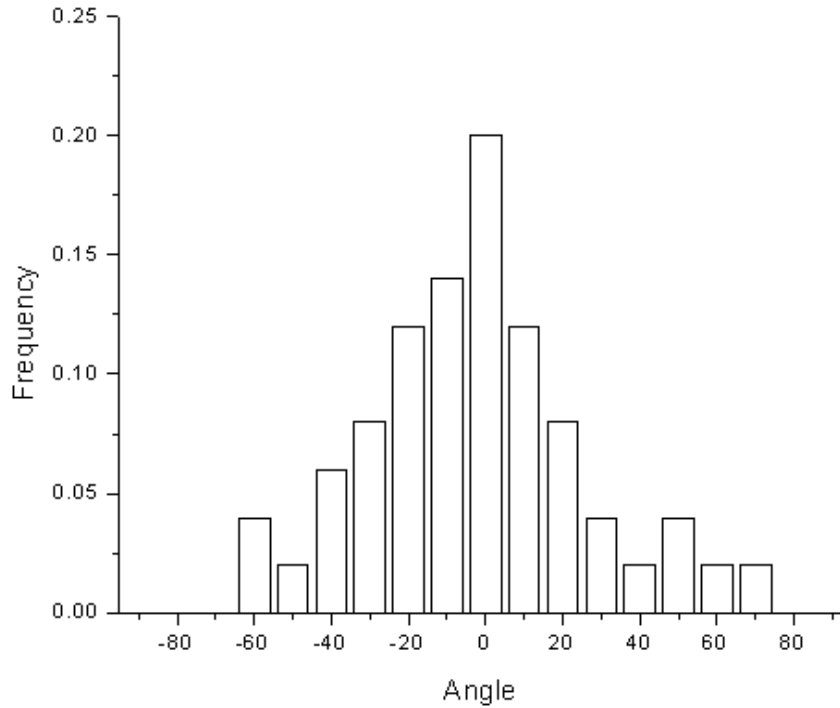


Figure 5.21. FOD for dogbone shaped C7.

Table 5.5. FOD angle percentages for the samples

Angle	Dogbone shaped samples			Rectangle bar shaped samples		
	C1	C4	C7	C1	C4	C7
$\pm 10^\circ$	50%	46%	46%	54%	48%	46%
$\pm 20^\circ$	66%	66%	66%	68%	66%	64%
$\pm 30^\circ$	78%	80%	78%	82%	78%	76%
	GF1	GF4	GF7	GF1	GF4	GF7
$\pm 10^\circ$	56%	54%	54%	54%	54%	44%
$\pm 20^\circ$	70%	68%	62%	72%	68%	60%
$\pm 30^\circ$	80%	76%	68%	80%	76%	68%

Table 5.5 gives the total fiber distribution percentages at $\pm 10^\circ$, $\pm 20^\circ$, and $\pm 30^\circ$ fiber orientation ranges. For all the samples, more than 65% of the fiber orientations are in the $\pm 30^\circ$ fiber alignment range.

As flow proceeds into the mold cavity, a core-shell structure occurs. Fibers are more located in the core structure and the shell is fiber free (Figure 5.22). When the mold is frozen, the sample has a multiple-layered structure that has different fiber orientations. The resin rich 'shell' which is the surface layer is approximately at 10 mm thickness. Inside the 'shell', the core structure consists of layers having different alignments of fibers to the flow direction. Under the surface layer, a thin layer of matrix which has parallel aligned fibers is observed. Under this layer, a thin layer having transverse aligned fibers is located [7].

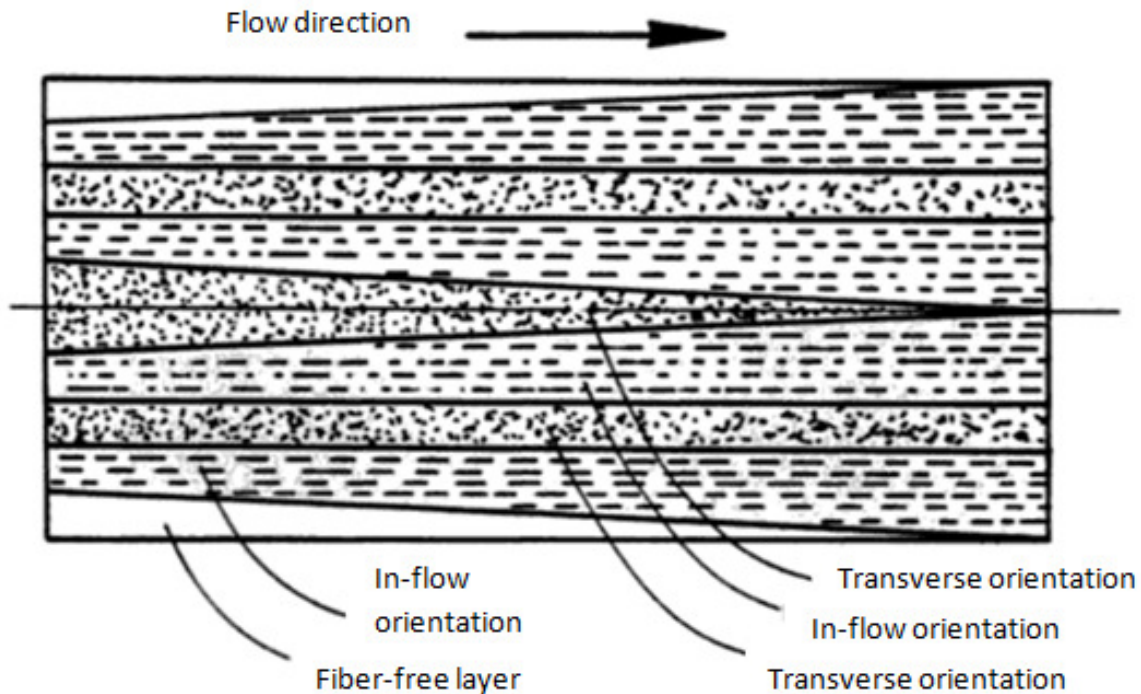


Figure 5.22. Schematic of fiber orientation development in injection molding [7].

Orientation of fibers, fiber concentration, and fiber distribution affect the strength and other mechanical properties of fiber reinforced composites. Several fiber orientations are shown in Figure 5.23.

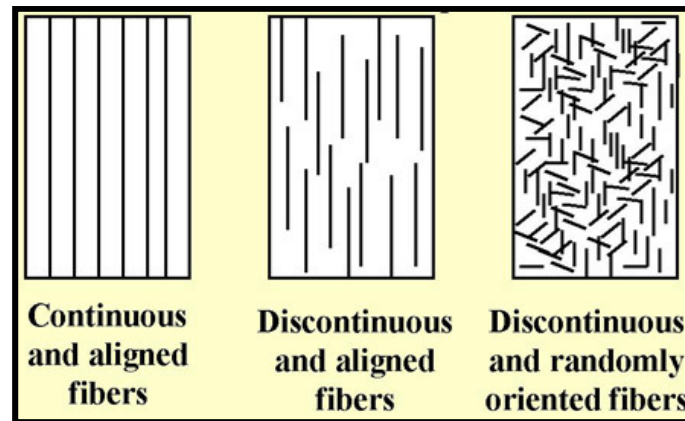


Figure 5.23. Example of fiber orientations [8].

5.3.4. Interfacial shear strength (IFSS)

The interfacial adhesion between the fiber and matrix affect the mechanical properties of fiber reinforced composites [9].

Experimental studies proved that a three dimensional region exists between the fiber subdomain and the matrix subdomain. This region is called “interphase” and includes the interface. ‘Interface’ is the two-dimensional contact area of the fiber and matrix and interface includes the whole surface of the fiber-matrix contact area [10]. The complex structure of the interphase makes it difficult to determine the interfacial properties and as a result it is difficult to predict the composite properties. Therefore, it is important to evaluate the interfacial forces [11]. There are different methods to evaluate the interfacial shear stress such as fiber pull-out test, fragmentation test, and microbonding test; none of them can correctly give the interfacial properties of a system ; the fiber pull-out method requires pulling the fiber out of the matrix

which can be a block, a disc or a droplet [12]. The maximum load to debond the fiber from the matrix is converted to an apparent interfacial shear strength as given in Equation 5.1.

$$\tau = \frac{F_{max}}{\pi \times d_f \times l_e} \dots\dots\dots (5.1)$$

where: τ : Mean interfacial shear strength

F_{max} : Maximum force from the force – displacement curve of the sample

d_f : Diameter of the fiber

l_e : Length of the embedded fiber

In the fragmentation method, a single fiber is totally encapsulated in the polymeric matrix shaped into a dog-bone sample. The sample is loaded and when the tensile strength of the fiber is exceeded, the fiber fractures inside the matrix. This process is repeated until the remaining fragments cannot produce further fracture. A simple shear-lag analysis is applied to calculate the interfacial shear strength using the length of resulting fragments, the fiber diameter and the fiber tensile strength. Even though there are many methods of determining IFSS, none of them is described to be the ideal method [13].

The IFSS was calculated using the pull-out method with 16 samples. The IFSS results of the fibers are given in Table 5.6. Polypropylene pellets were melted in the furnace at 300°C, one end of fibers were embedded in the melt so each fiber had PP matrix coating. The fibers were left drying in ceramic plates. Pull-out test was applied to each fiber on Instron 5565 universal testing machine making sure that fiber was getting apart from the PP matrix. IFSS values of carbon fibers were higher than glass fiber IFSS values. This may be due to the stronger bonding between carbon fiber and PP compared to bonding between glass fiber and PP matrix.

Table 5.6. IFSS of glass fibers and carbon fibers used.

Material	Diameter (μm)	IFSS (τ) (MPa)
E-Glass fibers	13	5.73
Carbon fibers	7	13.39

5.4. Suggested Models

5.4.1. Rule of Mixtures for Tensile Strength

For reinforced composites, the rule of mixtures (ROM) assumes that the solid domain (Ω_{solid}) can be subdivided into two subdomains: matrix (Ω_{matrix}) and fiber reinforcement (Ω_{fiber}).

Equation 5.2 gives the subdomain relation:

$$\Omega_{\text{solid}} = \Omega_{\text{matrix}} \cup \Omega_{\text{fiber}} \dots\dots\dots (5.2)$$

The volume of the solid domain is ‘V’, whereas ‘ V_F ’ and ‘ V_M ’ are the volumes of fiber and matrix subdomains, respectively. The domain volume is the total of the subdomains as indicated in Equation 5.3.

$$V = V_F + V_M \dots\dots\dots (5.3)$$

According to ROM, there are two possibilities based on the fiber reinforcement direction: parallel to the flow direction and vertical to the flow direction.

5.4.1.1. Fiber Reinforcement Parallel to the Flow Direction

In this case, as shown in Figure 5.24, the composite is assumed to be composed of two parallel springs: matrix and fiber. The strains of the constituent materials are assumed to be equal to each other (Equation 5.4). Equation 5.5 gives the general integration formula for tensile stress.

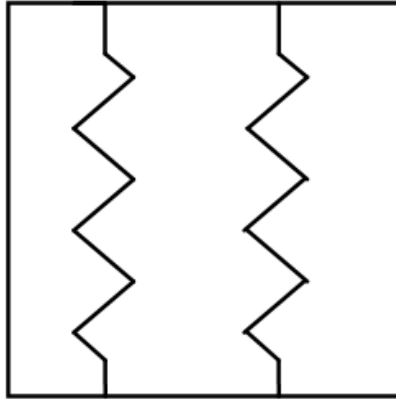


Figure 5.24. Simulation for fiber reinforcement parallel to the flow direction.

$$\varepsilon_C = \varepsilon_F = \varepsilon_M \dots\dots\dots (5.4)$$

$$(\sigma_{ij}) = \frac{1}{V} \int_0^V \sigma_{ij}(x) dV \dots\dots\dots (5.5)$$

Using Equation 5.5, the composite tensile strength formula is obtained as follows:

$$\sigma_c = \frac{V_F}{V} \sigma_F + \frac{V_M}{V} \sigma_M \dots\dots\dots (5.6)$$

In the parallel condition of ROM, the fiber strength has a parallel spring approximation.

The volume fraction can be denoted as ‘v’; fiber and matrix volume fractions are given as:

$$v_F = \frac{V_F}{V} \dots\dots\dots (5.7)$$

$$v_M = \frac{V_M}{V} \dots\dots\dots (5.8)$$

where: v_F : Fiber volume fraction

v_M : Matrix volume fraction

Then, equation 5.6 can be written as:

$$\sigma_c = v_F \sigma_F + v_M \sigma_M \dots\dots\dots (5.9)$$

5.4.1.2. Fiber Reinforcement Transverse to the Flow Direction

In this case, matrix and fiber are treated as a series of springs as shown in Figure 5.25, and the total strain of the composite is assumed to be the total of matrix strain and fiber strain as given in Equation 5.10.

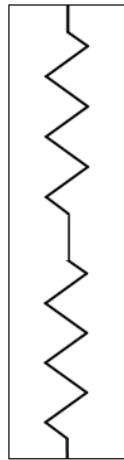


Figure 5.25. Simulation for fiber reinforcement transverse to the flow direction.

$$\varepsilon_c = \varepsilon_F + \varepsilon_M \dots\dots\dots (5.10)$$

$$(\varepsilon_{ij}) = \frac{1}{V} \int_0^V \varepsilon_{ij}(x) dV \dots\dots\dots (5.11)$$

Equation 5.11 gives the integration formula for strain. Using Equation 5.11, the composite tensile strength formula is obtained:

$$\frac{1}{\sigma_c} = \frac{V_F}{V} \frac{1}{\sigma_F} + \frac{V_M}{V} \frac{1}{\sigma_M} \dots\dots\dots (5.12)$$

ROM gives good approximation in parallel direction but does not give good approximation in transverse direction. ROM lacks accuracy as it does not use any information about the geometry and distribution of the fiber; moreover, ROM assumes perfect bonding between fiber and matrix [14].

5.4.2. Model for Tensile Testing

5.4.2.1. Effect of fiber Orientation Degree

In this model, we assume that the fiber sub domain consists of many springs having parallel and series combinations according to their distribution angle compared to the flow direction. The total fiber domain is a parallel spring to the matrix domain. Assuming θ as the angle between flow direction and fiber direction, Equation 5.9 can be re-written as:

$$\sigma_c = \sigma_F v_F^{\cos|2\theta|} + v_M \sigma_M \dots\dots\dots (5.13)$$

where: θ : The angle between flow direction and fiber (degree)

In the case of transverse direction, Equation 5.13 is still valid since the angle is 90° to the flow direction. For a composite having different fiber fractions at different fiber directions, Equation 5.13 can be modified as:

$$\sigma_c = \sigma_F v_F^{\sum_{i=-90^\circ}^{i=90^\circ} n_i \times \cos|2\theta_i|} + v_M \sigma_M \dots\dots\dots (5.14)$$

where: $n_i = \frac{N_i}{N}$

n_i : Fiber number fraction at a certain degree

N_i : Fiber number at a certain degree

N : Total fiber number in the sample

The suggested model will take into account the effects of void volume, interfacial shear strength, total surface area and fiber length.

5.4.2.2. Effect of Void

Equations 5.15 - 5.17 give the void and volume relations in a composite material [15].

$$V_{voided\ sample} = V_{void} + V_0 \dots\dots\dots (5.15)$$

$$v_{void} = \frac{V_{voided\ sample} - V_0}{V_{voided\ sample}} \dots\dots\dots (5.16)$$

$$V_{voided\ sample} = V_0 \left(\frac{1}{1 - v_{void}} \right) \dots\dots\dots (5.17)$$

where: V_{void} : Void volume in a sample

V_0 : Volume of a sample that has no void

v_{void} : Void fraction in a sample

As the length and width of the sample cannot change due to the mold shape, the only variable dimension of the sample is the thickness 't' [15]. Then, the following equation can be obtained:

$$v_{void} = \frac{t_{voided\ sample} - t_0}{t_{voided\ sample}} \dots\dots\dots (5.18)$$

where: $t_{voided\ sample}$: Thickness of voided sample

t_0 : Thickness of a sample that has no void

Tensile stress is defined as Equation 5.19:

$$\sigma = \frac{F}{A} \dots\dots\dots (5.19)$$

Equation 5.20 gives the relation between area and void volume. When this relation is implemented to Equation 5.19, equation 5.21 is obtained.

$$A_{voided\ sample} = A_0 \left(\frac{1}{1 - v_{void}} \right) \dots\dots\dots (5.20)$$

$$\sigma = \frac{F}{A_0} (1 - v_{void}) \dots\dots\dots (5.21)$$

Equation 5.22 gives the correlation between tensile stress and void volume:

$$\sigma \sim (1 - v_{void}) \dots\dots\dots (5.22)$$

5.4.2.3. Effect of Total Fiber Surface Area and IFSS

Using the total fiber volume and total fiber area formulas given in Equation 5.23 and Equation 5.24, respectively, Equation 5.25 gives the ratio between total fiber volume and total fiber area.

$$V_F = N_F \pi r_F^2 l_F \dots\dots\dots (5.23)$$

where: N_F : Total number of fibers

r_F : Fiber radius (m)

l_F : Fiber length (m)

$$A_F = N_F (2\pi r_F^2 + 2 \pi r_F l_F) \dots\dots\dots (5.24)$$

$$\frac{A_F}{V_F} = \frac{N_F (2\pi r_F^2 + 2 \pi r_F l_F)}{N_F \pi r_F^2 l_F} \dots\dots\dots (5.25)$$

After simplification:

$$A_F = \frac{2 V_F (r_F + l_F)}{r_F \times l_F} \dots\dots\dots (5.26)$$

IFSS is correlated to the area (A); the effect of IFSS x A on the tensile strength is investigated. Taking into account (5.14), (5.21) and (5.26), and applying them on exponential graph for glass fiber reinforced samples, the tensile strength is given by:

$$\sigma_c = \sigma_F v_F^{\sum_{i=0}^{i=n} v_i \times \cos|2\theta_i|} (1 - v_{void}) e^{0.089 \times IFSS \times A} + v_M \sigma_M \dots\dots\dots (5.27)$$

Figure 5.26 compares the calculated and measured values for tensile strength of glass fiber reinforced samples. The agreement between the calculated and measured values is in the range of 90%.

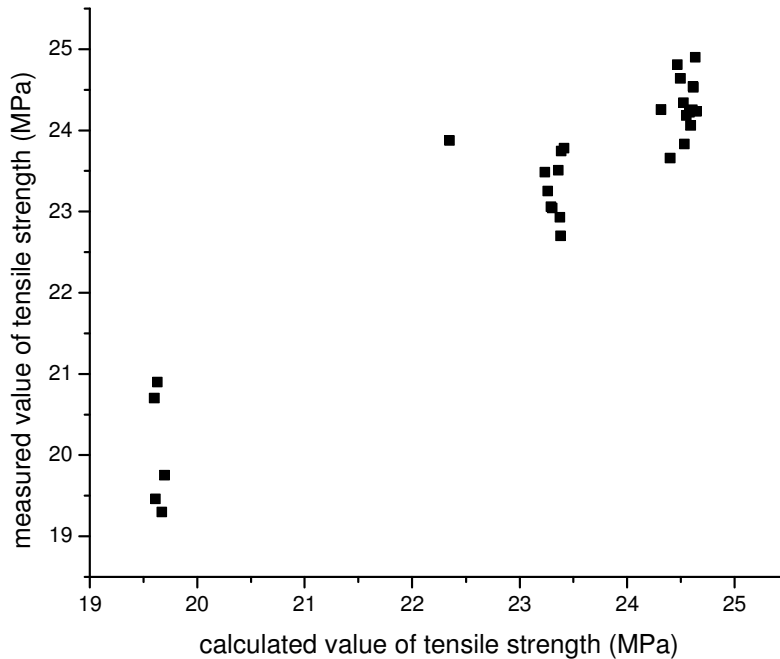


Figure 5.26. Measured and calculated tensile strength values of GF1, GF4 and GF7.

Applying Equations (5.14), (5.21) and (5.26) on exponential graph, for carbon fiber reinforced samples, the tensile strength is given by:

$$\sigma_c = \sigma_F v_F^{\sum_{i=0}^{i=n} v_i \times \cos|2\theta_i|} (1 - v_{void}) e^{0.924x IFSSXA} + v_M \sigma_M \dots\dots\dots (5.28)$$

Figure 5.27 compares the calculated and measured values for tensile strength of carbon fiber reinforced samples. The agreement between the calculated and measured values is in the range of 90%.

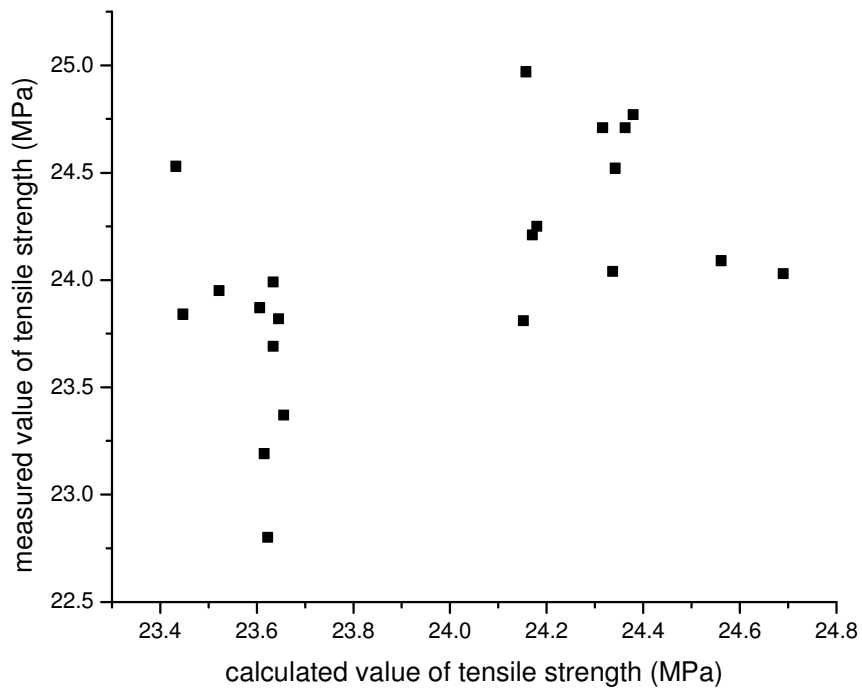


Figure 5.27. Measured and calculated tensile strength values of C1, C4 and C7.

5.4.3. Model for Flexural Testing

The effects of parameters given in Table 5.1 on flexural strength are investigated. According to the beam theory, flexural strength is defined as:

$$\sigma_{fl} = \frac{3 \times P \times L}{2 \times w \times t^2} \dots\dots\dots (5.29)$$

where: σ_{fl} : Flexural strength (MPa)

P: Load at maximum (N)

L: Support length (m)

w: Sample width (m)

t: Sample thickness (m)

5.4.3.1. Determination of Force Applied

When force is applied to a sample, deflection starts. The force applied vertical to the sample direction, $F_{vertical}$, is expressed as:

$$F_{vertical} = F \times \cos \alpha \dots\dots\dots (5.30)$$

where: $\alpha = \frac{d}{L/2}$

d : Deflection (mm)

$L/2$: Half of the support length (mm)

5.4.3.2. Effect of Void Volume

Flexural strength is inversely proportional to the cross sectional area as indicated in Equation 5.31; and void volume is inversely proportional to the area as given in Equation 5.32:

$$\sigma_{fl} \sim \frac{F}{A} \dots\dots\dots (5.31)$$

$$A \sim \left(\frac{1}{1-v_{void}} \right) \dots\dots\dots (5.32)$$

Regarding Equation 5.31 and equation 5.32, the relation between flexural strength and void volume is:

$$\sigma_{fl} \sim (1 - v_{void}) \dots\dots\dots (5.33)$$

In this case, when we apply the effects of v_{void} and α angle to the beam theory, the following is obtained:

$$\sigma_{fl} \sim \frac{3 \times P \times L}{2 \times w \times t^2} \times (\cos \alpha) \times (1 - v_{void}) \dots\dots\dots (5.34)$$

5.4.3.3. Effect of Fiber Orientation Degree

It is assumed that all fibers are vertical to the applied load. As the sample is being loaded, we will take into account the fiber load in the longitudinal direction of the sample is taken into account. In this case, the longitudinal component of the fiber volume is presented as $V_{effective}$ in Equation 5.35:

$$V_{effective\ fiber} = V_{fiber} \times \sqrt{(\sum_{i=-90^\circ}^{90^\circ} v_{fiber} \times \cos \theta_i)^2 + (\sum_{i=-90^\circ}^{90^\circ} v_{fiber} \times \sin \theta_i)^2} \dots\dots (5.35)$$

where: θ_i : Angle between fiber and longitudinal direction of sample (degree)

v_{fiber} : Volume fraction of fiber at a certain θ_i angle

Applying exponential graph for the relations of flexural strength of carbon fiber reinforced samples and glass fiber reinforced samples are given in Equation 5.36 and equation 5.37, respectively, assuming perfect bonding between matrix and fiber:

$$\sigma_{fl} = \frac{3 \times P \times L}{2 \times w \times t^2} \times (\cos \alpha) \times (1 - v_{void}) \times 18.32 \times e^{0.176 \times V_{effective\ fiber}} \quad (R^2:0.99) \dots \dots \dots (5.36)$$

$$\sigma_{fl} = \frac{3 \times P \times L}{2 \times w \times t^2} \times (\cos \alpha) \times (1 - v_{void}) \times 0.001 \times e^{0.298 \times V_{effective\ fiber}} \quad (R^2:0.94) \dots \dots \dots (5.37)$$

The measured and calculated values for flexural strength are shown in Figure 5.28. The difference between the measured and calculated values is not more than 10%, which means that there is a good correlation between the two value sets.

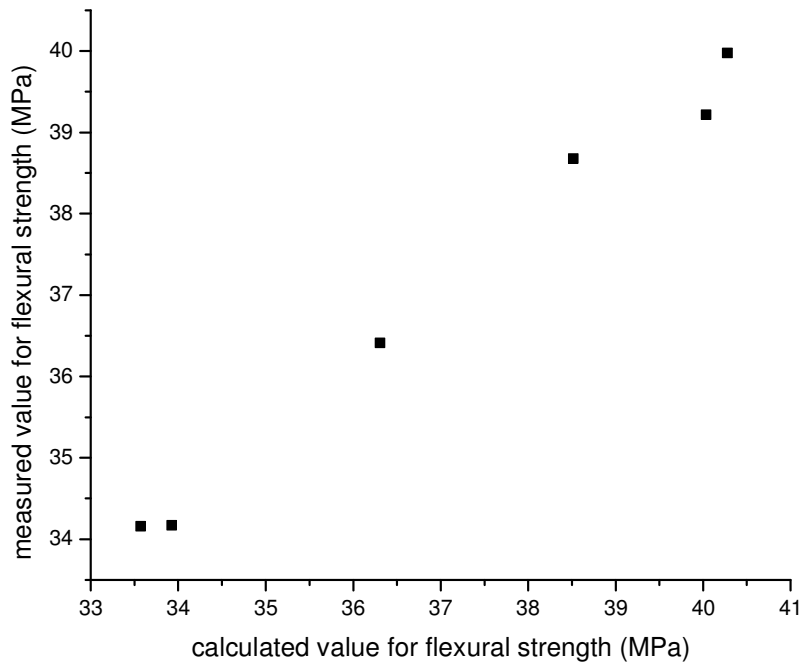


Figure 5.28. Measured and calculated values for flexural strength of glass fiber and carbon fiber reinforced samples.

5.4.4. Model for Impact Testing

Impact testing modeling is based on energy balance equations. According to the energy balance model given in Equation 5.38, the total absorbed energy is the sum of contact energy, bending energy, membrane energy and friction energy [16].

$$E_{absorbed} = E_C + E_{BS} + E_M + E_{friction} \dots\dots\dots (5.38)$$

where: E_C : Contact energy

E_{BS} : Bending-shear energy

E_M : Membrane energy

$E_{friction}$: Friction energy

When energy loss associated with friction is neglected, contact, bending and membrane energies can be calculated with the following equations.

The contact energy (Equation 5.39) depends on the contact force ‘ P_C ’ and the contact deformation α :

$$E_C = \int_0^\alpha P_C d\alpha \dots\dots\dots (5.39)$$

According to the Hertz law of contact, the contact force ‘ P_C ’ can be defined as:

$$P_C = \eta \alpha^{3/2} \dots\dots\dots (5.40)$$

η : the contact stiffness parameter

Combining Equation 5.39 and Equation 5.40:

$$E_C = \frac{2}{5} \eta \left(\alpha^{5/2} \right) \dots\dots\dots (5.41)$$

The contact stiffness parameter ‘ η ’ for a spherical isotropic rigid striker can be formulated as [16]:

$$\eta = \frac{4\sqrt{r_i}}{3\pi(k_i + k_{sample})} \dots\dots\dots (5.42)$$

where: $k_i = \frac{(1-\nu_i^2)}{\pi E_i}$

- k_i : stiffness of impactor
- k_{sample} : stiffness of sample
- ν_i : Poisson ratio of impactor
- E_i : Young modulus of impactor

The E_B energy due to bending deformations can be calculated using force-deformation relations [17]:

$$E_{BS} = \frac{1}{2} k_{BS} d^2 \dots\dots\dots (5.43)$$

where: k_{BS} : Bending shear stiffness

d : Deflection (m)

For samples having low thicknesses, the bending-shear stiffness is assumed to be equal to the bending stiffness as represented in Equation 5.35 [16]:

$$k_{BS} \cong k_B \dots\dots\dots (5.44)$$

In this case, Equation 5.34 can be expressed as:

$$E_{BS} = \frac{1}{2} k_B d^2 \dots\dots\dots (5.45)$$

where: k_B : Bending stiffness from flexural testing

d : Deflection (m) from flexural testing

$$E_m = \frac{1}{2} k_s x_s^4 \dots\dots\dots (5.46)$$

where: k_s : Sample stiffness

x_s : Sample deflection at impact

Given ' E'_m ' in Equation 5.46 [16] and assuming all the energy transferred to the sample is transferred as impact energy, then:

$$E_i = E_m \dots\dots\dots (5.47)$$

Applying values obtained for impact strength using exponential graph, Equation 5.48 is obtained. For glass fiber reinforced samples, impact energy is expressed using ' $v_{effective}$ ' given in Equation 5.35:

$$E_{impact} = \frac{1}{2} k_s x_s^4 \times 4.135 \times e^{(2.948 \times v_{effective})} \dots\dots\dots (5.48)$$

Using exponential graph for carbon fiber reinforced samples, impact energy is:

$$E_{impact} = \frac{1}{2} k_s x_s^4 \times 59.11 \times e^{(1.515 \times v_{effective})} \dots\dots\dots (5.49)$$

Figure 5.29 shows the measured and calculated impact energy values for glass and carbon fiber reinforced PP samples.

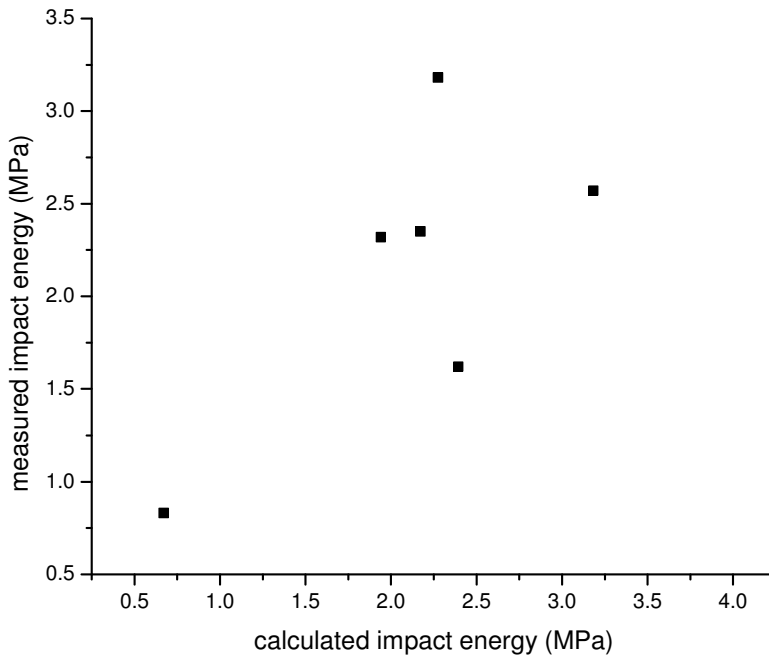


Figure 5.29. Measured and calculated values for impact energy of glass fiber and carbon fiber reinforced samples.

5.4. References

- [1] Kalaitzidou, K., Fukushima, H., Miyagawa, H., and Drzal, L.T., Flexural and Tensile Moduli of Polypropylene Nanocomposites and Comparison of Experimental Data to Halpin-Tsai and Tandon-Wang Models, *Polymer Engineering and Science*, **47**(11), 1796-1803 (2007).
- [2] Fu, S.Y., Lauke, B., Mader, E., Yue, C.Y., Hu, X., Mai, Y.W., Hybrid Effects on Tensile Properties of Hybrid Short-Glass-Fiber- and Short-Carbon-Fiber-Reinforced Polypropylene Composites, *Journal of Materials Science*, **36**(5), 1243-1251 (2001).
- [3] Mohsen, R.S., Saied, N.K., Ali Z., Hosein E.M., and Hasan P., Theoretical and Experimental Determination of Tensile Properties of Nanosized and Micron-Sized CaCO₃/PA66 Composites, *Polymer Composites*, **30**(3), 274-280 (2008).
- [4] Beckermann, G.W., Pickering, K.L., Engineering and Evaluation of Hemp Fibre Reinforced Polypropylene Composites: Micromechanics and Strength Prediction Modelling, *Composites Part A- Applied Science and Manufacturing*, **40**(2), 210-217 (2009).
- [5] Singh, U.P., Biswas, B.K., and Ray, B.C., Evaluation of Mechanical Properties of Polypropylene Filled with Wollastonite and Silicone Rubber, *Materials Science and Engineering A*, **501**, 94-98 (2009).
- [6] Fu, S.Y., and Lauke, B., Effects of Fiber Length and Fiber Orientation Distributions on the Tensile Strength of Short-Fiber-Reinforced Polymers, *Composites Science and Technology*, **56**, 1179-1190 (1996).
- [7] S.T. Peters, *Handbook of Composites*, Chapman & Hall, ISBN 0412540207, pg131-155; 525-555 (1998).
- [8] <http://info.lu.farmingdale.edu/depts/met/met205/composites.html>, access date 04.10.2009.

- [9] Pocius, A.V., Dillard, D.A., Chaudhury, M., “Adhesion Science and Engineering Volume 2”, Elsevier, 605-606 (2002).
- [10] Ash, J.T., Cross, W.M., Svalstad, D., Kellar, J.J., and Kjerengtroen, L., Finite Element Evaluation of the Microbond Test: Meniscus Effect, Interphase Region, and Vise Angle, *Composites Science and Technology*, **63**(5), 641-651 (2003).
- [11] Foster R. J., Hine P. J., and Ward I. M., Characterisation and Modelling of polypropylene/carbon Nanofiber Nanocomposites, *Polymer*, 50, 4018-4027 (2009).
- [12] DiFrancia, C., Ward, T.C., and Claus, R.O., The Single-Fibre Pull-Out Test. 1: Review and Interpretation, *Composites Part A: Applied Science and Manufacturing*, **27**(8), 597-612 (1996).
- [13] Thomason, J.L., Micromechanical Parameters From Macromechanical Measurements on Glass Reinforced Polyamide 66, *Composites Science and Technology*, **61**(10), 2007-2016 (2001).
- [14] Seymour S.A., The Aligned Discontinuous Fiber Process: Extension Into Manufacturing, Masters of Science Thesis, Department of Chemical Engineering, Michigan State University, page 9-10 (2000).
- [15] Hagstrand, P. O., Bonjour, F., and Manson, J. A. E., The Influence of Void Content on the Structural Flexural Performance of Unidirectional Glass Fiber Reinforced Polypropylene Composites, *Composites Part A: Applied Science and Manufacturing*, **36**, 705-714 (2005).
- [16] Sierakowski R.L., and Chaturvedi S.K., Dynamic Loading and Characterization of Fiber Reinforced Composites, pp 220-224 (2001).
- [17] Volmir A.S. 1967, A Translation of Flexible Plates and Shells, report number AFFDL-TR-66-216 (1967).

CHAPTER 6

CONCLUSIONS AND RECOMMENDATIONS

6.1. Conclusions

For toughening study of polypropylene with two different elastomers, tensile, three point bending and impact tests are conducted. Tensile test results show that the brittle characteristic of PP turns to be ductile when elastomers are blended in the polypropylene matrix. Three point tests show that flexural strength decreases when PP is toughened with elastomers F1 and F2. Impact tests give higher impact strength for elastomer blended PP.

DSC analysis shows the relation between crystallinity and toughness. PP blended with F1 and F2 elastomers give higher ductility and higher toughness while the overall crystallinity of blends decreases.

SEM analysis proves that both F1 and F2 elastomeric particles are evenly distributed in the PP matrix. Even distribution has a great effect on toughness increase in elastomer-polymer blends. SEM images also reveal that F2 particle sizes are smaller than F1 particle sizes.

The mixture samples are tougher than PP samples. Therefore, the toughness property of PP may be improved by adding F2 and F1 in PP.

In the reinforcement study of polypropylene with carbon fibers and glass fibers, improvement in tensile, flexural and impact properties is achieved. For prediction of the

composite tensile strength, impact energy and flexural strength models are developed using fiber volume content, void volume, interfacial shear strength, and total fiber surface area parameters.

When fiber orientation degrees are examined, it is seen that for all the samples, more than 65% of the fiber orientations is in the $\pm 30^\circ$ fiber alignment range. Even though fibers have a distribution from parallel to vertical within the samples, The mean orientation degrees are close to parallel orientation to the flow direction. This indicates that, it is important to find a fiber orientation factor for modeling. In the modeling of tensile strength, fiber orientation degree (FOD) has a power effect, while in impact and flexural models, FOD has a component of x-axis and y-axis orientations.

Using the models formed, the measured and calculated values are compared to evaluate the validity of the models. The difference between calculated and measured values is in the range of 90% acceptance for the tensile strength of glass fiber reinforced samples.

The difference between calculated and measured values is in the range of 90% acceptance for tensile strength of carbon fiber reinforced samples.

The comparison of calculated and measured values shows that the suggested models are in good correlation with the measured values for tensile strength, flexural strength and impact energy.

6.2. Recommendations

In the rubber toughening study, additional study may be conducted to investigate the suitability of PP/F1 and PP/F2 blends to extrude tougher fibers. Stiffness decrease is a sacrifice in rubber toughening. To obtain a good balance between pure PP and PP/elastomer blends, the addition of fillers such as CaCO_3 and silica nanoparticles to PP/elastomer blends may be helpful.

In the fiber reinforcement study, the fiber reinforcement weight percentages were 1 wt%, 4 wt% and 7 wt% which do not cause entanglements. Additional samples having higher fiber weight percentages may be produced to see the effect of fiber entanglements and compare the improvement in composite properties. The suggested models may be evaluated for higher weight percentages of fiber. In the suggested models, the interfacial shear strength is assumed to be the same for all samples, since the study is in micro scale.

Additional interdisciplinary study may be conducted with chemists to evaluate the bond strength between fibers and matrix using chemical modeling methods.

For nanoclay reinforced samples, the dispersion of nanoclay particles in the matrix and the spacing between nanoclay platelets may be evaluated using TEM analysis and models for predicting the overall strength properties of nanoclay composites may be developed.